MINERAL PROVINCES 37

AGSO
AUSTRALIAN GEOLOGICAL SURVEY ORGANISATION

Landsat–5 Thematic Mapper Image Correlations: Application to NGMA Mapping of the Western Musgrave Block, central Australia

A Y Glikson

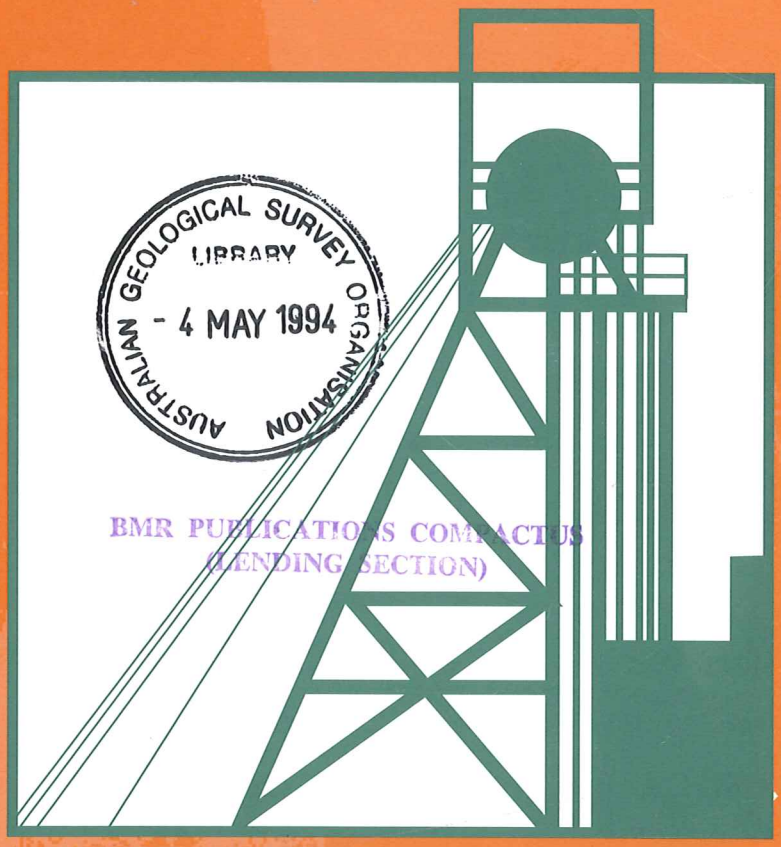

Record 1994/17

MINERALS AND LAND USE PROGRAM

AUSTRALIAN GEOLOGICAL SURVEY ORGANISATION

AGSO Record 1994/17

Landsat–5 Thematic Mapper Image Correlations: Application to NGMA Mapping of the Western Musgrave Block, Central Australia

Tomkinson Ranges, western Musgrave Block, central Australia

part of Landsat-TM scene p105r78 RGB pc2[4/3, 5/7] : 5/4 : 4/3 (clay : Fe-oxide : green vegetation) scale 1:100 000

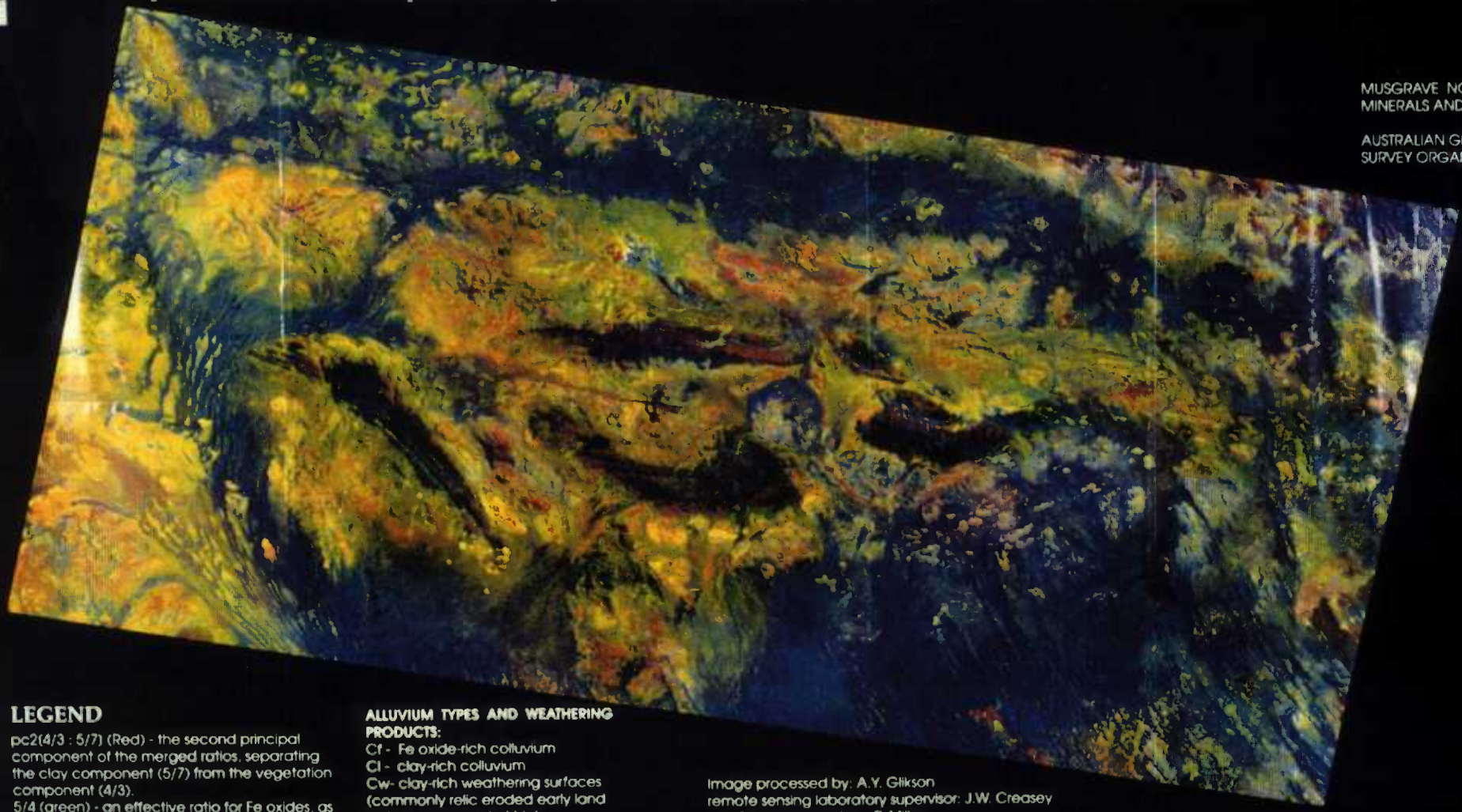

MUSGRAVE NGMA PROJECT
MINERALS AND LAND USE PROGRAM

AUSTRALIAN GEOLOGICAL
SURVEY ORGANISATION

LEGEND

pc2(4/3 : 5/7) (Red) - the second principal component of the merged ratios, separating the clay component (5/7) from the vegetation component (4/3).
5/4 (green) - an effective ratio for Fe oxides, as distinguished from the lower 5/4 ratios of vegetation and clay.
4/3 (blue) - green vegetation ratio.

BEDROCK TYPES:
P - peridotite
Px - pyroxenite
Gb - gabbro, gabbronorite, anorthosite
Gf - Fe oxide-rich gabbro
Mn - mafic granulites
Fn - felsic granulites and granitoids
BD - basic dykes

DURICRUST TYPES:
L - laterite (ferricrete)

ALLUVIUM TYPES AND WEATHERING PRODUCTS:
Cf - Fe oxide-rich colluvium
Cl - clay-rich colluvium
Cw- clay-rich weathering surfaces (commonly relic eroded early land surface preserved at high topograpdhic elevations

FIRE/VEGETATION PATTERNS:
F - fireburns
SV - vegetated southern slopes
DV - vegetated dunes

method:

Landsat Thematic Mapper (30X30 metre pixel) imagery, part of scene p105r78 (Cooper, Western Australia, Northern Territory and South Australia). Warped to Universal Mercator Grid (UTM) and image processed using IIS software.

Image processed by: A.Y. Glikson
remote sensing laboratory supervisor: J.W. Creasey
SUN System suspervisor: P. Miller

Minerals and Land Use Program,
Australian Geological Survey Organization,
P.O. Box 378,
Canberra, A.C.T. 2601

February, 1994

AGSO

AUSTRALIAN GEOLOGICAL SURVEY ORGANISATION

Landsat–5 Thematic Mapper Image Correlations: Application to NGMA Mapping of the Western Musgrave Block, Central Australia

Record 1994/17

Andrew Y. Glikson

DEPARTMENT OF PRIMARY INDUSTRIES AND ENERGY

Minister for Resources: Hon. David Beddall, MP
Secretary: Greg Taylor

AUSTRALIAN GEOLOGICAL SURVEY ORGANISATION

Executive Director: Harvey Jacka

ISSN: 1039-0073
ISBN: 0 642 20257 5

Contents

List of Figures and Tables

Figures

Tables:

SUMMARY

A study of Landsat-5 Thematic Mapper multispectral image data (7 bands, 30x30 metre pixel size) was conducted in conjunction with the detailed geological mapping of the Tomkinson Ranges, western Musgrave Block, within the framework of the National Geoscience Mapping Accord (NGMA)(Glikson et al., 1989; Ballhaus and Glikson, 1989; Stewart and Glikson, 1991; Clarke, 1992; Sun and Sheraton, 1992; Feeken, 1992; Ballhaus, 1993). The detailed geological and environmental field work conducted during 1987-1991 allows meaningful correlations between image data and lithological surface types, providing a test area for the development of spectral-lithological correlations in other parts of the Musgrave Block and similar terrains in central Australia. In this study correlations were conducted in terms of both bedrock types and surface deposit types. The Tomkinson Ranges consist of a series of up to about 1000 metres high ranges separated by alluvial valleys or dunes. Good outcrop, sparse vegetation and the dry climatic conditions of the terrain, located at the fringe of the Gibson Desert, combine to provide an environment highly suited for the application of remotely sensed imagery. The terrain is underlain by about c.1.3-1.5 b.y. old felsic/intermediate granulites intruded by layered about c.1.2 b.y. old mafic/ultramafic bodies of the Giles Complex and younger granites coeval with c. 1.06 b.y. old volcanics. The Landsat-5-TM imagery was warped to the Australian Metric Grid. Image processing was conducted according to the following methods: (A) single band dark pixel-correction; (B) band ratioing; (C) logarithmic residual (Green and Craig, 1985); (D) principal components analysis of single bands; (E) principal components of band ratios (Fraser and Green, 1987); (F) pixel unmixing analysis applying radiance correction for atmospheric scatter and resolving the proportions of individual end members (Bierwirth, 1991); (G) devegetation of single band images, subtracting the vegetation end members resolved by the pixel unmixing analysis of Bierwirth (1991); and (H) unsupervised classification. Significant correlations are observed between the scanned reflectance patterns of iron oxide and clay/carbonate-dominated weathering surfaces and the primary rock types. Identification of iron oxides is facilitated by several methods, including (1) log residual of bands 5 and 7; (2) the 5/4 band ratio, and (3) the iron oxide end-member of pixel-unmixed images. The identification of iron oxide by the 3/1 band ratio is partly masked by the corresponding vegetation ratio. Identification of clay and/or carbonate is facilitated by (1) high bands 5/7 ratio; (2) the clay end-member of pixel-unmixed images; (3) pc2(4/3, 5/7) (Fraser and Green, 1987), and (4) where clay-rich soils support green vegetation, indirectly by band 4. Method (3) was found to be particularly effective in resolving clay from vegetation. Discrimination between carbonate and clay is difficult, but calcrete banks along creeks are characterised by higher reflectance relative to clay. The quartz component of weathering crusts on bedrock is masked by clay/iron oxide coatings. In contrast, alluvial and dune deposits display higher reflectance thanks to their higher content of abraded quartz grains. The combination of the various resulting images with a sound field knowledge of the petrological, structural and morphological characteristics of the terrain, allows discriminations between several surface types, including (1) peridotite (partly magnesite covered); (2) orthopyroxenite (iron oxide-rich weathering); (3) clinopyroxenite (weaker iron oxide weathering), gabbro (clay and carbonate-dominated weathering); (4) ferrogabbro (iron oxide-rich weathering); (5) anorthosite (high reflectance carbonate-rich weathering); (6) mafic granulites (iron oxide and silica-rich crusts); (7) felsic granulites and granites (clay and silica crusts) commonly crossed by lineaments representing the iron oxide-rich weathering of dykes; (8) laterite (iron oxide-rich); (9) calcrete (high reflectance, common along creeks); (10) silcrete (very high reflectance); (11)

mafic source-derived alluvium (iron oxide-dominated); (12) felsic source-derived alluvium (clay and quartz dominated); and (13) clay pans and silty (in places ferruginous) dry lake (playa) deposits. Identification of the composition of small isolated bedrock outcrops (inselbergs) is facilitated by associated haloes of derived detritus – namely iron oxide-rich detritus around mafic outcrops and clay/quartz rich detritus around felsic outcrops. Discrimination between old vegetation and fireburn vary between mafic terrains, where the small increase in reflectance is highest in band 4, and felsic terrains which show a strong increase in reflectance with a maximum in band 5. Fireburnt dune areas show a maximum reflectance increase in band 4, signifying green vegetation regrowth. Correlations between Landsat-5-TM spectra and ground observations were tabulated in order to facilitate their application to the mapping of other parts of central Australian metamorphic/igneous terrains. Examples of correlations and discriminations between lithological assemblages and boundaries allowed by the Landsat-5-TM data are: (1) discrimination between felsic granulites and interbanded layers and lenses of anorthosite in the Teizi area due to the clay/carbonate weathering surfaces of the anorthosites; (2) discrimination between gabbro and mafic granulites derived by recrystallisation of the gabbro in conjunction with intrusion of felsic veins. The mafic granulites are characterised by a higher iron oxide signature than the gabbro and by surface coating of silica, which results in spectral features more similar to felsic granulites than to the parent gabbro; (3) clear distinctions between ferrogabbro – characterised by cumulate magnetite and thick weathering coatings of iron oxide – from normal gabbro; (4) distinctions between orthopyroxene-dominated pyroxenite (iron-rich) and clinopyroxene-rich pyroxenite (plagioclase-bearing). Preliminary image processing of two 5 km-wide strips of Geoscan Mark-I (13 bands, 10x10 metre pixel) airborne scanner imagery flown over the Tomkinson Ranges point to the superior spatial resolution and the significance of the thermal bands of this imagery (Honey and Daniels, 1986; 1987). Free quartz and silcrete rich areas are expressed by a high band 11/10 ratio. Logarithmic residual images, for example RGB log residual 9:4:1, effectively resolve detailed lithological contrasts on a scale close to that of individual outcrops. An example is furnished by the Wingellina lateritic nickel deposits, where logarithmic residual images are capable of outlining areas underlain by fresh to weakly weathered gabbro from areas underlain by lateritised mafic and ultramafic rocks.

1. INTRODUCTION

This study forms part of the Musgrave NGMA project underataken jointly by the Australian Geological Survey Organisation, the Geological Survey of the Northern Territory, the Geological Survey of Western Australia and the South Australia Department of Mines. The National Geoscience Mapping Accord, endorsed by the Australian (now Australian and New Zealand) Minerals and Energy Council in August 1990 is a joint Commonwealth/ State/Territory initiative to produce, using modern technology, a new generation of geoscientific maps, data sets, and other information on strategically important regions of Australia over the next 20 years.

The study of multispectral LANDSAT-5 Thematic Mapper and GEOSCAN Mark-I multispectral imagery is associated with a 1:100K mapping program of the Tomkinson Ranges within the framework of the National Geological Mapping Accord (NGMA). Field work has been facilitated by 1:20k colour aerial photography, flown for AUSLIG (May, 1987) over the Tomkinson Ranges (Fig. 1). The purpose of the study is to (1) correlate rock types and units mapped in the field with multispectral reflectance patterns; (2) attempt to model the observed spectra in terms of realistic end members, using laboratory measured spectra; (3) interpolate and extrapolate the observed geological units within the Tomkinson Ranges, and (4) identify image processing methodology best suited to the Musgrave Block, with the aim of extending the mapping program into new areas.

The application of remotely sensed imagery to regional mapping of unmetamorphosed terrains and greenschist to amphibolite facies metamorphic terrains utilizes the characteristic absorption spectra of hydrosilicates (amphibole, mica, chlorite) and their alteration products (clay minerals, serpentine, carbonates and iron oxides). In these terrains remotely sensed data in the visible, near-infrared (NIR) and shortwave infrared (SWIR) can be correlated with a range of lithologies (e.g. Simpson et al., 1987). The application of these data requires careful screening of weathering, vegetation and fireburn effects (Simpson, 1978), while in some instances recent fireburns provide little-obscured bedrock windows, as observed in the central Pilbara region using Geoscan Mark-I imagery (Glikson, 1987, unpubl.).

In contrast, the geology of the Tomkinson Ranges is dominated by igneous and granulite facies assemblages dominated by feldspar, pyroxene, olivine accompanied by only a minor hydrosilicate component. The scarcity of characteristic hydroxyl-controlled absorption features in the granulite facies rocks, as contrasted with their abundance in greenschist facies terrains, complicates their remotely sensed identification. However, characteristic weathering crusts, i.e. clay, carbonate, haematite, goethite, etc., offer diagnostic fingerprints for primary lithologies. Application of Landsat-5-TM imagery and Geoscan Mark-I imagery in the Tomkinson Ranges has involved processing of band ratio images, log residual images (band radiance divided by mean pixel radiance divided by mean image radiance), principal components images (band covariance indices), pixel-unmixed images, devegetated mineral images and unsupervised classification images

Systematic geological mapping of high grade metamorphic terrains in central Australia (Stewart et al., 1984; Warren, 1982; Shaw & others, 1984; Glikson, 1987; Glikson, 1990; Stewart, 1991) has produced a series of regional maps on the 1:100K and 1:250K scale. Inherent in the mapping of these terrains is the interpolation and extrapolation of outcrop-scale (mesoscale) data to map-scale (macroscale: 10^2 metres) units, aided by aerial photography and airborne geophysical and remotely sensed information. Penetrative deformation and recrystallization associated with high grade metamorphism commonly result in dismemberment of original rock units into interdigitated mesoscale,

handspecimen-scale and microscopic units, as well as imperceptible transitions between macroscale units. Partial melting, remobilization and anatectic injection of veins, bands and migmatite units occur on all scales. Consequently, interpolation of field data and identification and charting of map-scale units may require numerous field traverses and petrographic examinations.

2. THE TOMKINSON RANGES, CENTRAL AUSTRALIA

2.1 GEOGRAPHY

The Tomkinson Ranges straddle the Western Australia-South Australia border, centering about longitude 129°00'E and latitudes 26°00'- 26°23'S - forming an east-west elongated block about 80X40 km large within the Bell Rock 1:100k sheet (Western Australia, sheet no. 4645), Davies 1:100k sheet (South Australia, sheet no. 4745), and the southwestern part of the Bates 1:100k sheet (Western Australia, sheet no. 4646 (Fig. 1). The terrain consists of a series of ridges and inselbergs occupying about 40 percent of the area. The highest points reach elevations ~1000 metre above sea level in the Hinckley Range (1014 m), Mount Davies (1053 m), Ewarara hills (1018 m), Mount Kalka (1009 m), Teizi hills (871 m), Mount Aloysius (982 m), Bell Rock Range (874 m), Michael Hills (838 m) and the Mount West massif (858 m). The geography of the region has been documented by Daniels (1974) and Feeken (1992).

Duricrusts may form low rises above valley floors and plains. Major elevated morphological units in the Tomkinson Ranges consist of mafic and to a lesser extent ultramafic rock, including the Hinckley Range, Bell Rock Range, Mount Kalka, Mount Davies, Michael Hills and the southern part of the Mount West massif. Other elevated units consist of felsic granulites and granitic gneiss, including Mount Aloysius, Mount West, Ewarara hills and numerous scattered outcrops. Ridges consisting of gabbro or pyroxenite display jagged skylines and may contain prominent rock piles consisting of slumped subangular boulders several metres across with little soil or vegetation in-between. Examples of such boulder piles are common in the Bell Rock Range, consisting largely of gabbro, and Mount Kalka and Ewarara intrusion, where the slumped boulders consist mainly of pyroxenite. Mafic granulites are, as a rule, less resistant to erosion than the gabbro, and form more subdued morphological features. Mafic dykes form linear depressions within gabbro terrains and stand out as narrow linear ridges in mafic granulite and felsic granulite and granite terrains.

2.2 SURFACE DEPOSITS

Bedrock ridges are engulfed by colluvial collars. Pediments are observed mainly in association with colluvium and to a lesser extent are interspersed with alluvial fans, jutting out into the plains. The intermontane valleys and intersecting plains in the Tomkinson Ranges show a general decline in elevation toward the southwest. Plains and valleys consist of lithic materials, grading from gravels in parts of the flood plains and alluvial plains south of Michael Hills and coarse sands in alluvial fans to clayey red to red-brown soils in the centre of alluvial plains. Sandplains, including dunes, are widespread in the northwest, north and northeast of the map area, as well as along the southern margin. The materials of the plains and dunes include coarse to medium-grained red-brown sands, which tend to become quartz-rich in the west, and coarse to medium-grained brown lithic sands in the east. Dune fields engulf the Tomkinson Ranges and individual dunes may reach 10 meters in height. Several types can be identified, including network dunes and broadcrested linear dunes. Some dunes, contain interbeds of fine magnetite grains and flakes. Commonly dunes coincide with isolated inselberg outcrops and form in conjunction with a

Fig.1

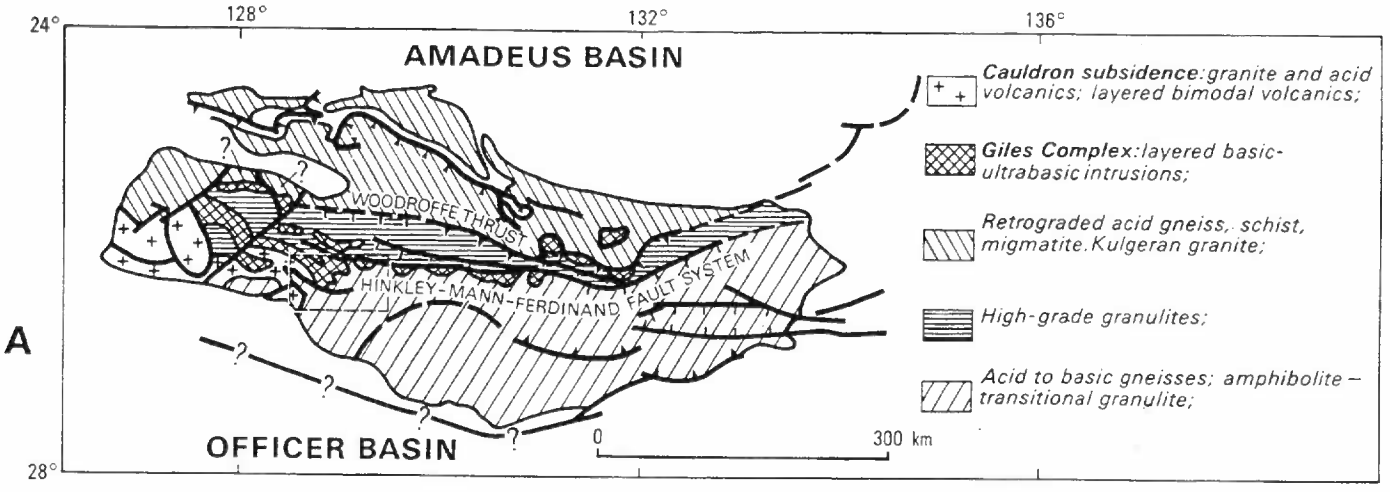

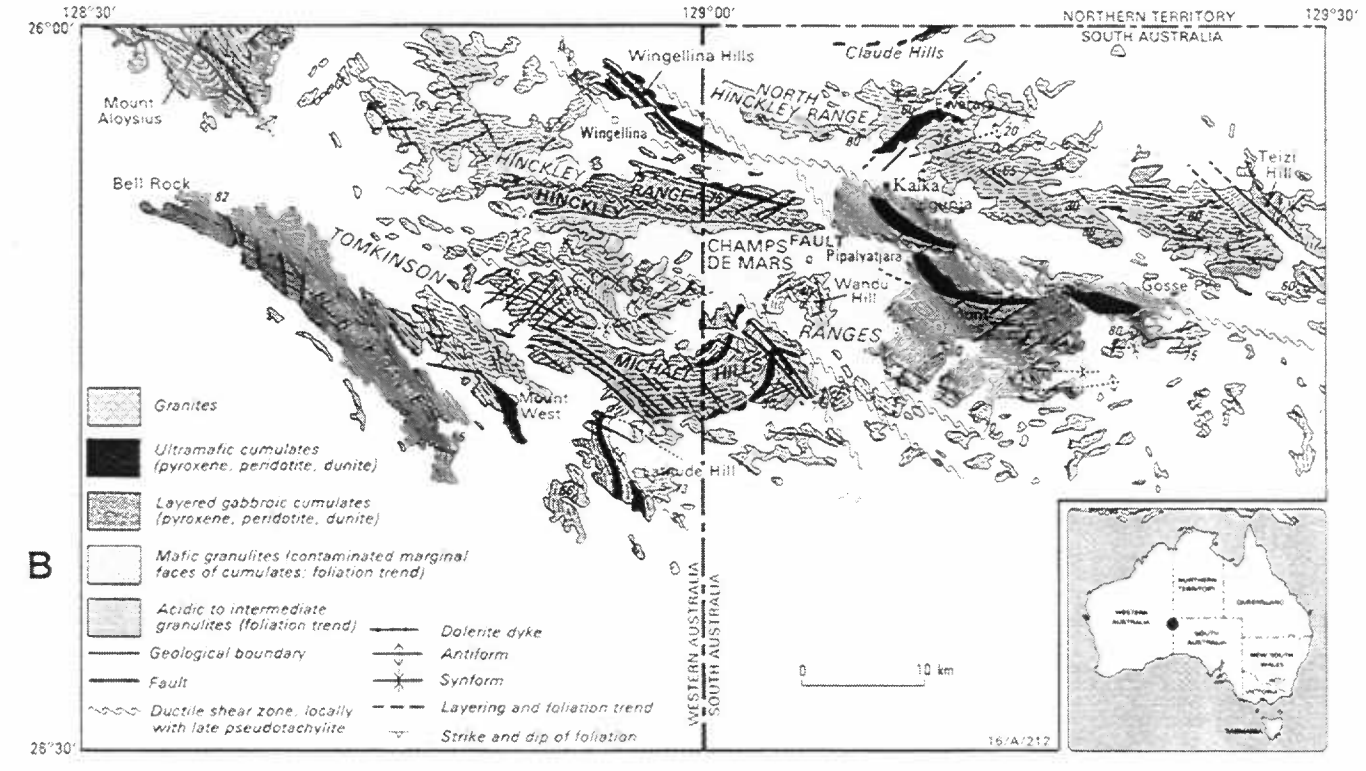

Fig. 1. Location and geological sketch map of the Tomkinson Ranges, Western Australia and South Australia. A - The Musgrave Block, frame defines location of Fig. 1B; B - Tomkinson Ranges.

wind shadow effect. Duricrusts are common, including calcrete horizons, which are common in the vicinity of mafic and ultramafic outcrops, but are less common or absent around felsic rock outcrop. Fericrete outcrops occur mainly above ultramafic rocks, for example north of Wingellina, north of Mount Kalka Hill and at Mount Davies, but also occur above felsic granulites west of Teizi soak. Silcrete crops out in conjunction with lateritic profiles, and may be locally interbedded with calcrete.

2.3 VEGETATION

Vegetation distribution patterns in the Tomkinson Ranges can be correlated with surface deposits (Feeken, 1992). The floral habitat is dominated by mulga, spinifex and annual and perennial grasses. Mulga can occur on plains, outcrops or among dunes, with or without association with other growth. A reciprocal relationship is seen between mulga and spinifex, and mulga decreases or is totally absent where heavy spinifex growth occurs. Mulga has died back extensively in the near past, a decline not obviously correlated with burning or with the rabbit population. An example is the region south of the Michael Hills from Purnawarra bore eastward, where over 70% of the mulga has died from lack of moisture and/or disease. Very little regeneration of the mulga is evident. Spinifex tussocks dominate mafic and ultramafic rock outcrops, but are also common on some felsic terrains, for example Mount West, and in plains. Bunch grasses dominate on the plains and are also important on felsic granulite and granitic outcrops. Corkwood trees (of the Hakea family are locally prominent and often occupy the margins of outcrops, including pediments and alluvial fans. Other prominent plant growth include two species of Grevillea in dune fields on or near the crest of dunes, often the very dense interdunal desert heath (Thryptomene), and species of native fuchsia and cassias.

2.4 GEOLOGY

Regional geological mapping in the Tomkinson Ranges was conducted by Daniels (1974) and Thomson et al. (1962), and detailed studies by workers of the University of Adelaide (Nesbitt and Kleeman, 1964; Nesbitt and Talbot, 1966; Nesbitt et al., 1970; Goode and Krieg, 1967; Goode and Moore, 1975; Goode, 1978). The most important geological unit in the Tomkinson Ranges - the Giles Complex - consists of a suite of deformed, partly recrystallized, massive gabbroic to interlayered gabbro/pyroxenite intrusions emplaced in the southern granulite-facies block of the upper-middle to upper Proterozoic Musgrave Block (Fig. 1) (Nesbitt et al.,1970, Goode, 1978; Moore and Goode, 1978; Daniels, 1974; Ballhaus and Glikson, 1989; Glikson et al., 1990; Glikson, 1992). The Giles Complex is emplaced into a suite of felsic granulite facies orthogneiss and paragneiss, and is intruded in turn by a suite of porphyritic granites about 1185 Myr (Sun and Sheraton, 1992). The high-grade metamorphic suite is intruded by several sets of mafic dykes and succeeded by volcanics of the Bentley Group about 1060 Myr old. The NGMA project (1987-1992) included investigations of the field relations between the Giles Complex and country rocks in the western Musgrave Block (Glikson, 1990; Glikson et al., 1990; Pharaoh, 1990; Stewart and Glikson, 1991; Clarke et al., 1992), the petrology/geochemistry of the mafic/ultramafic rocks (Ballhaus and Glikson, 1989; Ballhaus and Berry, 1991; Ballhaus et al., 1992; Ballhaus, 1992), the age and composition of felsic igneous rocks (Sun and Sheraton, 1992), and the tectonic fabrics and thermobarometric indices (Clarke et al., 1992; 1993).

For the purposes of the remotely sensed investigation of the Tomkinson Ranges area, the lithological assemblages are classified in terms of the following groupings, as based on geological mapping (Glikson et al., in prep.) and field observations of the surface deposits (Feeken, 1991, 1993):

1. bedrock

A. banded to massive felsic to intermediate granulites.

B. massive to foliated granitoids associated with felsic granulites.

C. mafic granulites: C1 – associated with felsic granulites; C2 – representing recrystallized products of gabbro of the Giles Complex.

D. gabbro, gabbronorite and norite of the Giles Complex.

E. anorthosites of the Giles Complex.

F. pyroxenites of the Giles Complex.

G. peridotites of the Giles Complex.

H. mafic/ultramafic plugs.

I. mafic, intermediate and felsic volcanic rocks

2. duricrust

K. calcrete and magnesite.

L. ferricrete and laterite.

M. silcrete

3. surface deposits

N. colluvium (coarse grained arenites and conglomerates associated with pediments).

O. alluvium (including plains and creek terrace deposits).

P. clay pans

These rock and surface cover types were tested in relation to the imagery with the aim of establishing correlations as a basis for the preparation of synoptic geological and environmental maps in the Musgrave Block. The correlations include testing of training areas of a size of about 10-20 pixels as well as other areas mapped in detail in the field.

3. LANDSAT-5 TM SPECTRA AND IMAGES

3.1 REMOTELY SENSED MULTISPECTRAL DATA

Remotely sensed data available for the Tomkinson Ranges includes the LANDSAT-5 Thematic Mapper 180X180 km scene p105r78 consisting of 7 spectral bands (pixel size 30X30 metre for bands 1-5 and 7; 120X120 metre for band 6):

band 1:	.45-.52	micrometer	visible blue/green (VIS)
band 2:	.52-.60	"	" green/red
band 3:	.63-.69	"	" red
band 4:	.76-.90	"	near-infrared (NIR)
band 5:	.1.55-1.75	"	short wave infrared (SWIR)
band 7:	.2.08-2.35	"	"
band 6:	.10.4-12.5	"	thermal infrared (TIR)

Statistical data for this scene, including minimum, maximum and mean DN values, standard deviations, correlation matrix, Eigen values and Eigen vectors are given in Table A. The present report is based on a 4805 X 2678 pixels large sub-scene of this image, including 6 bands (bands 1, 2, 3, 4, 5, 7). The thermal band 6 has been deleted because atmospheric interference effects make it unusable. Statistical data for the dark pixel-subtracted sub-scene is given in Table B.

Table A - Image statistics for Landsat Thematic Mapper image p105r78.image
Size : 6160 x 5800 x 7 x 1; Brick size : 128 x4; Data type: byte

bands:	1	2	3	
	4	5	6	7
Minimum Vector:				
	54.000	20.000	21.000	
	16.000	24.000	129.000	15.000
Maximum Vector:				
	172.000	103.000	158.000	
	148.000	241.000	180.000	137.000
Mean Vector:				
	74.210	38.137	61.886	
	63.240	120.630	161.785	74.942
Standard Deviations:				
	3.915	3.150	8.295	
	8.945	18.724	4.336	12.089

Correlation Matrix for 7 bands:

1	1.000	.744	.442	.332	.312	-.136	.272
2	.744	1.000	.839	.760	.674	-.109	.645
3	.442	.839	1.000	.949	.873	.070	.882
4	.332	.760	.949	1.000	.877	.098	.895
5	.312	.674	.873	.877	1.000	.067	.965
6	-.136	-.109	.070	.098	.067	1.000	.155
7	.272	.645	.882	.895	.965	.155	1.000

Eigen Values		Eigen Vectors:						
		pc1	pc2	pc3	pc4	pc5	pc6	pc7
band 1	.897	-.053	-.091	-.308	-.334	-.745	-.016	-.477
band 2	.040	-.448	-.348	-.519	-.435	.352	.236	.199
band 3	.031	.227	.080	-.191	-.322	.337	-.807	-.191
band 4	.018	.718	.200	-.088	-.419	.160	.485	-.035
band 5	.008	-.185	.028	.061	.188	.426	.236	-.830
band 6	.004	.297	-.073	-.723	.619	-.001	-.005	.016
band 7	.001	.327	-.904	.255	.036	.018	-.045	-.080

Table B - pixel array statistics for a dark pixel-corrected sub-image of the Landsat Thematic Mapper image p105r78
size : 4805 x 2678 x 6 x 1 ; Brick size : 128 x4; data type:byte
User Coordinate System: mapproj; Type: Linear
Ax: .030 Bx: 430.722
Ay: -.030 By: 7143.845

statistics: 6 bands (1,2,3,4,5,7)

bands:	1	2	3
	4	5	7
minimum Vector: 0 (dark-pixel-corrected)			
maximum Vector:	118.000	83.000	116.000
	112.000	175.000	121.000
Mean Vector:	13.721	12.255	26.525
	30.450	60.471	47.966
Standard Deviations:	9.577	8.529	18.599
	21.133	42.290	33.022

Correlation Matrix for 6 bands:

1	1.000	.977	.944	.934	.929	.930
2	.977	1.000	.976	.966	.954	.954
3	.944	.976	1.000	.992	.981	.981
4	.934	.966	.992	1.000	.985	.988
5	.929	.954	.981	.985	1.000	.994
6	.930	.954	.981	.988	.994	1.000

Eigen Values		Eigen Vectors:					
		pc1	pc2	pc3	pc4	pc5	pc6
band 1	.989	-.146	-.133	-.299	-.340	-.685	-.535
band 2	.006	.512	.413	.476	.353	-.425	-.189
band 3	.003	.649	.246	-.275	-.543	.341	-.177
band 4	.002	-.249	-.004	.319	.091	.475	-.776
band 5	.001	-.224	.105	.657	-.675	-.087	.209
band 7	.000	.428	-.860	.275	-.016	-.013	-.029

3.2 IMAGE PROCESSING METHODOLOGY

The Landsat-5-TM and Geoscan images used in this study were processed at the AGSO Image Processing Centre using the IIS System 600 Version 3.0 (International Imaging Systems, 1500 Buckeye Drive, Milpitas, Calif. 95035) and the ERMAPPER software Version 4.0 (Earth Resources Mapping, 87 Colin St., West Perth, W.A. 6005), using the Unix Operating System (Unix Systems Laboratories Inc.) run on a Sun 4/280 mainframe computer (Sun Microsystems Inc., 2550 Garcia Avenue, Mountain View, Calif. 94043-1100, USA) connected to 3.36 Gb NEC 2363 disc drives. Backups of image files and other data are stored on 1.9 Gb Exabyte 8 mm tapes. The Sun system at AGSO is supervised by P. Miller and the image processing laboratory supervised by J. Creasy.

The procedures performed in the present study were conducted in the following sequence on the IIS (for details of these procedures refer to the above references):

1. Loading image from tape reels, running the program: t'lgso

2. Cutting of a 4805 X 2678 pixels-large subimage from the Landsat-5-TM p105r78: c'copy (xx;yy;bands).

3. Dark pixel subtraction (subtracting minimum DN values in each band): c'stat, c'print_stat, u'add. The minimum DN values for the studied subimage are: band 1 - 54; band 2 - 20; band 3 - 21; band 4 - 16; band 5 - 24; band 6 - 129; band 7 - 15.

4. Warping of the subimage to the Australian Metric Grid, (on the M75 Station): m'process, c'gcp'collect, c'gcpbyhand, c'cpwarp (forming auxiliary [header] User Coordinate System [UCS] files).

5. Copying of the auxiliary statistics file from the file header of the unwarped image to the file header of the warped image (to avoid the null values of the surrounds of the

warped subimage), running c'aux'copy. Subsequent c'stat operations on the warped file always have to be conducted on a subarea of the image, to avoid null pixels.

6. Creating RGB images: c'copy.

7. Spatial filtering images: c'convolve.

8. Creating ratio images (section 3.7): c'divide, c'scale, and merging RGB band ratio images: c'merge.

9. Creating log residual images (section 3.6): u'logress; inverting bands in log residual images: c'neg.

10. Creating principal components images (section 3.8): c'kl.

11. Creating pixel unmixing images (sections 3 and 9): prepare a spectral selelction file, tmspectsel, selected from file tmspeclib (spectral library of Landsat-5-TM data for standard surface types). Run: %bemix,)b'stat (statistics program), berad2 (reflectance estimates), spmix (pixel unmixing program not including RMS errors) or spermix (including RMS errors).

12. The spmix and spermix programs include an option for subtracting the vegetation end members from original spectral bands, allowing preparation of de-vegetated images.

12. Log residual analysis can be conducted on devegetated images.

13. Unsupervised classification conducted on warped dark-pixel unmixed images: c'cluster, involving choice of desired number of classes.

Processing on the ERMAPPER software system was conducted principally in view of the storage space economy allowed for small (kb) algorithm files, instead of entire image files. The procedure included (1) transfer of image files from the IIS system; (2) processing of band ratios, including band streching and filtering; (3) storage of algorithms; (4) transfer of image files back to the IIS system. The latter step was necessary since the resolution of the IVAS workstations connected to the IIS system was found to be better than the resolution on the 24 bit workstations connected to the ERMAPPER system.

3.3 CALIBRATION OF LANDSAT-5-TM DATA

Landsat-5-TM data are affected by the additive atmospheric radiance (path radiance or multiple atmospheric scatter) and by multiplicative factors (including atmospheric transmittance of solar radiation, solar illumination variations, reflected radiation at specific solar zenith and satellite nadir view angles, and sensor gains), and should be calibrated, i.e. converted to pixel reflectance values. Such calibration involves removal of the atmospheric influences, sensor gains and sensor offsets from the scanned data. Ideally, direct comparisons are performed between the remotely sensed data and field or laboratory spectral measurements. For this purpose, relatively homogeneous pixels are selected, e.g. water, uniform green vegetation cover, open cuts of monomineralic material or known uniform rock/weathering crust composition and compared with available mineral or rock spectra. Potential test pixels were examined in the Tomkinson Ranges by C. Simpson (1987). No perfectly homogeneous pixel consisting of a pure component is identified in the area. Open cuts of silica--dominated chrisoprase in silcrete near Wingellina and Kalka settlements display high reflectance (band 5, DN = 120-140), but also show spectral features suggestive of contamination with iron oxides and clay. Nor can the silica-rich airstrip at Wingellina be considered a pure component. A Eucalypt and green grass-rich patch of the Wingellina school was also tested. The DN values for test pixels are presented in Table C.

Where uniform pixels can not be identified, approximate calibrations can be obtained by the application of log residuals. The treatment represents ***within-scene relationships*** within pixels and between pixels, and is thus independent from the overall atmospheric and gain corrections which apply uniformly to ***all*** the pixels. Band ratio images are less affected by shade component, which does not alter the within-pixel spectral ratios.

In the present study radiance data were converted to reflectance by means of the two following methods (1) dark pixel [DPS], namely subtraction in each band of the minimum pixel DN value in the entire scene, assuming that the minimum DN values represents additive atmospheric scatter, and (2) A correction that takes illumination, atmospheric transmittance, incidence/reflectance angles, global ground radiance, additive atmospheric scatter, sensor gains and sensor offset into account (Forster, 1984; Richards, 1986; Bierwirth, 1990). The method uses band means and and an inferred reflectance mean, and it estimates the pixel reflectance (R) for any particular wavelength interval on the basis of corrections for dark pixel radiance, sensor gains and the average solar spectrum.

Estimated reflectance spectra are plotted along with vegetation-removed spectra in Fig. 10. Comparisons between the raw spectra, dark pixel-corrected spectra, radiation-corrected spectra and field/laboratory measured end member spectra are complicated by the differences in the conditions under which each spectral set has been measured or scanned. Thus, whereas comparisons of spectra ***within*** any particular spectral set may be meaningful, comparisons ***between*** the different spectra sets (DPS spectra, corrected spectra using program BERAD2 (P.N. Bierthwirth, pers. com., 1993), field-measured spectra [solar

Table C - Landsat -TM mean radiance values (in DN) for training areas in the Tomkinson Ranges. Values on the left - dark pixel-corrected mean radiance values. Values on the right - atmospheric effects-corrected mean reflection values.

Landsat-TM band	1	2	3	4	5	7
1. igneous and metamorphic rocks						
opx-rich rocks-GP	13 / 12	10 / 18	16 / 21	20 / 34	40 / 43	38 /62
cpx-rich rocks-EW	15 / 14	13 / 24	27 / 33	29 / 48	66 / 68	57 / 91
gabbro-BR	20 / 18	18 / 30	35 / 42	38 / 62	69 / 71	59 / 94
ferrogabbro-BR	22 / 14	18 / 23	35 / 32	39 / 44	78 / 72	62 / 95
gabbro-HG	23 / 20	19 / 33	33 / 40	36 / 59	47 / 50	42 / 68
weather. gabbro-HG	17 / 15	17 / 30	35 / 42	38 / 63	56 / 59	47 / 75
mafic granulite-HG	21 / 19	16 / 27	27 / 33	30 / 51	69 / 71	54 / 86
norite-KA	23 / 21	22 / 37	42 / 51	41 / 68	64 / 67	57 / 91
leucogabbro-KA	24 / 21	21 / 36	38 / 46	39 / 64	72 / 74	57 / 91
anorthosite, TEIZI	27 / 23	27 / 45	52 / 63	54 / 87	89 / 91	65 / 104
gabbro-MH, fireburn	20 / 18	18 / 30	33 / 40	36 / 59	57 / 60	46 / 74
gabbro-MH, old veg	21 / 19	16 / 28	26 / 32	28 / 46	51 / 54	42 / 69
felsic granulites	22 / 20	20 / 34	39 / 47	45 / 73	93 / 95	69 / 109
granite gneiss	19 / 17	16 / 28	30 / 37	35 / 57	76 / 78	58 / 93
weathered felsic granulites	18 / 16	17 / 29	34 / 42	41 / 66	74 / 76	53 / 85
2. duricrust						
laterite-WIN	17 / 16	13 / 24	25 / 31	30 / 50	78 / 80	59 / 95
laterite-KA	17 / 16	14 / 23	30 / 31	33 / 46	88 / 76	67 / 96
calcrete-PID	44 / 37	36 / 58	62 / 74	68 / 108	125 / 127	86 / 136
calcrete-CDM	27 / 24	25 / 42	52 / 62	57 / 91	116 / 118	87 / 137
silcrete-WIN	51 / 43	41 / 67	65 / 77	65 / 104	120 / 122	81 / 129
silcrete-KA	55 / 46	43 / 69	63 / 75	67 / 107	139 / 141	87 / 138
3. alluvial deposits						
alluvium, basic source	23 / 20	19 / 33	35 / 45	37 / 64	75 / 83	62 / 106
alluvium, felsic source	19 / 17	20 / 34	51 / 61	56 / 90	119 / 121	86 / 136
silt and clay-CDM	22 / 19	22 / 37	50 / 59	52 / 84	95 / 97	77 / 122
silt and clay-LW	31 / 27	24 / 40	38 / 46	38 / 63	98 / 100	82 / 129
dunes, fireburn	21 / 19	18 / 31	45 / 54	52 / 84	102 / 104	78 / 123
dunes, old growth	24 / 21	18 / 31	35 / 43	40 / 65	91 / 93	67 / 108

illumination], laboratory-measured spectra [artificial illumination]) must take their measurment conditions into account. Further, variations in the grain size of chemically and mineralogically similar materials preclude direct correlations between standard laboratory-measured end members and the remotely sensed pixel data, unless field calibrations are available. An example is the marked difference in the reflectance of gabbro and mafic granulites in the Tomkinson Ranges. Although these materials are mineralogically and chemically very similar, the mafic granulites are finer grained than and are in places intruded by granitic veins and coated by silica-rich thin weathering crust. The gabbro, by contrast, is typically coated by clay/carbonate/iron oxide-bearing weathering crusts. These differences are expressed by the spectral characteristics of these rocks, allowing their discrimination and mapping.

The discussion of Landsat-5-TM data in this report is illustrated by single band black and white images of selected areas, principally the Mount Davies sub-scene. This area covers a wide range of surface types, including the Mount Davies and Kalka gabbro-pyroxenite, Gosse Pile pyroxenite (websterite, orthopyroxenite, peridotite), felsic granulites, lateritic duricrust, calcrete duricrust, mafic source-derived alluvium and free quartz-bearing felsic source-derived alluvium.

3.4 VEGETATION, FIREBURN AND WEATHERING EFFECTS

Correlations between spectral data and lithological/mineralogical components are affected by older vegetation, vegetation regrowth and recent fireburns. Laboratory data for green (chlorophyll-rich) vegetation indicate absorbtion in the visible bands 1, 2 and 3, and high reflectance in band 4. Dry vegetation (cellulose-rich) reflects strongly in band 5. Quantitative estimates of the effects of green and dry vegetation and the separation of their effects from that of lithological surface types are considered in section 3.9.

Comparisons between reflectance values in spatially contiguous burnt and regrowth training areas overlying the same lithological units indicate higher reflectance of fireburn zones which, with some exceptions in band 1, show increases in reflectance in most bands (Table D). The regrowth of young green spinifex and other bushes in fireburn areas contributes to higher reflectance in band 4.

Table D - Reflectance differences (DN) between fireburn areas and old vegetated areas in gabbroic terrains and dune terrains. (+) increased reflectance in fireburn areas relative to old vegetation; (-) decreased reflectance in fireburn areas relative to old vegetation.

	band 1	band 2	band 3	band 4	band 5	band 7
gabbro	-1	+2	+7	+8	+6	+4
felsic granulite	+11	+10	+22	+23	+41	+25
dunes	-3	0	+10	+12	+11	+11

The marked increases in reflectance in fireburnt felsic terrains and to a lesser extent over dunes, as compared to small increases in mafic terrains, may be due to the high reflectance of quartz and clay of the exposed felsic rocks. In contrast, removal of vegetation over low-reflelcting mafic rocks results in smaller increases in reflectance. Since the contrast between fireburn and old growth areas increases from bands 1-2 to bands 3-5, images in the visible range manifest fireburns to a lesser extent than in the near-infrared range.

A well pronounced feature of single band images in the Tomkinson Ranges is the marked

reflectance in band 4 on some topographically elevated surfaces, including ridge tops and high level spurs. Field observations indicate more advanced weathering of some of these surfaces, i.e. at Mount Aloysius, parts of the Hinckley Range, Mount Davies, Ewarara ridge and elsewhere. The deep weathering results in clay-rich weathered rock and soil, expressed by high pc2(4/3:5/7) (section 3.8.2). The clay-rich soil supports denser spinifex vegetation. These surfaces are interpreted as relict weathering profiles subjacent to a pre-existing uplifted erosion surface (peneplain), and are correlated with remnant lateritic mesa throughout central Australia.

3.5 SINGLE BAND IMAGES

3.5.1. General comments

The broad spectral windows of Landsat-5-TM bands allows only first order approximations of the more detailed spectral patterns of each pixel (Fig. 2). Narrow absorption features may be identified by multispectral scanners such as MK-II (37 channels), Geris-band (69 channels) or Aviris (224 channels). Despite these limitations, useful empirical correlations of spectral profiles are made with lithologically relatively uniform training areas examined in the field. Modelling of end members proportions in each pixel according to the method of Bierwirth (1990) is discussed in section 3.9. Dark pixel-subtracted radiance data for training areas is presented in Table C and Fig. 3. Single band grey scale sub-scene images are displayed in Fig. 4. The characteristics of Landsat-5-TM bands 1,2,3,4,5,7 are examined vis-a-vis spectra of silica, clay, iron oxides, carbonates, green vegetation and dry vegetation.

3.5.2. The visible range (bands 1-3)

The absorption of visible wavelengths by iron oxides and by chlorophyll in green plants, result in a low reflectance of iron oxide-rich materials and green vegetated areas in the visible Landsat-5-Tm 1-3 band range. For green vegetation, reflectance in band 2 forms a visible peak relative to bands 1 and 3. In contrast, clay minerals reflect strongly in the visible bands, allowing a useful distinction between materials with different proportions of iron oxide and clay. Carbonate, silica and free quartz reflect more strongly than clay minerals, consequently, calcrete and silcrete duricrusts and free quartz-rich alluvial deposits and dunes display distinctly higher reflectance in the lower channels as compared to clay-bearing weathered bedrock surfaces. In contrast, iron oxide-rich materials, including laterites, weathering crusts of ferrogabbro and iron-rich pyroxenites, as well as derived detritus, show low reflectance in the visible range - due to iron oxide absorption in bands 1-2.

Characterization of the usually altered peridotitic rocks is complicated as weathering surfaces include carbonate (magnesite), hydrated magnesium silicates and iron oxides - resulting in a typical DN range similar to carbonate-clay mixtures in training areas. Spectral data for dark pixel-corrected images indicate that, in general, orthopyroxene-rich rocks, clinopyroxene-rich rocks, gabbroic rocks and anorthosite display an increasing reflectance in this order (Fig. 3). This is due to the increasing abundance of carbonate/clay weathering crusts in cpx and plagioclase bearing rocks. Thus, orthopyroxene-rich (calcium-poor) rocks may have low reflectance values in the visible range - a result of the abundance of iron oxide coatings on their iron-rich weathering surfaces. In contrast clinopyroxene-bearing Websterite shows a higher reflectance due to higher Ca and Al and thereby the greater abundance of clay and carbonate in their weathering surfaces. For these reasons mafic igneous rocks - including gabbro, gabbronorite, norite, anorthosite and

Fig. 2 LANDSAT THEMATIC MAPPER SPECTRA

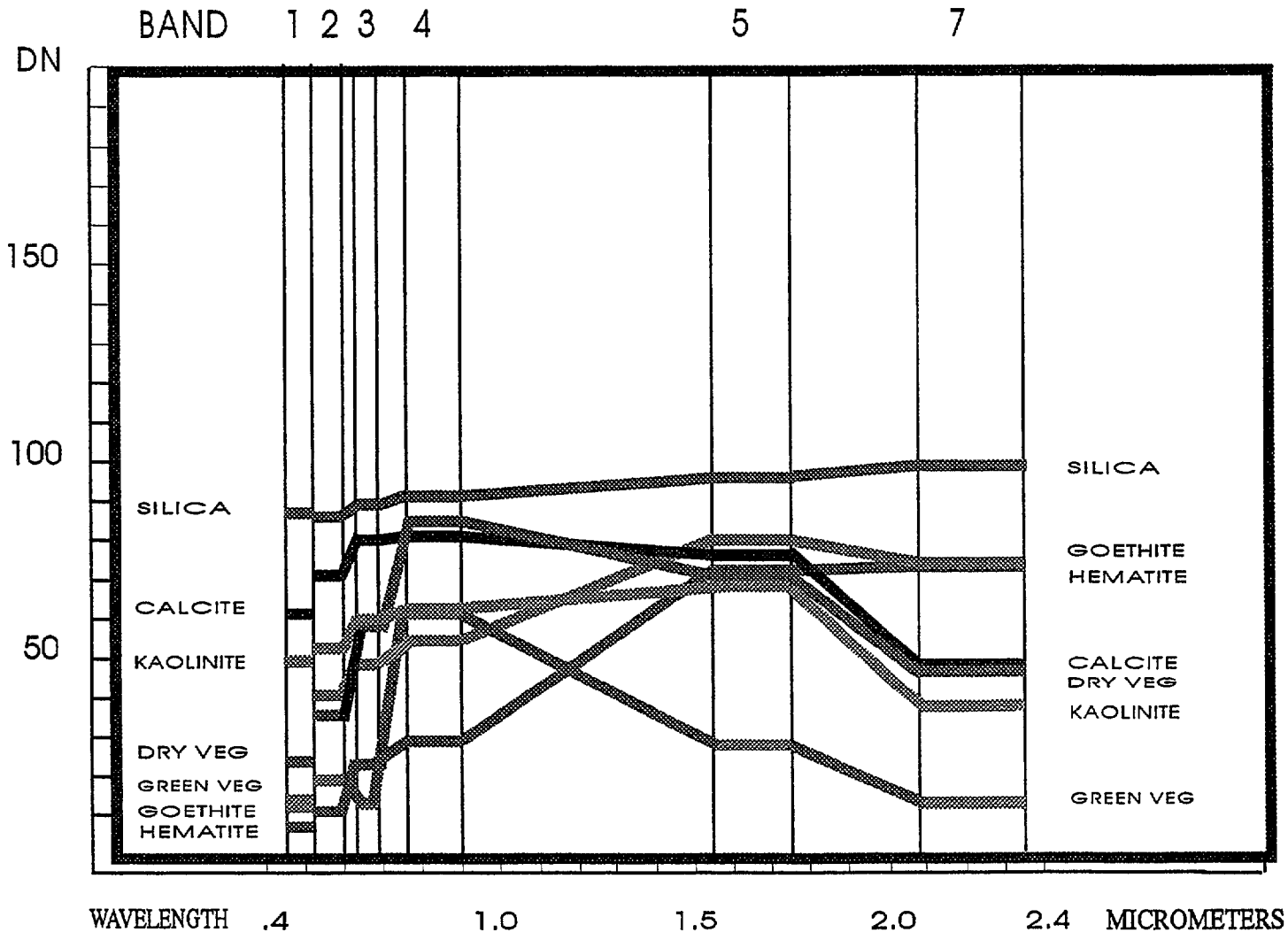

Fig. 2. Landsat-5-TM spectra of characteristic mineral and vegetation end members. (TMSPECLIB file, P.N. Bierwirth, pers. comm., 1993).

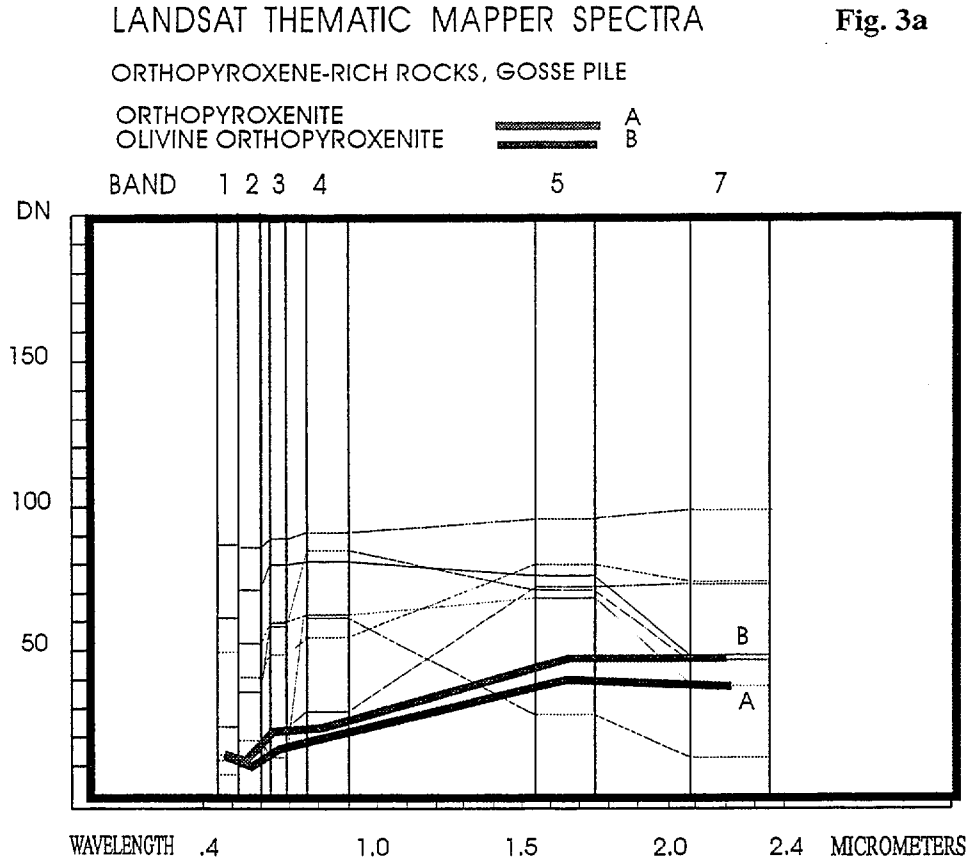

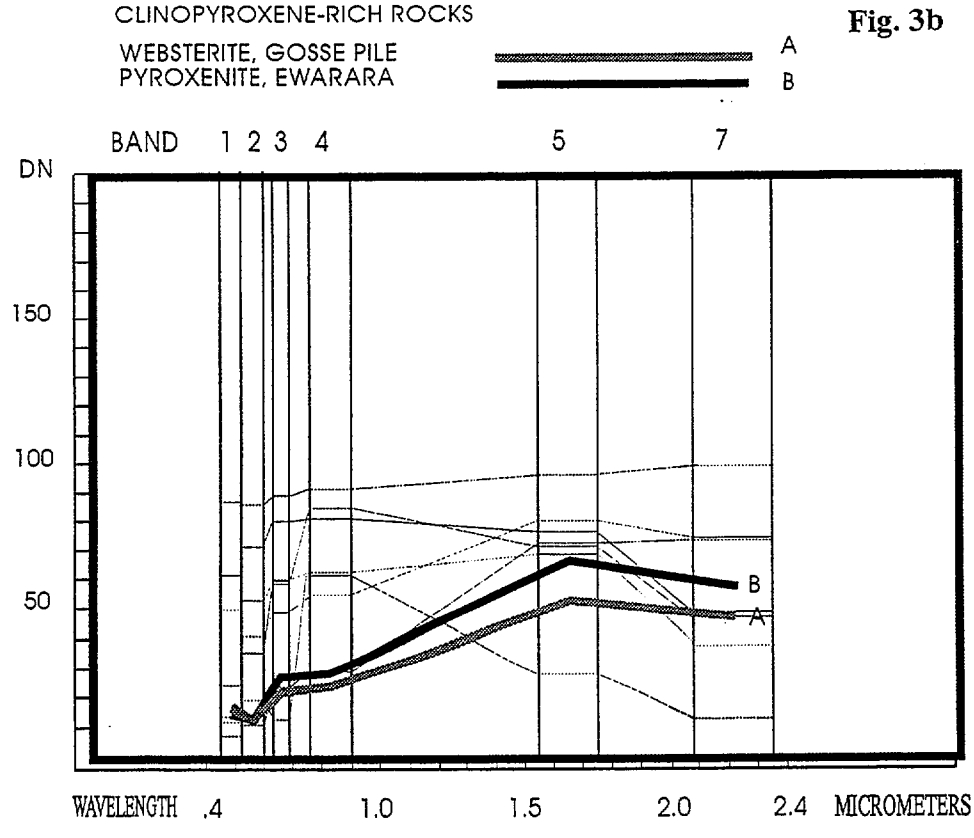

Fig. 3. Dark-pixel subtracted radiance data plots for mean radiance data of training areas in the Tomkinson Ranges. 3a - orthopyroxenite and olivine orthopyroxenite; 3b - websterite and pyroxenite; 3c - gabbro, norite and leucogabbro; 3d - gabbro and ferrogabbro; 3e - gabbro, mafic granulite and weathered gabbro; 3f - anorthosite; 3g - felsic granulite and porphyritic granite; 3h - weathered felsic granulite; 3i - laterite; 3j - calcrete; 3k - ssilcrete; 3l - alluvial pediments, mafic-derived and felsic-derived; 3m - silt and clay; 3n -dunes, fireburns and vegetated; 3o - fireburn and old vegetation over gabbro. Spectra of Landsat-5-TM end members (Fig. 2) are plotted for comparisons.

LANDSAT THEMATIC MAPPER SPECTRA

Fig. 3c

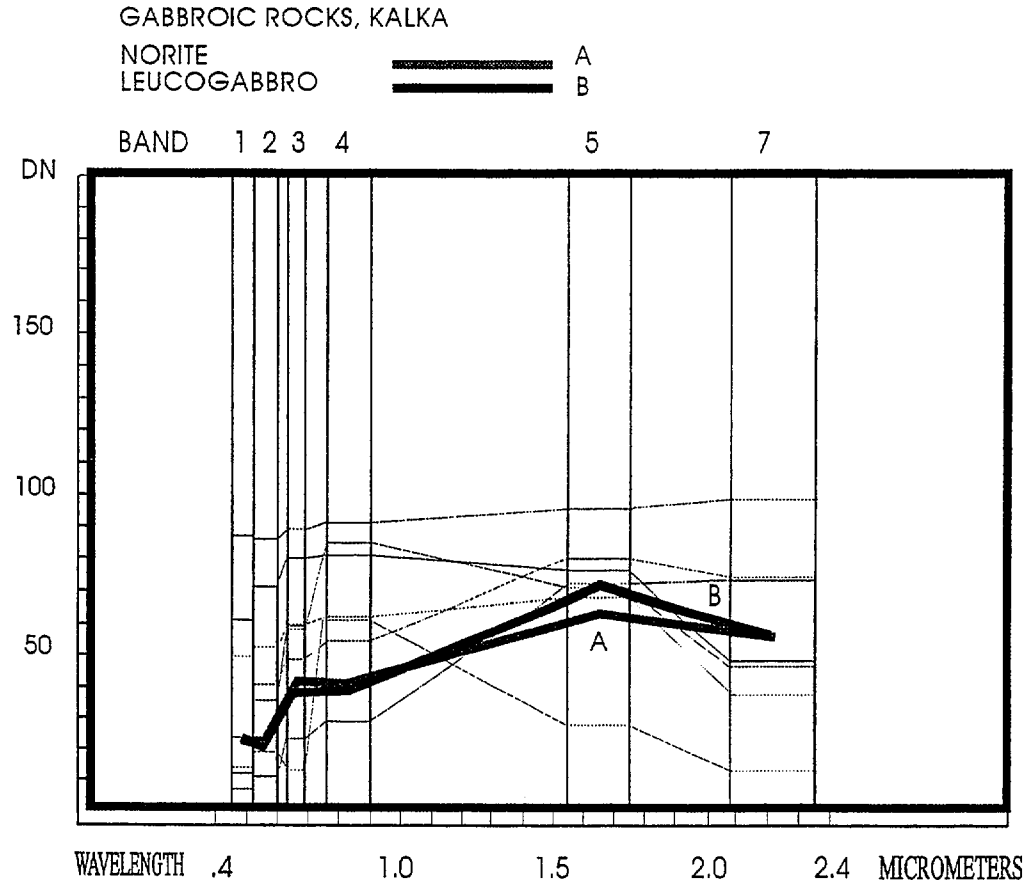

Fig. 3d

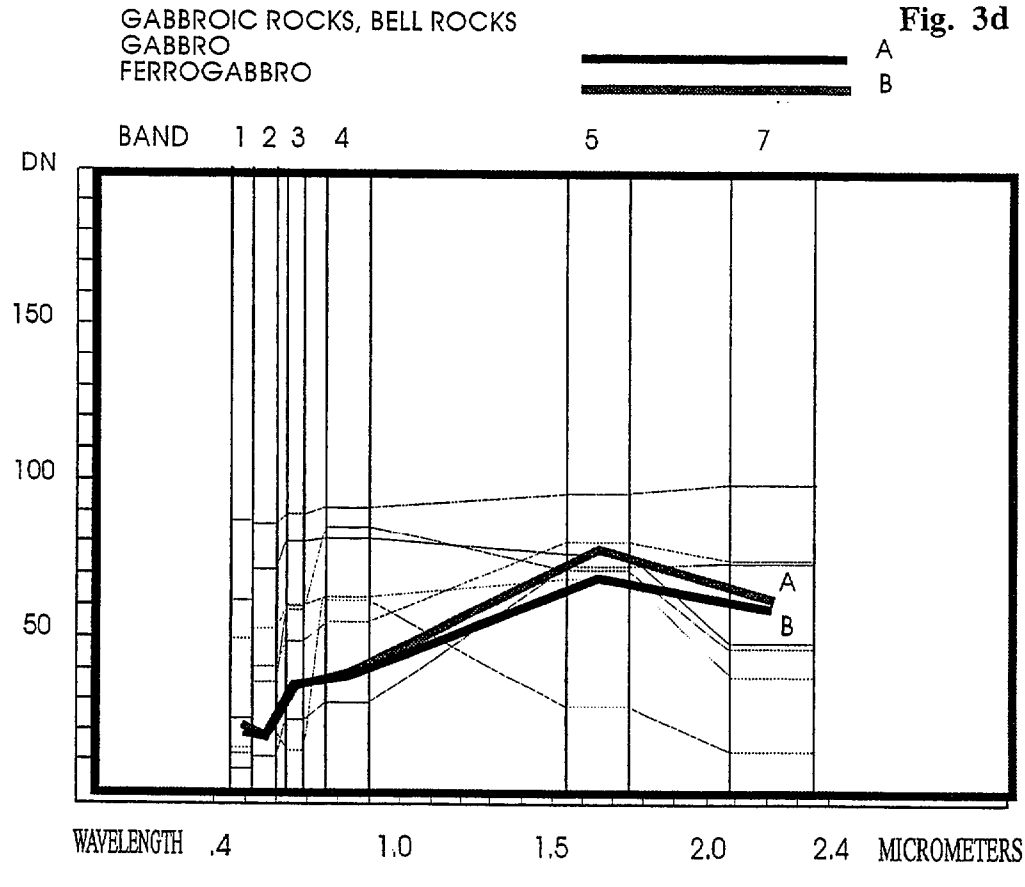

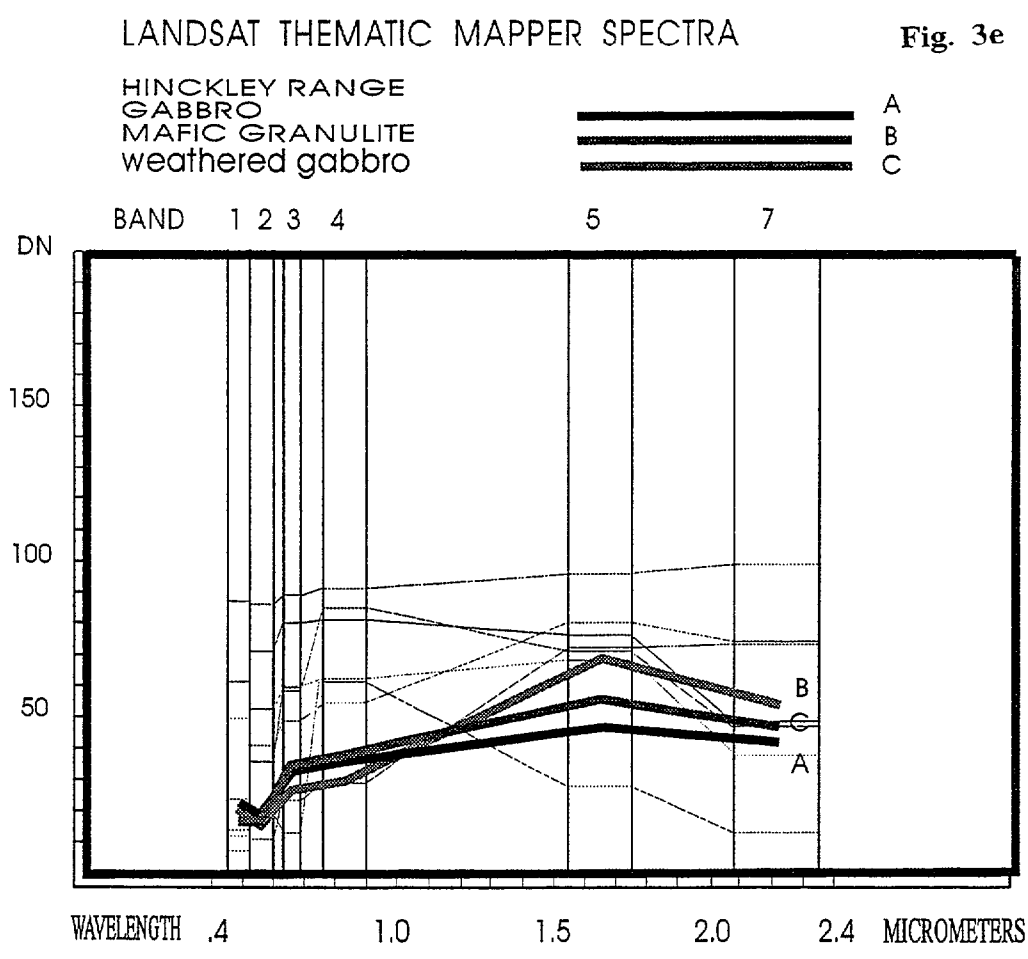

Fig. 3e

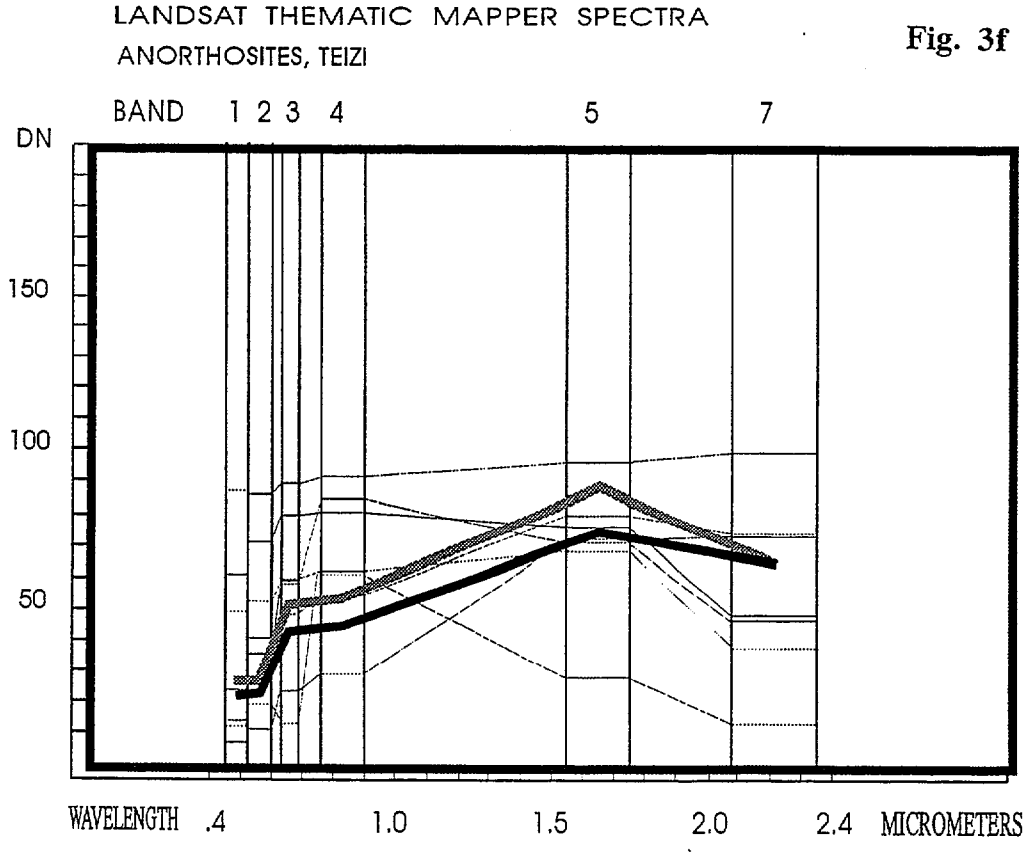

Fig. 3f

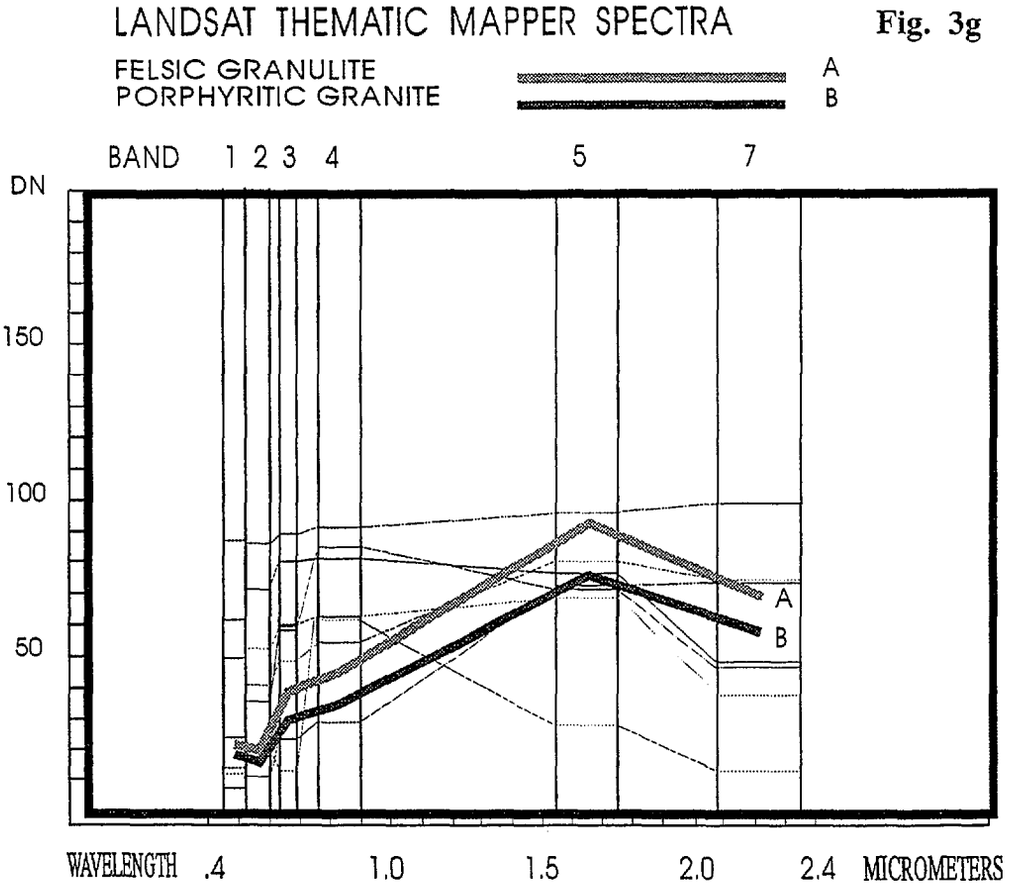

Fig. 3g

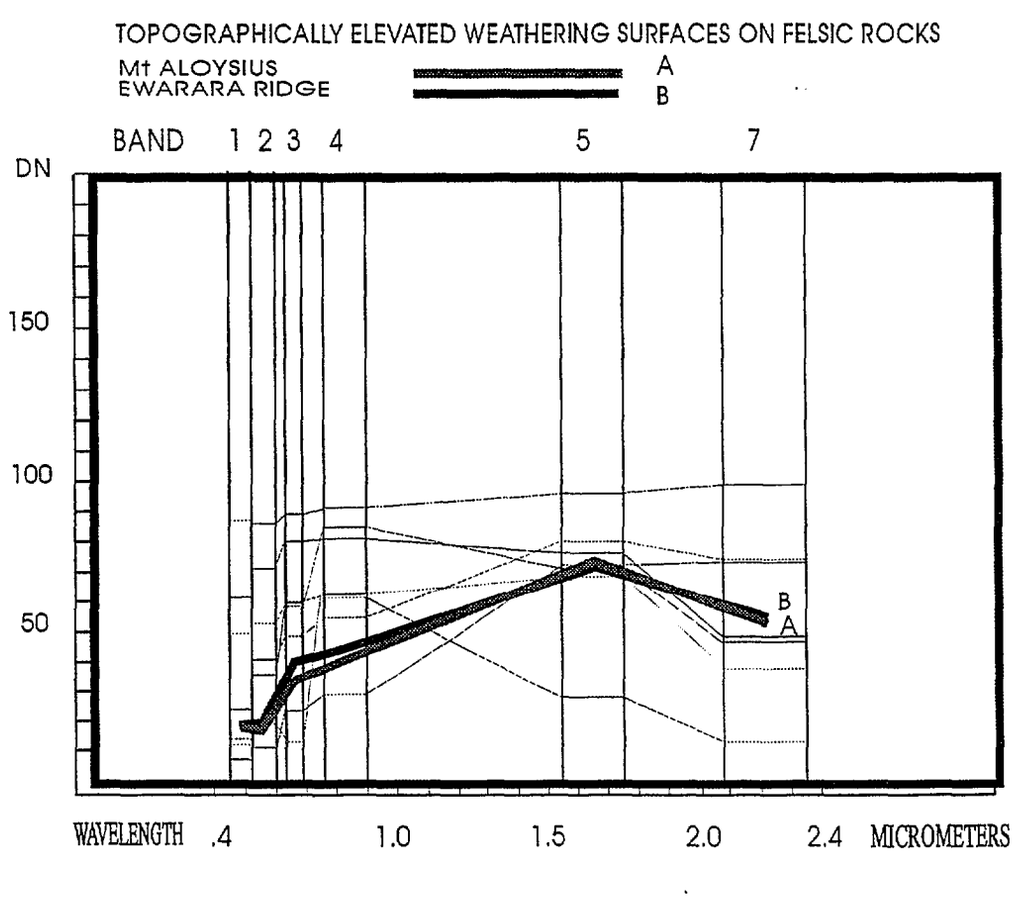

Fig. 3h

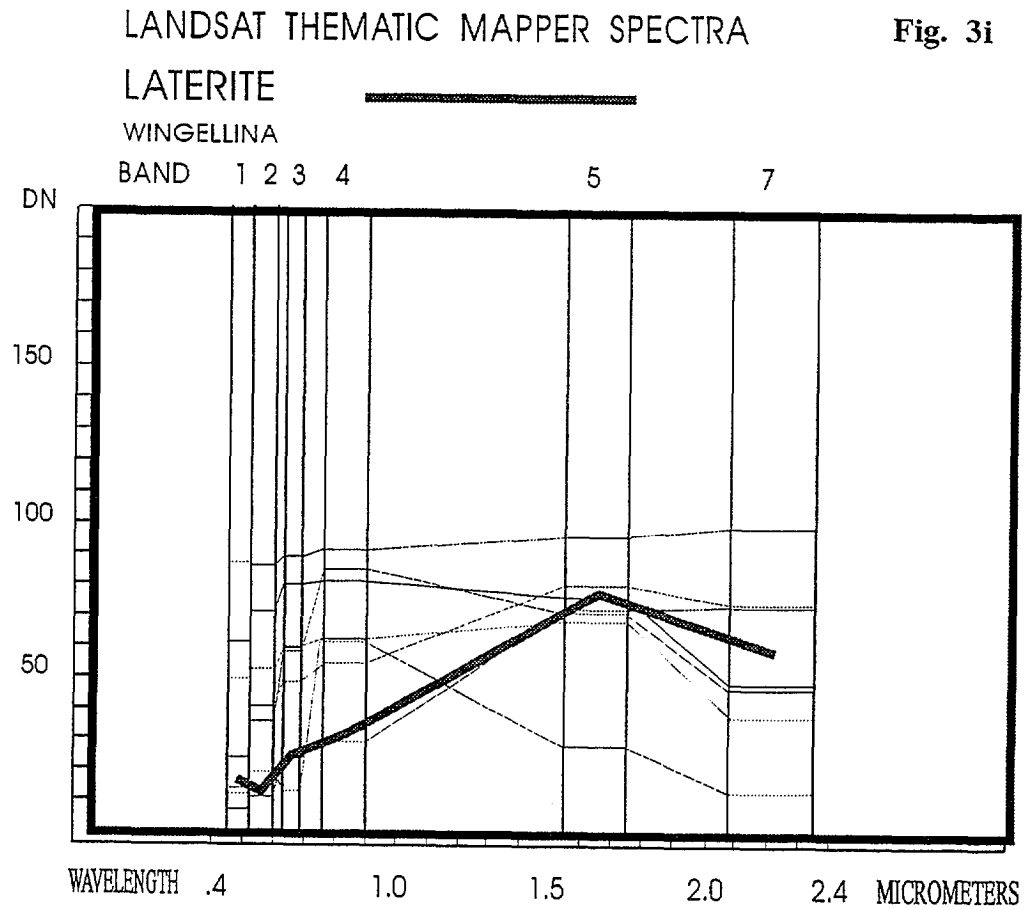

Fig. 3i

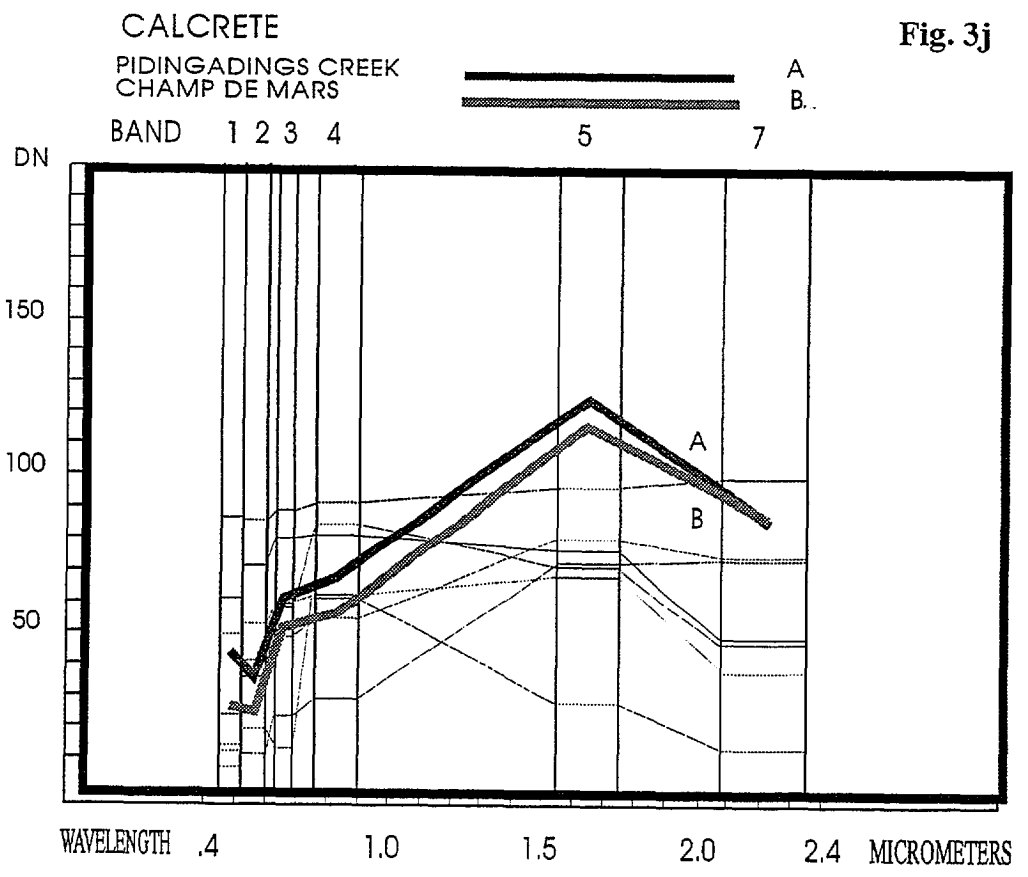

Fig. 3j

LANDSAT THEMATIC MAPPER SPECTRA

Fig. 3k

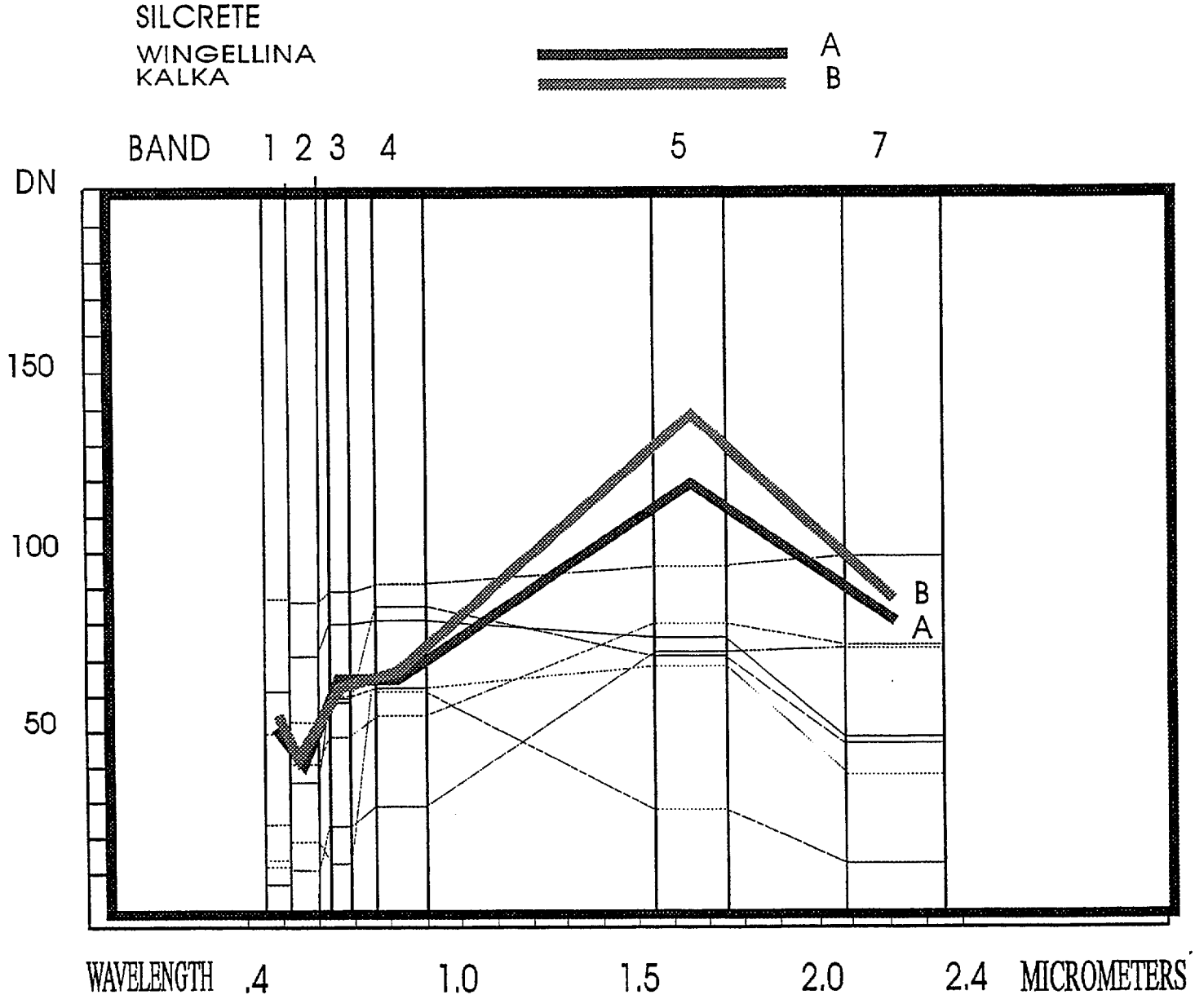

LANDSAT THEMATIC MAPPER SPECTRA

Fig. 3l

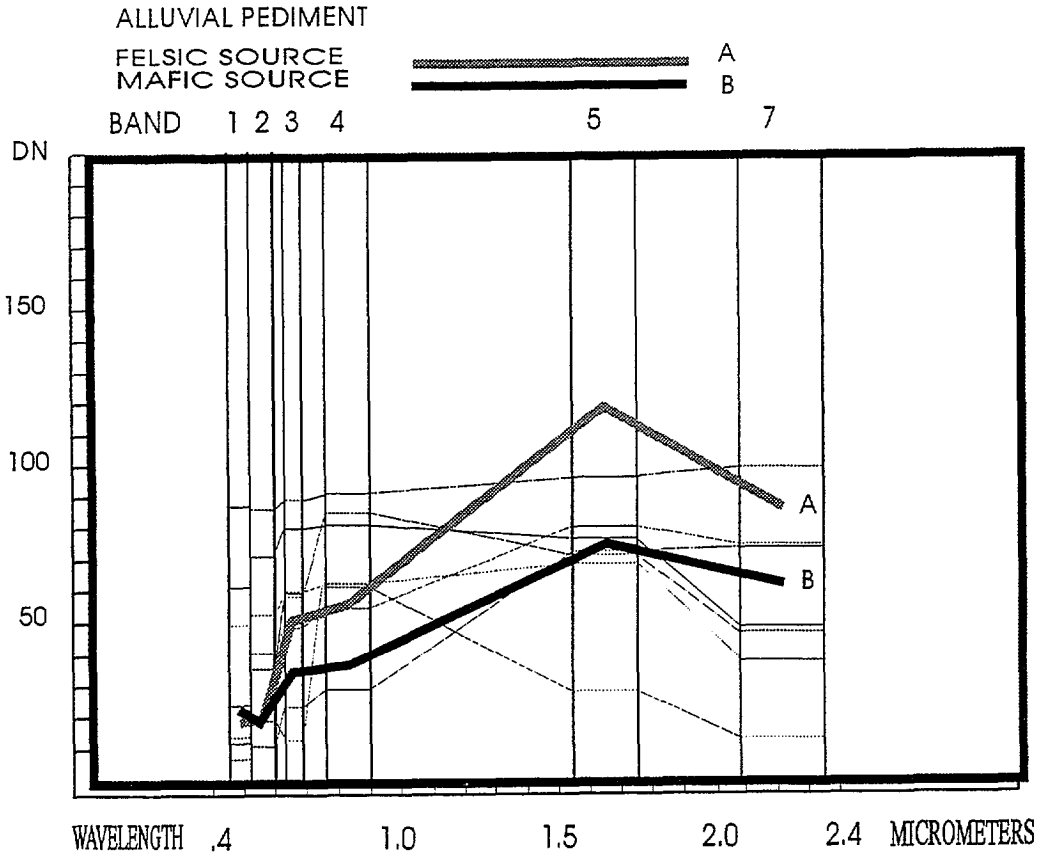

Fig. 3m

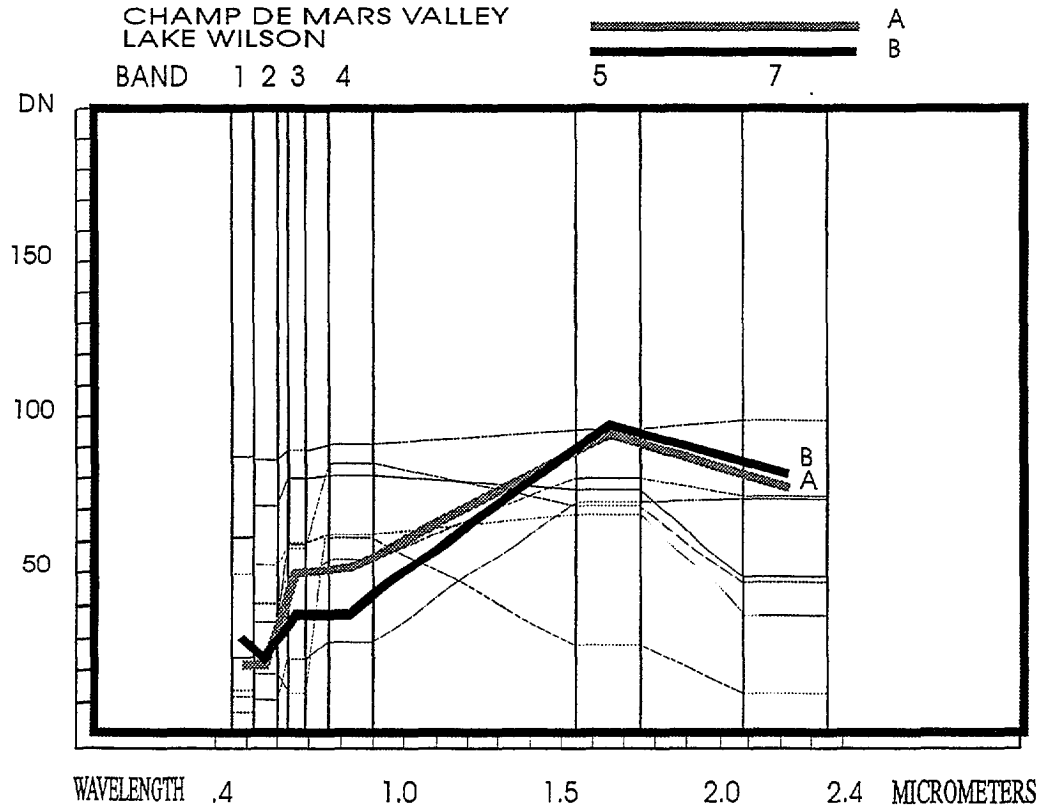

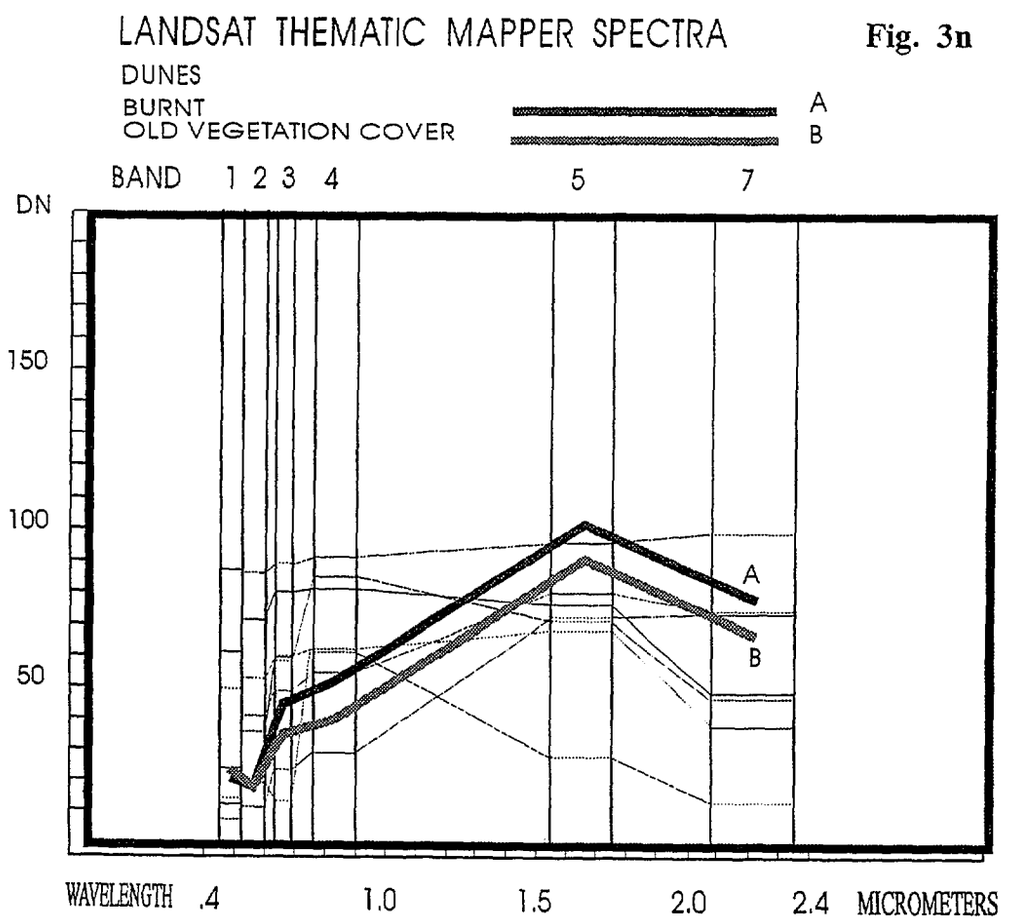

Fig. 3n

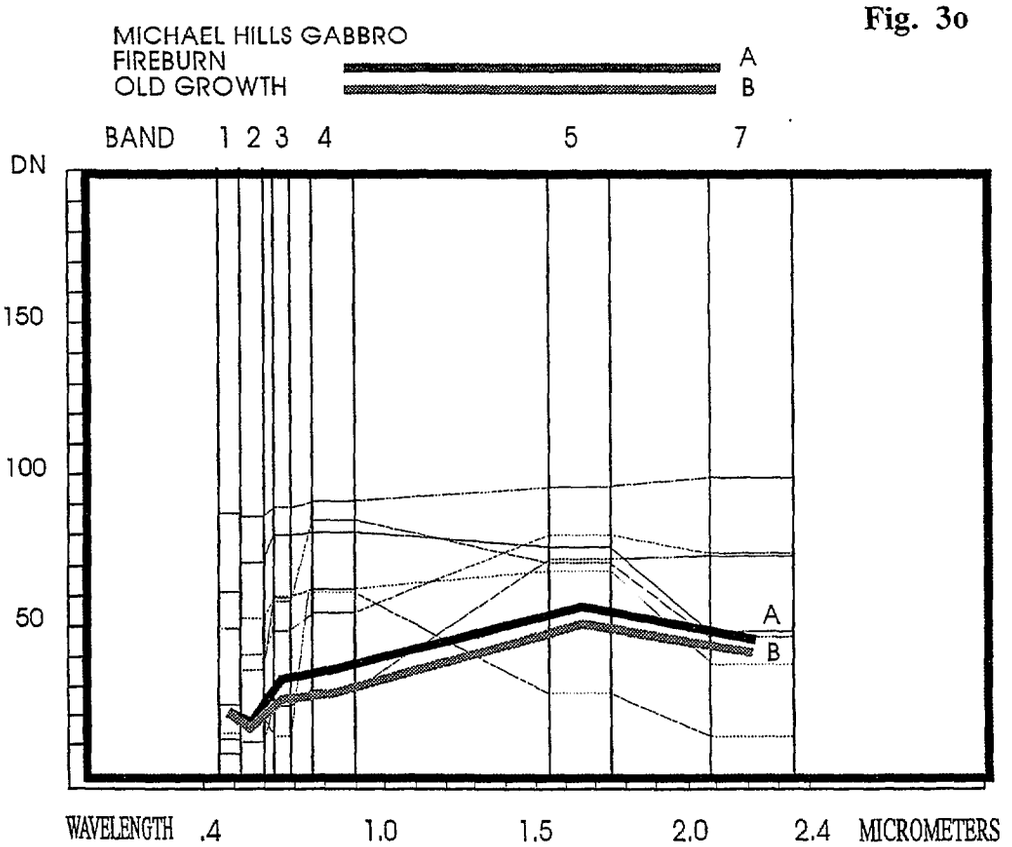

Fig. 3o

ferrogabbro - are characterized by generally higher reflectance than pyroxenites. For example, in dark pixel-corrected images the average values for norite are 24 (band 1), 22 (band 2) and 41 (band 3) - significantly higher than pyroxenites. Anorthosites display a high reflectance in the lower visible band due to high clay/carbonate content of their weathering surfaces, which display in bright cyan on RGB 7:4:1 images relative to the darker blue of gabbro. Felsic granulites and granitoids, which in the infrared range generally show higher reflectance than mafic materials, are not readily distinguished from the latter in the visible range (overlapping bands 4-5 of Landsat-5-MSS), which is thus unsuitable for lithological discriminations. Dry vegetation has a higher reflectance than green vegetation in bands 1-3, resulting in that old growth areas show higher reflectance than fireburn-affected areas, where young green regrowth occurs.

3.5.3 The Near Infrared Range (band 4)

The NIR band 4 is characterized by strong reflectance of green and dry vegetation and of carbonate and clay minerals. The iron oxides is subdued by comparison. Although the calibrated reflectances of end members (clay, hematite, carbonate, goethite) are relatively closely grouped in this band (Fig. 2), the Landsat-5-TM data show distinct differences between high-reflectance felsic granulites, lower-reflectance mafic rocks and lowermost-reflectance pyroxenites - allowing effective lithological separations of these rocks and their derived detritus. The high reflectance of the felsic materials is interpreted in terms of the combined effects of silica and clay. The differences between mafic rocks and orthopyroxene-rich ultramafics may be due to the role of carbonates in weathering crusts of the former. The reflectance of dry vegetation exceeds that of green vegetation, allowing their separation on images.

3.5.4 The Short Wave Infrared Range (bands 5 and 7)

Data for the short wave infrared bands 5 and 7 indicate similar high reflectance by silica and iron oxides. Accordingly iron oxide-rich materials (laterite and weathering surfaces of ferrogabbro and some pyroxenites) yield high reflectance in these bands, allowing their effective discrimination from mafic components of the layered intrusions (gabbro, gabbronorite, norite, anorthosite). The role of silica results in high reflectance of felsic granulites, granitoids and derived detritus relative to mafic rocks and their derivatives, compensating for the lower reflectivity of the clay component on weathering surfaces of these materials. In the SWIR band 5 the high reflectance of silica and to a lesser extent of carbonate result in high reflectance of silcrete and calcrete relative to laterites.

The combination of single bands, described above, allowing the effective comparisons of selected attributes of the multispectral data, is particularly useful where the more clearly identifiable correlations are displayed. A clear example is the combination of bands 7, 4 and 1 (RGB) - emphasising the role of iron oxide in band 7 (red), the role of vegetation in band 4 (green) and the role of clay and/or carbonate in band 1 (blue). Consequently, RGB 7:4:1 and 5:4:1 images display gabbroic rocks in blue/black (kaolinite and carbonate bearing weathering crusts); anorthosite in bright cyan (carbonate-weathered plagioclase in bands 1 and 4); felsic granulites and granites in purple (clay showing in blue in band 1 combined with contribution of iron oxide from mafic dykes showing in red in band 7); calcrete in light blue (band 1); iron oxide-rich pediments and laterite in red (band 7); vegetated areas in green, and alluvial planes in yellow (representing combined effects of silica, iron oxide [red] and vegetation [green]). A useful application for regional mapping is the composition of alluvial/pediment collars around or along unidentified bedrock outcrops.

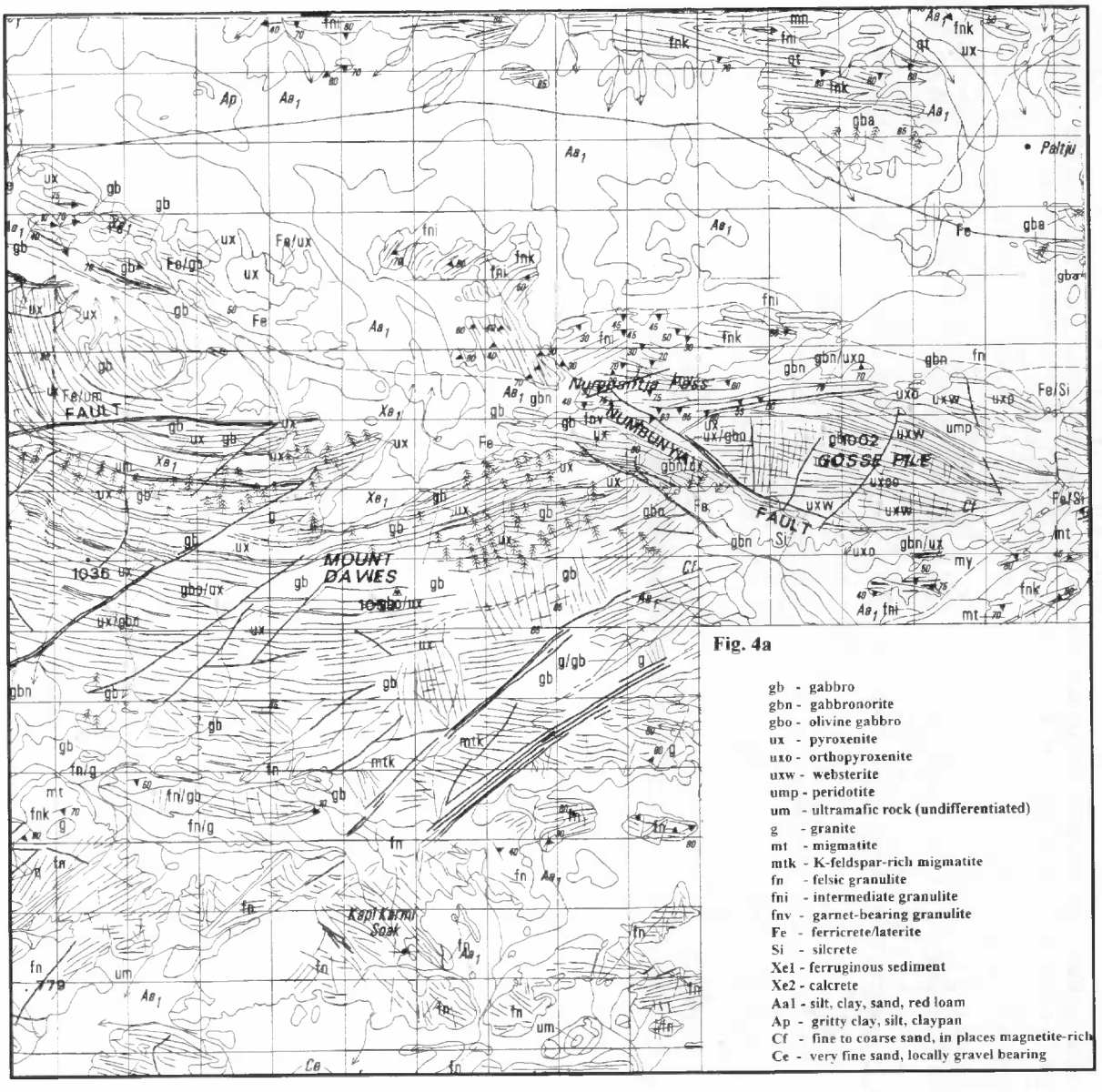

Fig. 4. Single band images of the Mount Davies sub-scene. 4a - geological sketch map of the Mount Davies area; 4b - Landsat-5-TM band 2 image (G - gabbro; P - pyroxenite - U - ultramafics; F - felsic granulite; L - laterite; Fe - ferruginous alluvium; 4c - Landsat-5-TM band 7 image (symbols as for 4b).

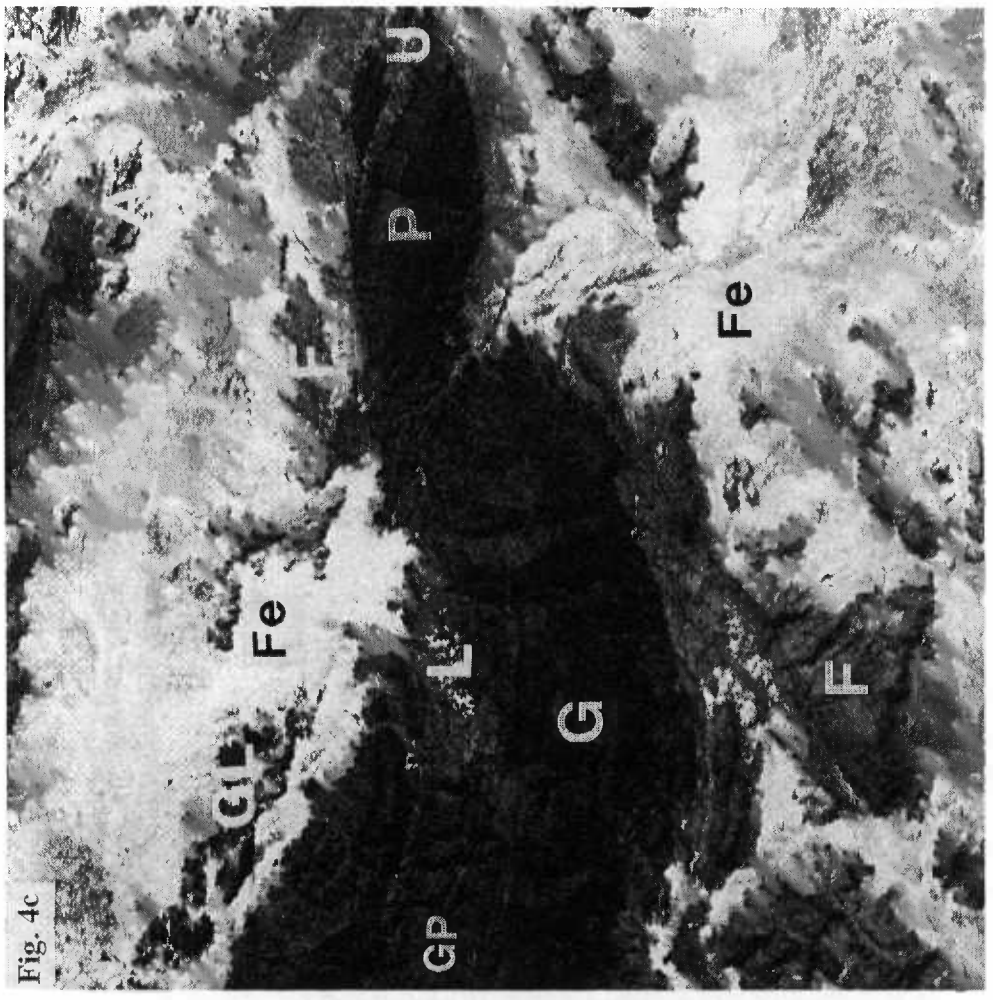

Fig. 4c

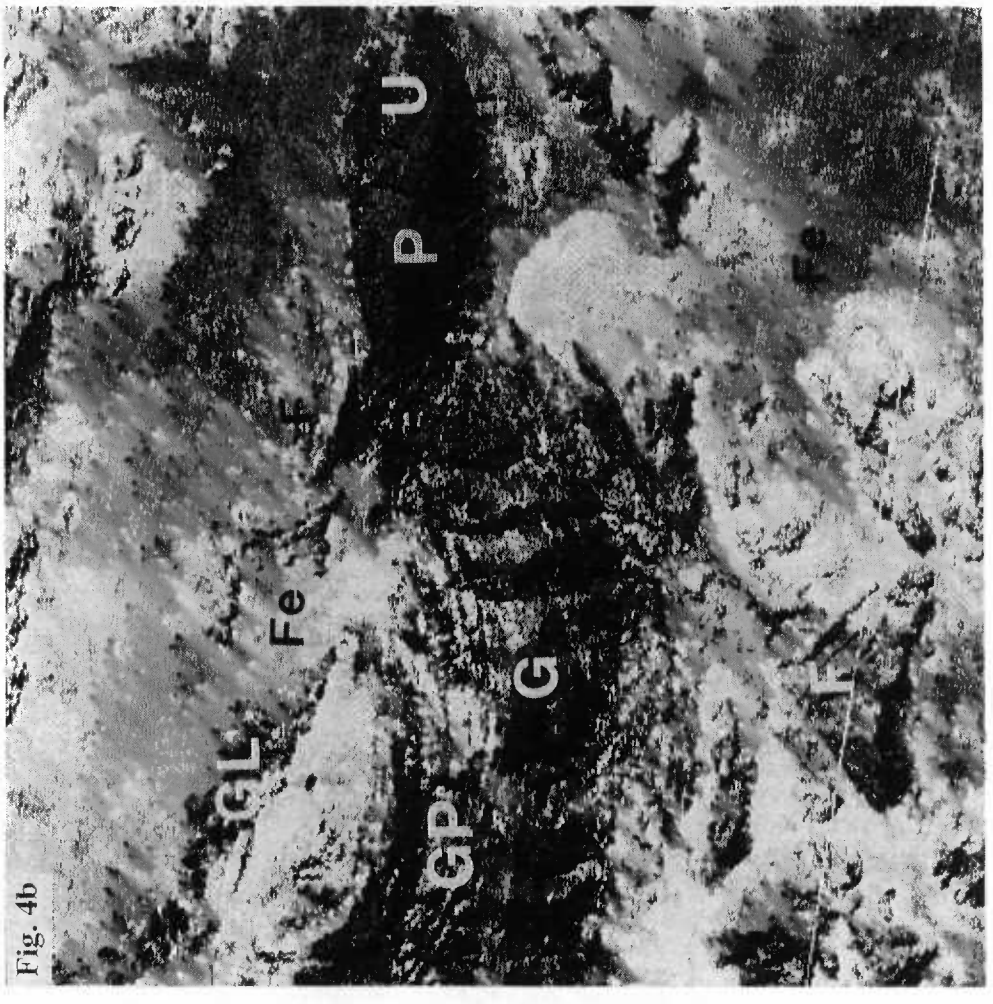

Fig. 4b

Since these outcrops are at times too small for their bedrock spectra to display clearly on the imagery, the spectral characteristics of broader zones of derived detritus yield an indication of the source composition. Thus, mafic bedrock are mostly fringed/surrounded by iron oxide-rich detritus (red collars on RGB 7:4:1), whereas felsic outcrops are associated with quartz and clay-rich detritus (light cyan collars on RGB 7:4:1).

The relationships between estimated reflectance spectra of different training areas, applying the BERAD2 program of Bierwirth (pers. comm., 1993), are consistent with those between dark pixel-corrected spectra of different training areas, since the corrections affect all pixels. The estimated reflectance spectral patterns vary from those of dark pixel-corrected data, resulting in an overall steepening of the reflectance spectrum from short to long wavelengths relative to the dark pixel-subtrated radiance spectrum.

3.6 LOG RESIDUAL IMAGES

Log residual (LR) values represent the radiance values for any particular band in any single pixel (R_{bp}), normallized by divison by the bands mean within the pixel (R_{bmp}), further divided by the multispectral mean radiance of the entire image or subimage (R_{mmi}):

LR value = $R_{bp} / R_{bmp} / R_{mmi}$

This normalization cancels out multiplicative effects such as atmospheric absorption, solar illumination and sensor gains. The log residual program separates a shadow component, which can be subsequently recombined with LR bands or with dark pixel-corrected radiance bands in any particular image to enhance topography and structure. Log residual images help to identify the significance of any single band DN value relative to the pixel bands mean and the image pixels mean, and thus expression of within-pixel and between-pixels relationships. Examinations of log residual images of the Tomkinson Ranges shows in many instances superior discriminations relative to single band and band ratio images, allowing meaningful discriminations and correlations of surface types. The values of log residual-normalized spectra for individual training areas (Fig. 5) and single band log residual images for the Mount Davies sub-scene (Fig. 6) allow the following observations:

3.6.1. Single log residual (LR) band images

- LR band 1 (Fig. 6a) - The generally higher DN values of mafic materials as compared to felsic materials in LR band 1 allow a ready discrimination between the mafic-ultramafic intrusions of the Gidles Complex and felsic granulites. The reflectance of laterites is also high in LR band 1. The contrast is best represented by alluvial cover, where felsic source-derived alluvium is significantly darker than mafic source-derived debris. Fireburn areas in LR band 1 show lower DN values than old vegetation, and appear as dark patches on mafic rock surfaces.

- LR band 2 (Fig. 6b) - Mafic materials display higher DN values than felsic materials, by analogy with LR band 1 reflectance. The marked absorption by iron oxides in this LR band results in the dark display of laterite of the Mount Davies and Greenwood fault jasper zones and of oxidized colluvium, particularly in gullies which drain mafic sources.

- LR band 3 (Fig. 6c) - The contrast between the high DN values of mafic rocks and the low value of iron oxide is accentuated in this LR band, resulting in good discrimination between gabbro, pyroxenite and laterite. Thus, pyroxenite bands, lateritic zones and oxidized colluvium in the Mount Davies intrusions are well pronounced. The DN values

of felsic materials remain significantly lower than those of mafic materials. This LR band shows a reversal in the values of fireburn and old growth areas, the former being displayed by high DN on mafic rock surfaces, i.e. the eastern and northern parts of Mount Davies.

- LR band 4 (Fig. 6d) - The contrast between the DN values of mafic and felsic rocks almost disappears, or is slightly reversed in this LR band. Iron oxide-rich laterites and weathering crusts are low. There is little distinction between alluvial materials of different sources. Fireburn effects are maximized, with a distinctly high value of fireburn areas as compared to unburnt old growth areas over mafic terrains.

- LR band 5 (Fig. 6e) - This LR band displays high DN value of felsic rocks as compared to mafic rocks and a very high value of laterite. Clinopyroxene-rich rocks (websterite) have a higher DN value than orthopyroxenites at Gosse Pile. Oxidized colluvium helps to outline gullies and strike-controlled depressions underlain by pyroxenite in mafic terrains (Mount Davies gabbro/pyroxenite).

- LR band 6 (Fig. 6f) - this LR band - derived from the original LR band 7 of the Landsat-5-TM image - shows little distinction between mafic and felsic materials but marked high value of iron oxide-rich materials, including orthopyroxenite, laterite and oxidized mafic colluvium.

- LR band 7 (Fig. 6g) - representing the shade or albedo component of the image, is very useful in expressing structure and in combination with other LR bands in RGB images where combination of surface types with relief is desired.

3.6.2 Log residual RGB images

Orthopyroxene-dominated and clinopyroxene-dominated rock types display similar log residual patterns, and are similar to that of ferrogabbro (Fig. 5). LR band 7 DN values are consistently high, and LR bands 4 and 3 DN values consistently low, as compared to norite and gabbro. These variations are attributed to the high iron oxide levels (i.e. higher value in LR band 7) and lower plagioclase and thereby lower clay/carbonate weathering products (lower value in LR bands 3 and 4) on weathering crusts of pyroxenites and ferrogabbro. These variations are clearly manifested on RGB log residual 7:4:1 images through the orange red color of pyroxenites and ferrogabbro, for example the Gosse Pile, north Kalka, Ewarara and Latitude Hill pyroxenites and the Bell Rock ferrogabbro LR band. The Bell Rock ferrogabbro pattern displays higher iron oxide and lower clay/carbonate signature as compared to the dominant gabbroic component of this intrusion. The signatures of anorthosites and leucogabbro are broadly similar to those of gabbro, or show higher values in LR bands 3 and 4 (higher clay/carbonate signatures). In the latter case the higher reflectance in the green channel results in a light azur greenish blue color of anorthosites relative to the deeper blue of gabbro on RGB log residual 7:4:1 images. A similar effect is imparted by weathering profiles of gabbro at topographically elevated positions, reflecting the combined effects of clay and vegetation in LR bands 4 and 5. Anorthosites can be readily distinguished from felsic granulites thanks to the stronger value of the former in the lower visible LR bands, for example bright cyan on log residual 7:4:1 images. Mafic granulites of the western Hinckley Range, while showing a lower DN values in LR band 7 relative to pyroxenites and ferrogabbro, are similar to the latter in terms of their low signatures in LR bands 3 and 4. This is attributed to the lesser development of clay/carbonate weathering crusts on the mafic granulites, discussed above. However, the

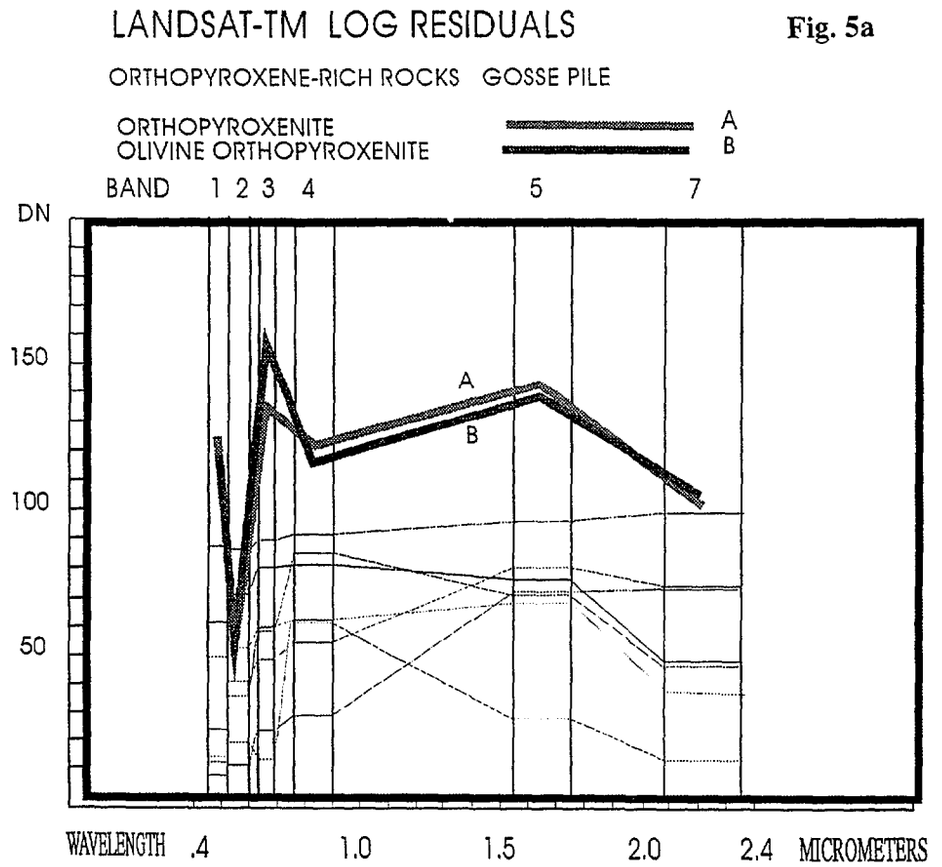

Fig. 5a

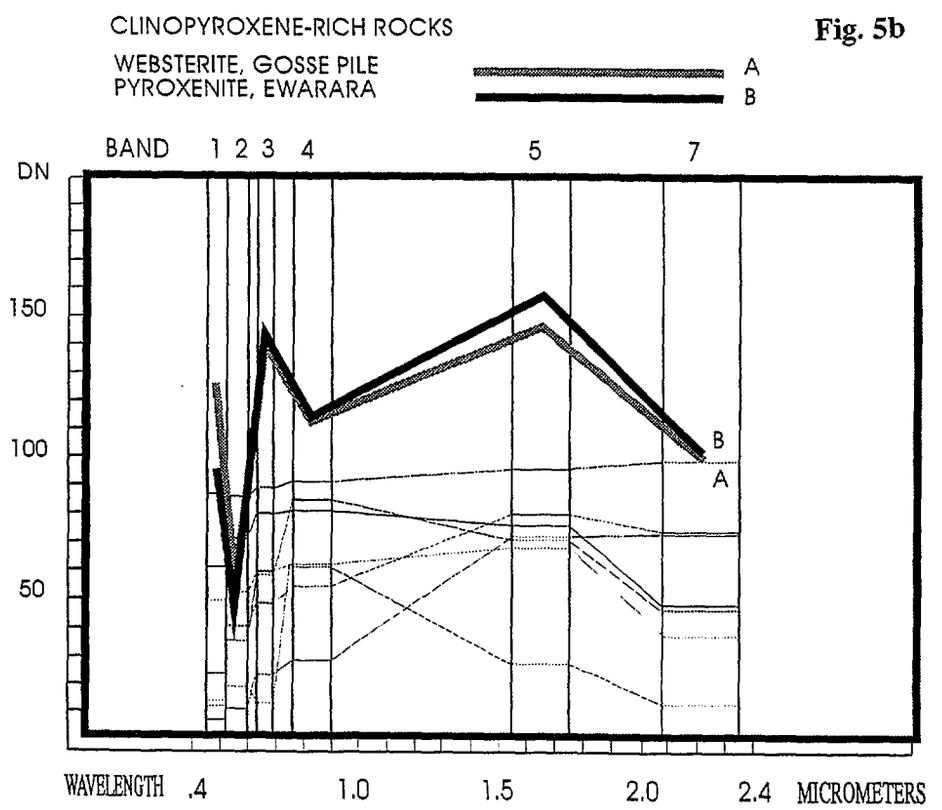

Fig. 5b

Fig. 5. Log residual plots of Landsat-5-TM mean radiance data of training areas in the Tomkinson Ranges (see section 3.6 for explanation). Surface types as in Fig. 3. Spectra of Landsat-5-TM end members (Fig. 2) are plotted for comparisons.

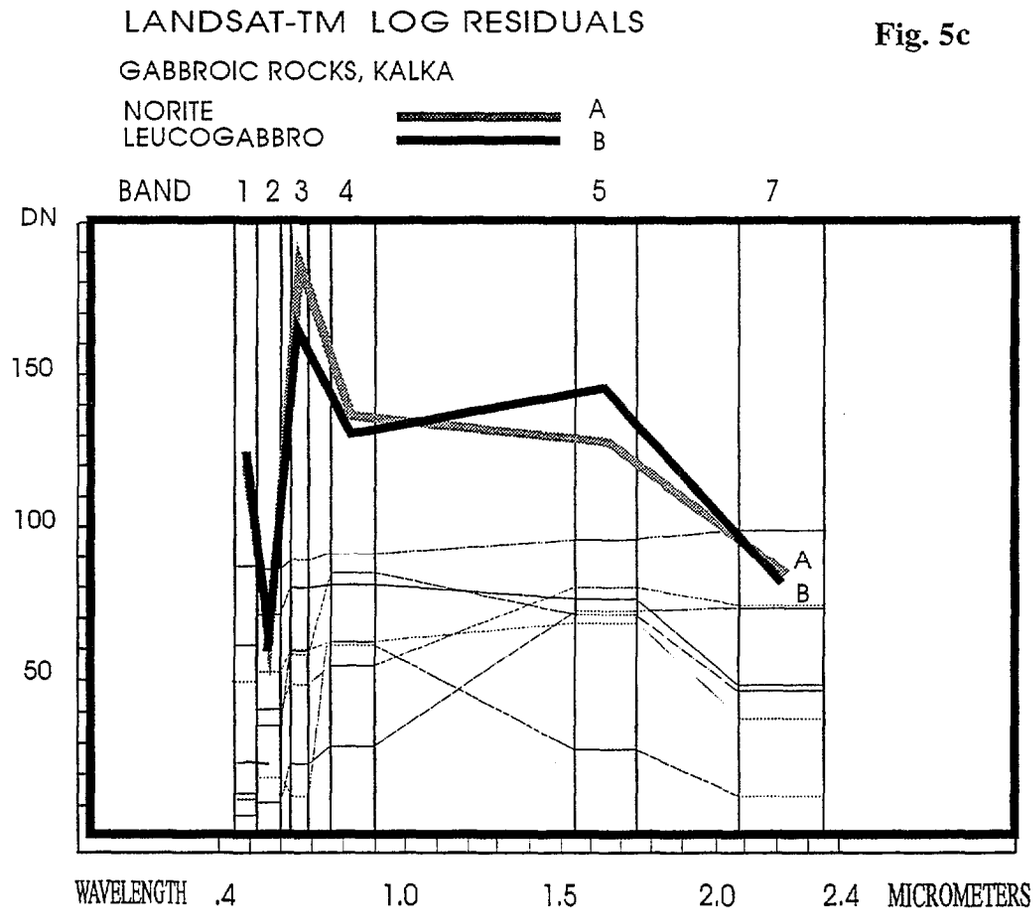

Fig. 5c

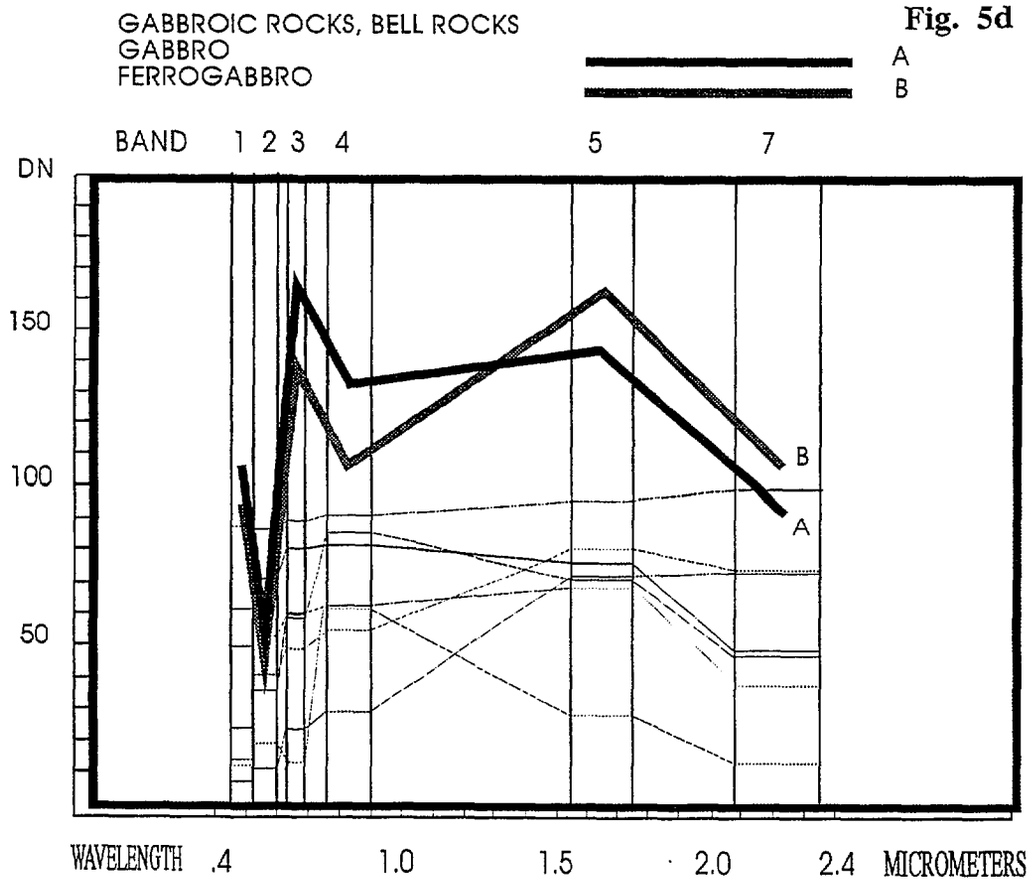

Fig. 5d

Fig. 5e

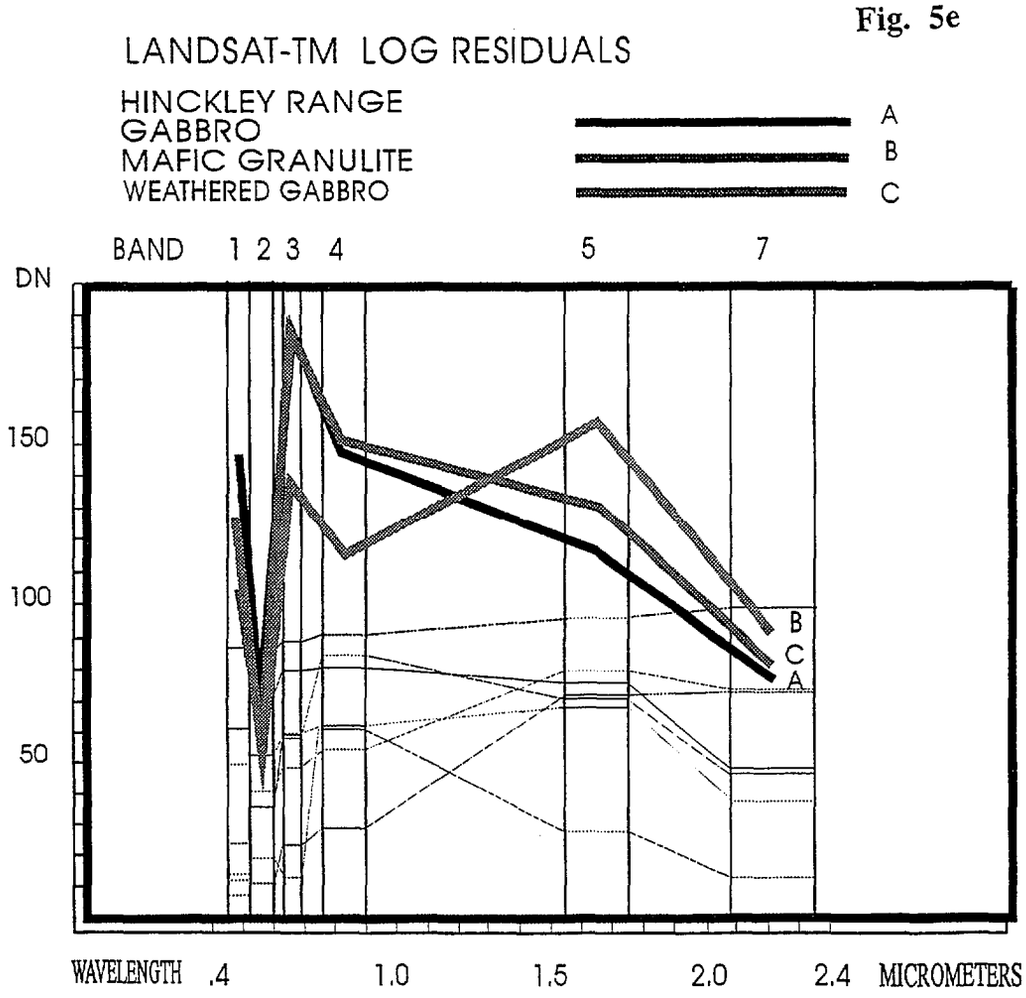

Fig. 5f

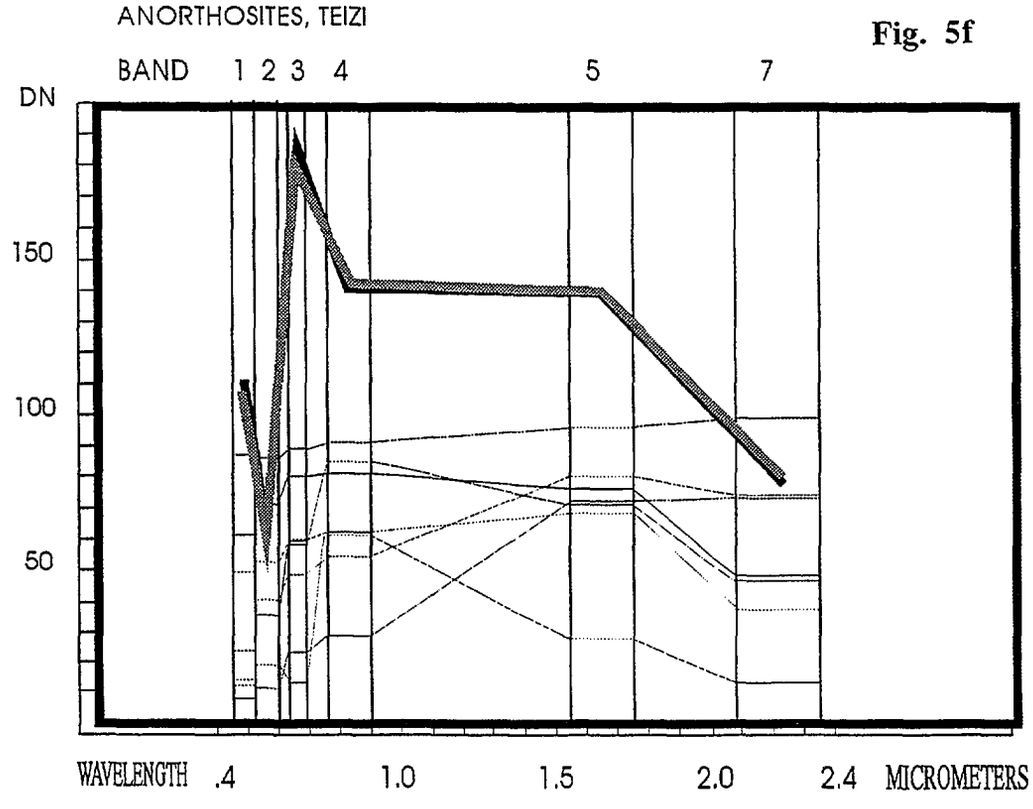

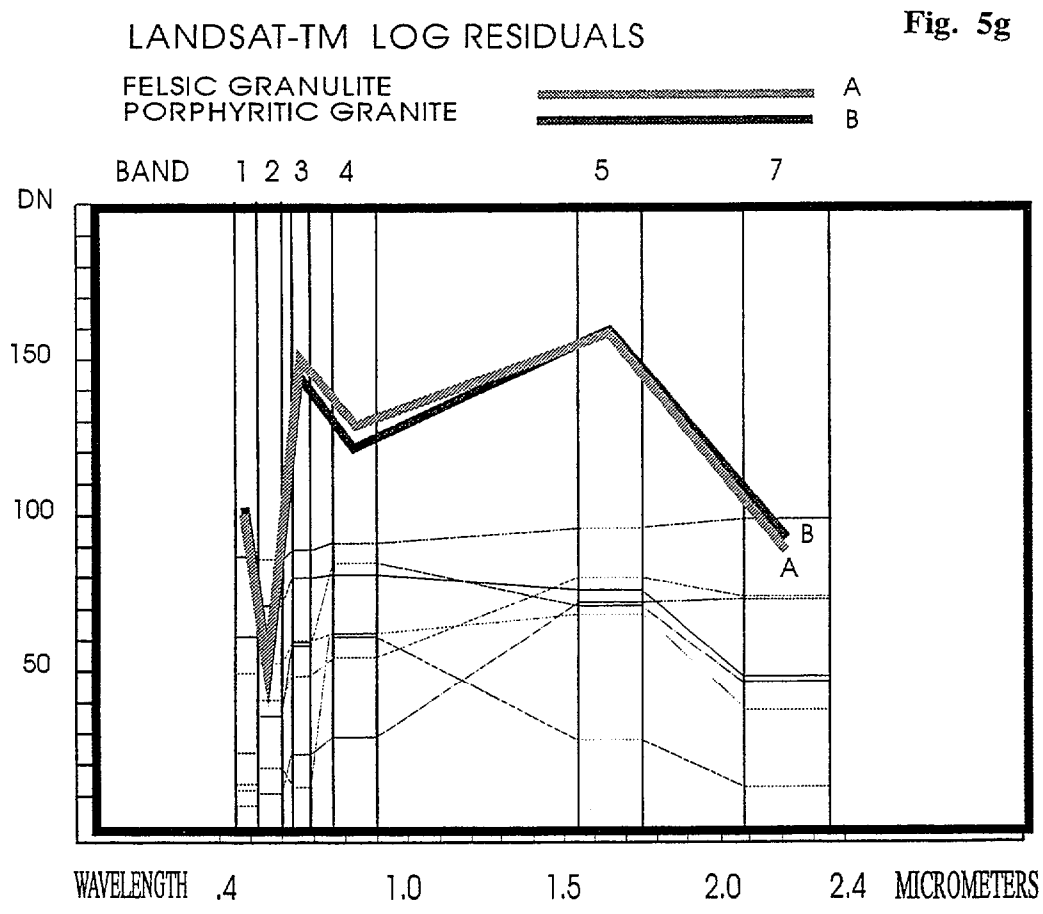

Fig. 5g

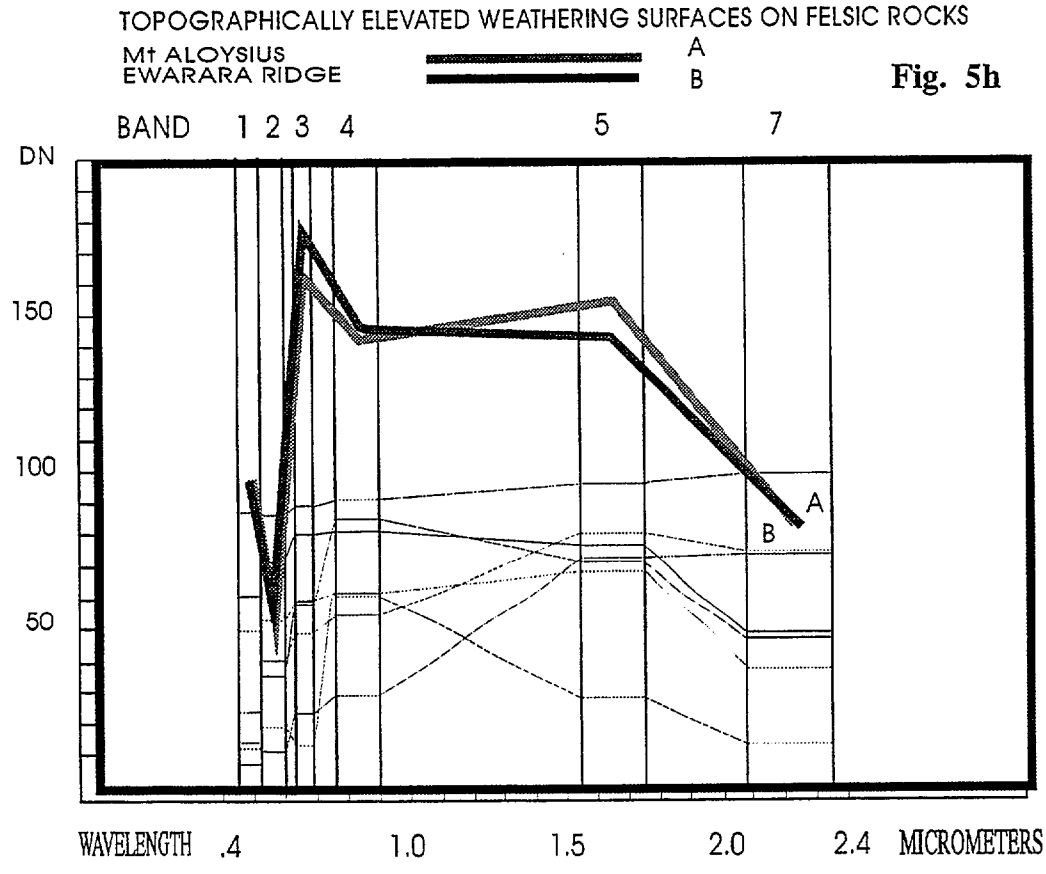

Fig. 5h

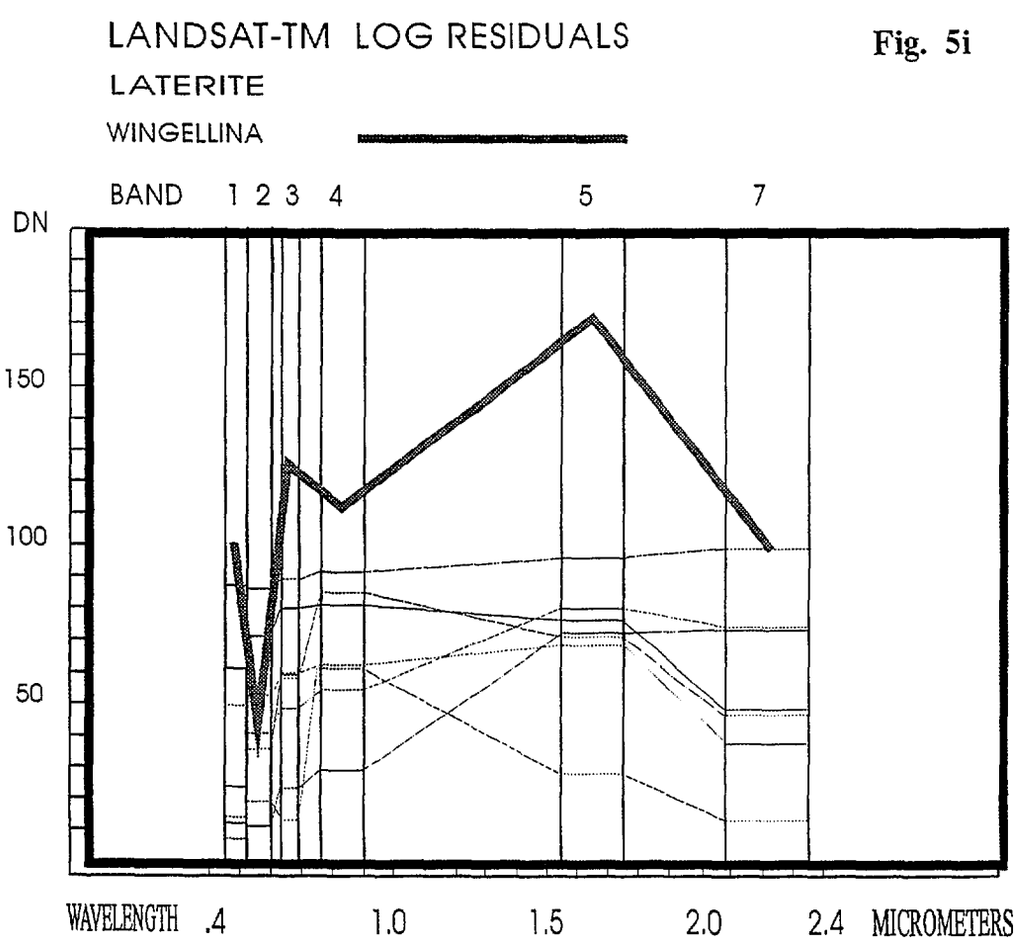

Fig. 5i

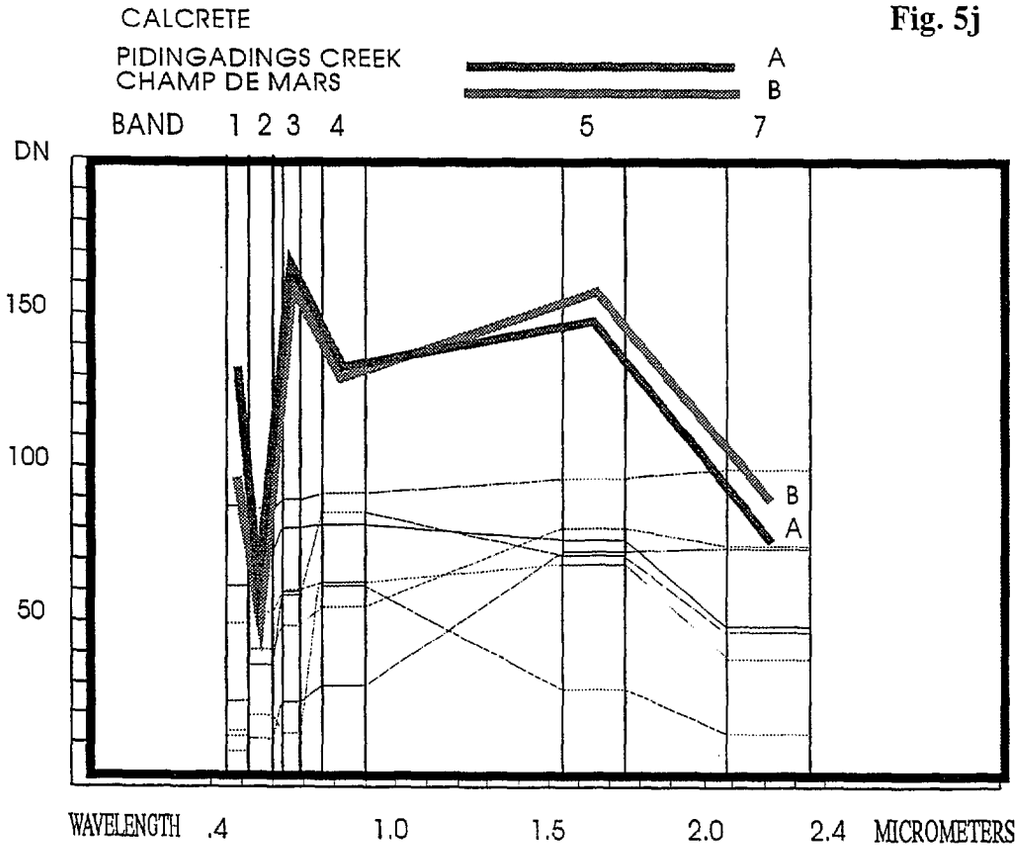

Fig. 5j

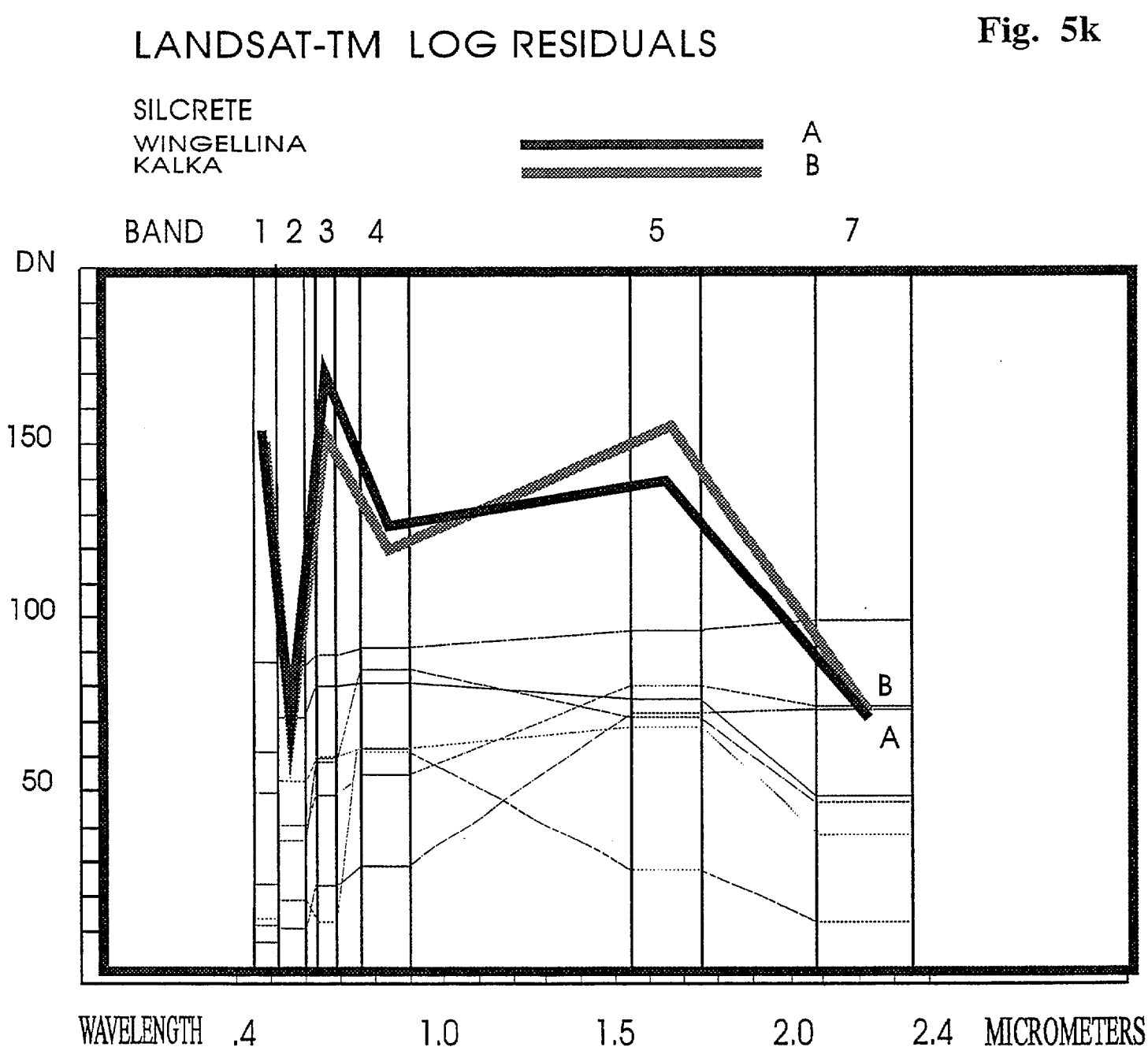

Fig. 5k

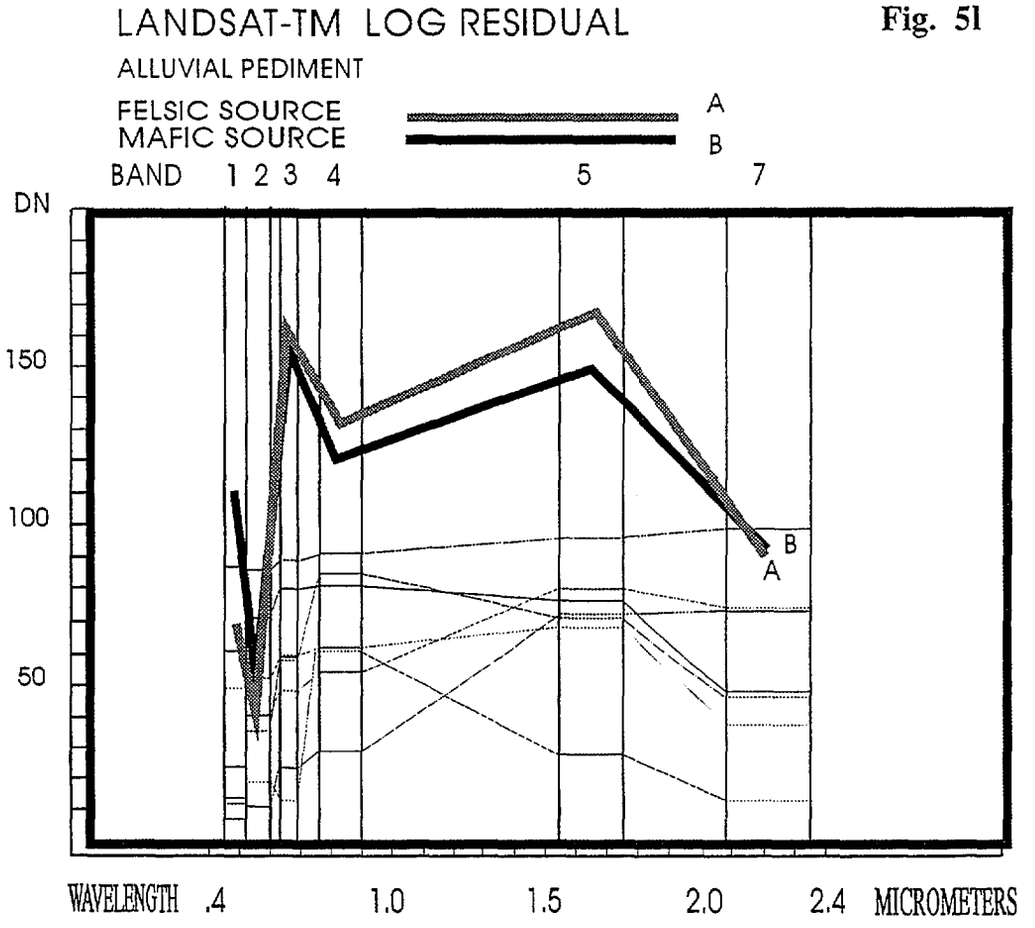

Fig. 5l

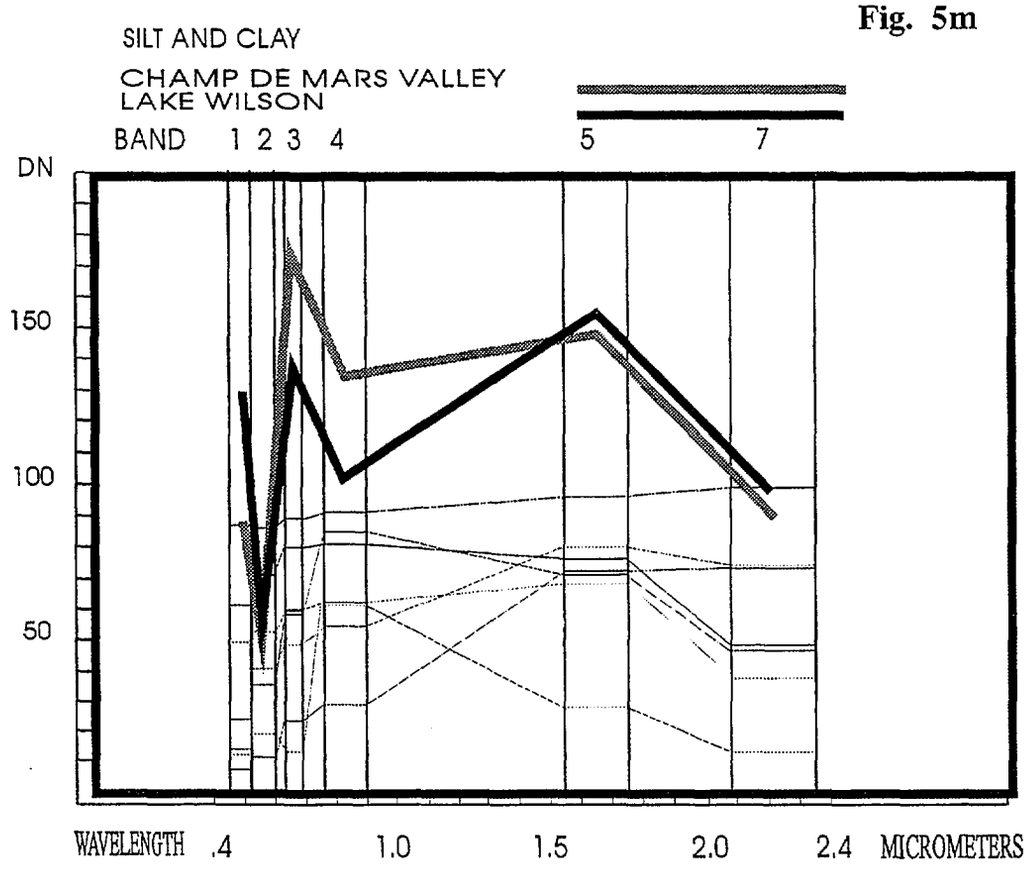

Fig. 5m

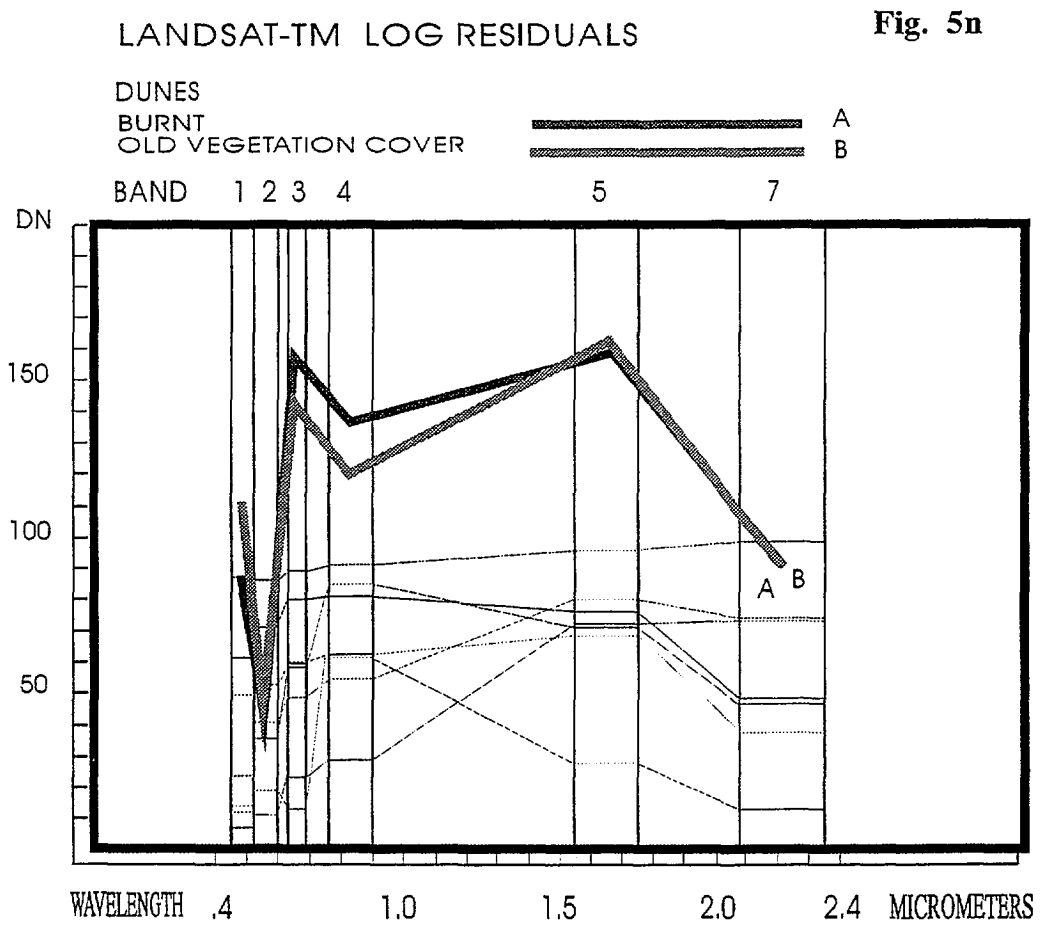

Fig. 5n

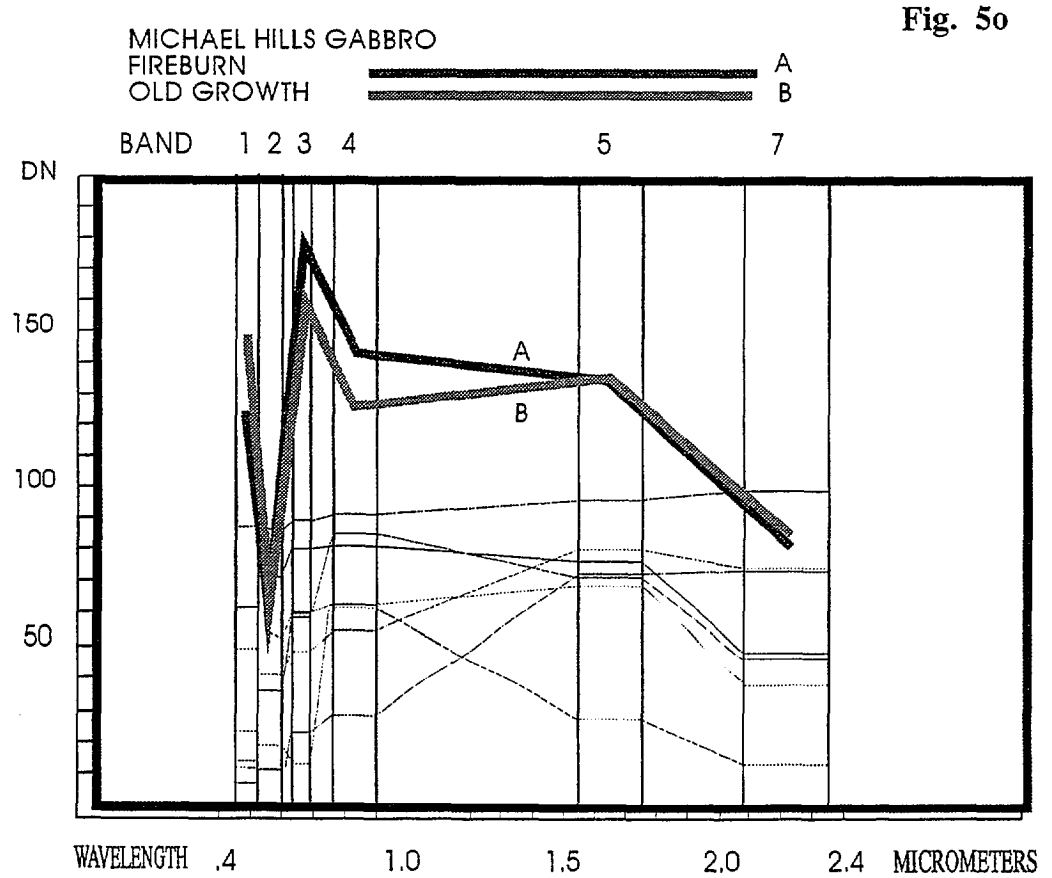

Fig. 5o

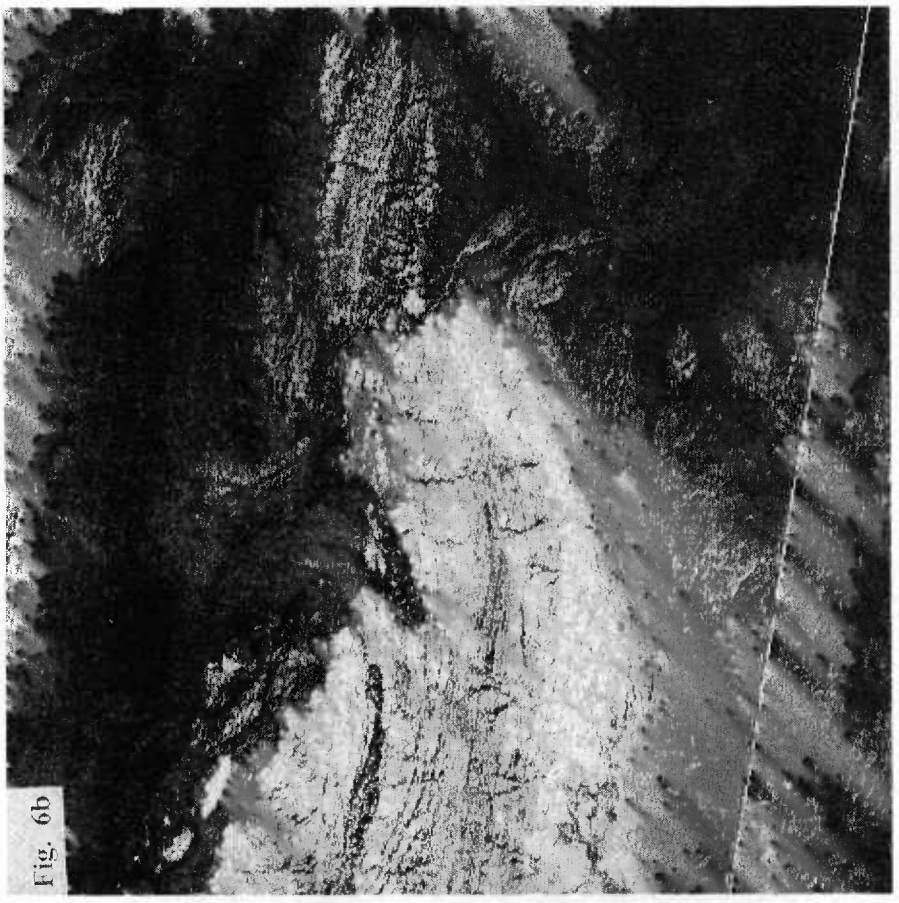

Fig. 6. Log residual images of the Mount Davies sub-scene. 6a - log residual of band 1; 6b - log residual of band 2; 6c - log residual of band 3; 6d - log residual of band 4; 6e - log residual of band 5; 6f - log residual of band 7; 6g - shade component. For geological explanation refer to Fig. 4.

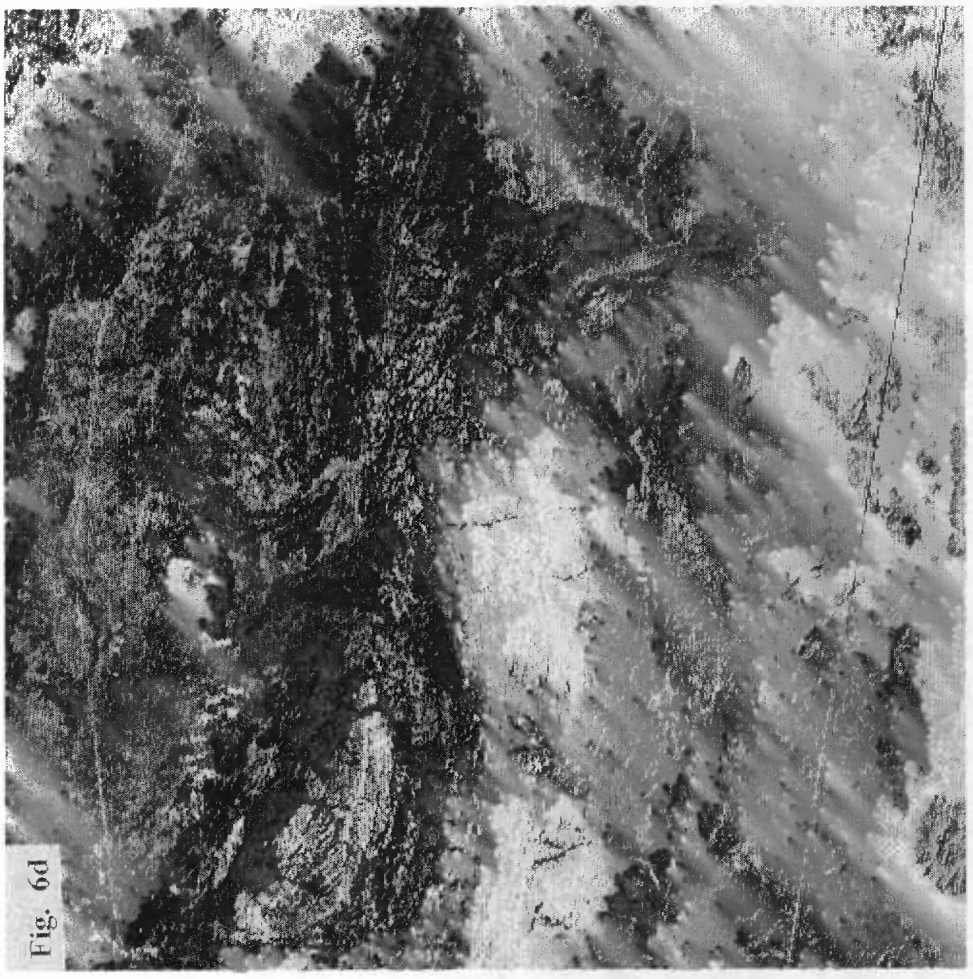

Fig. 6d

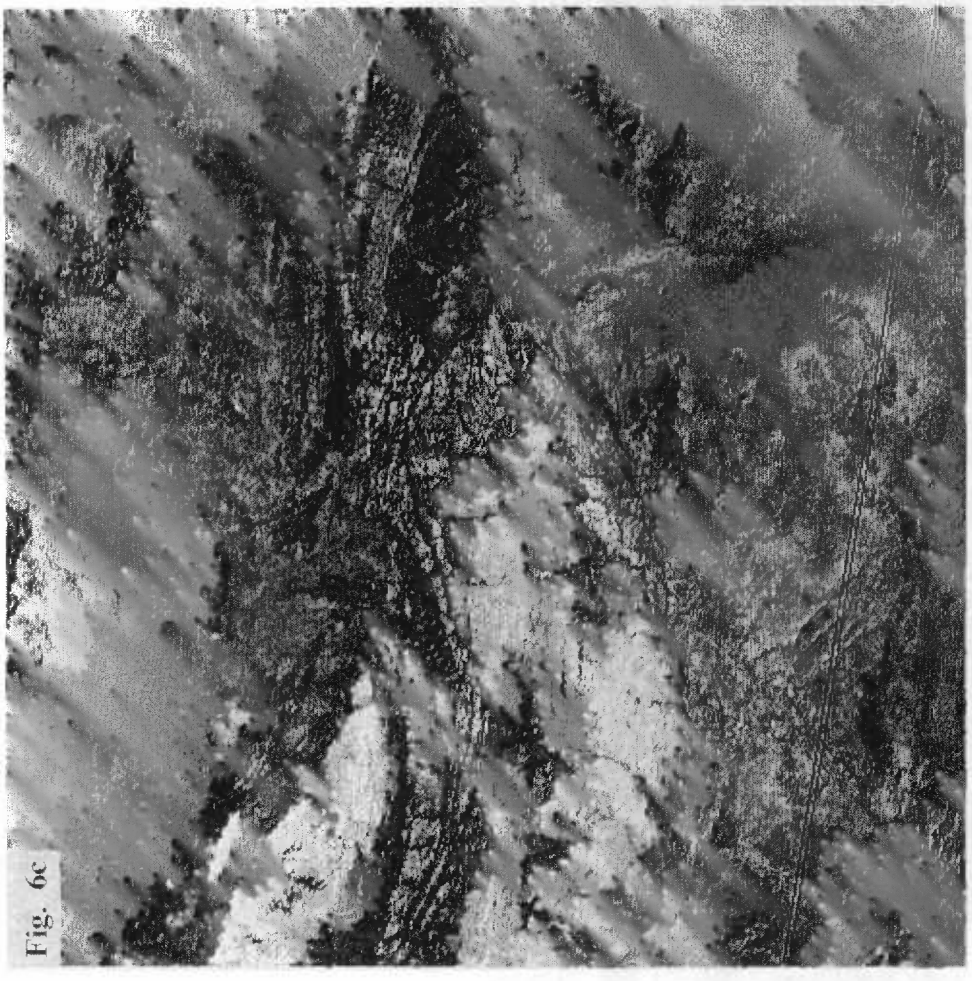

Fig. 6c

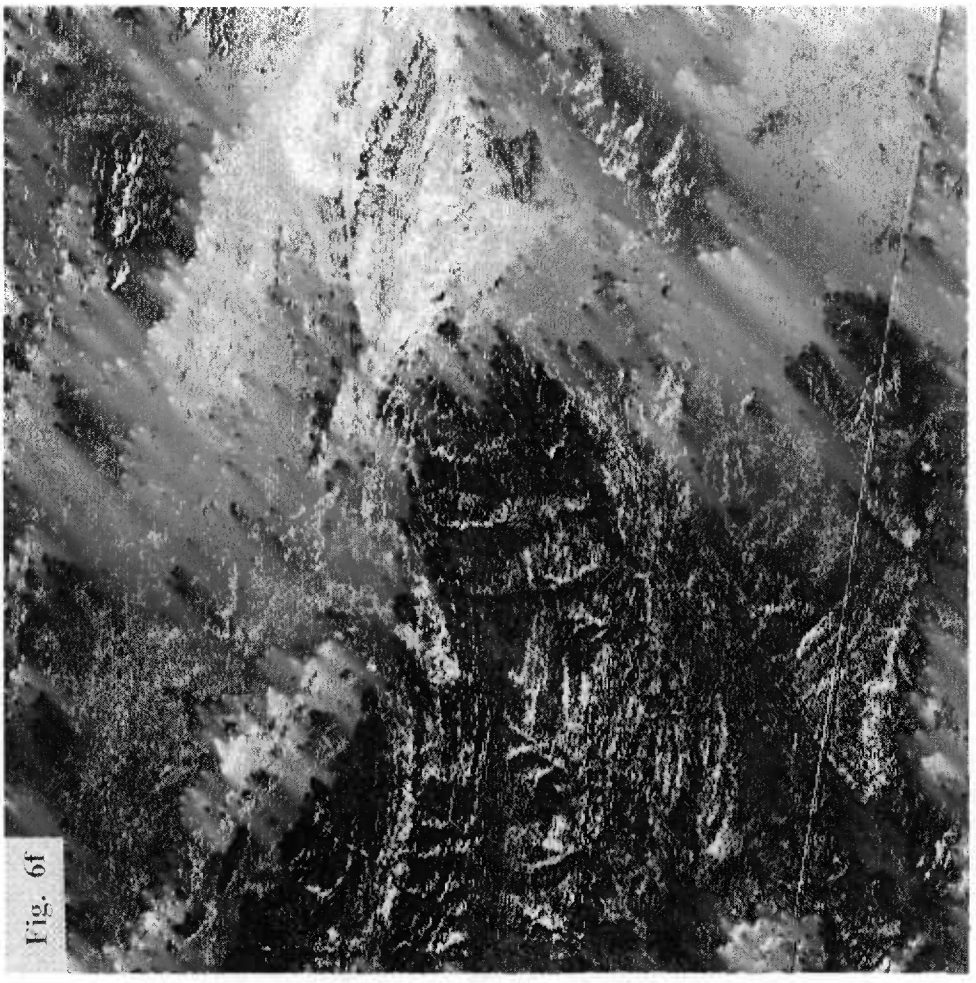

Fig. 6f

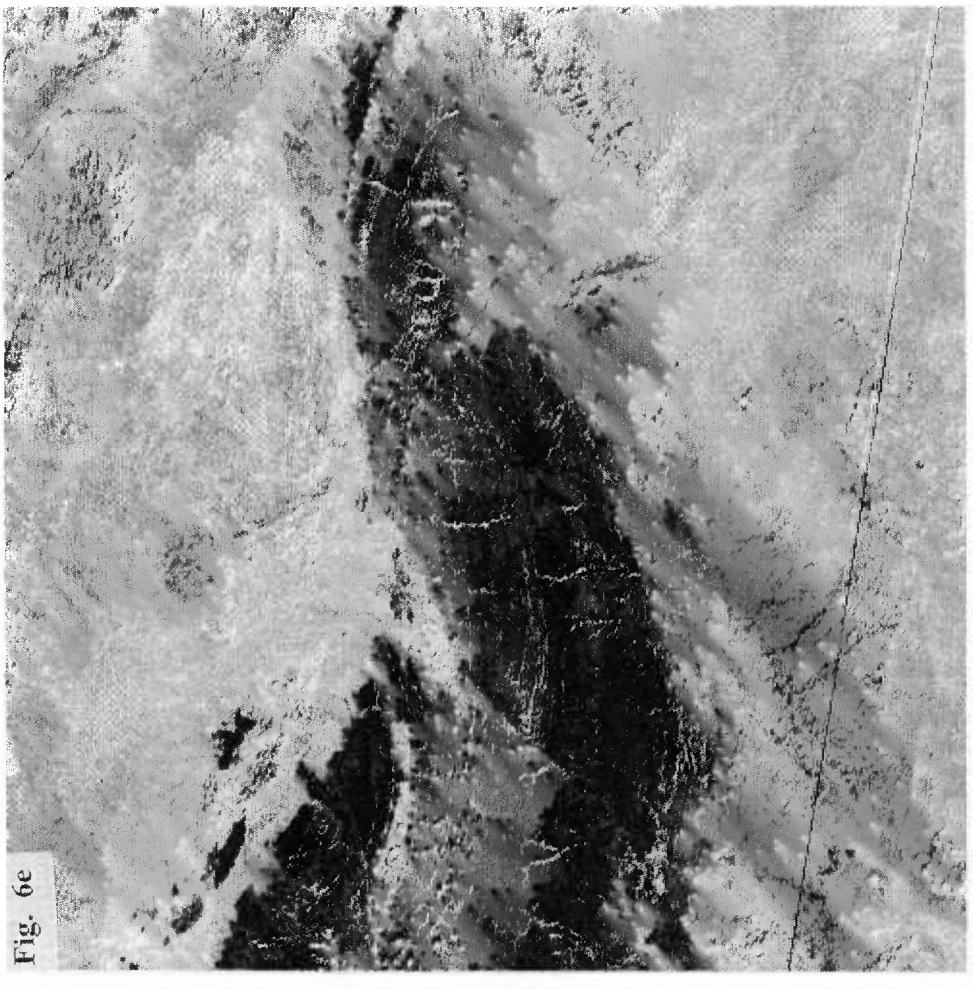

Fig. 6e

Fig. 6g

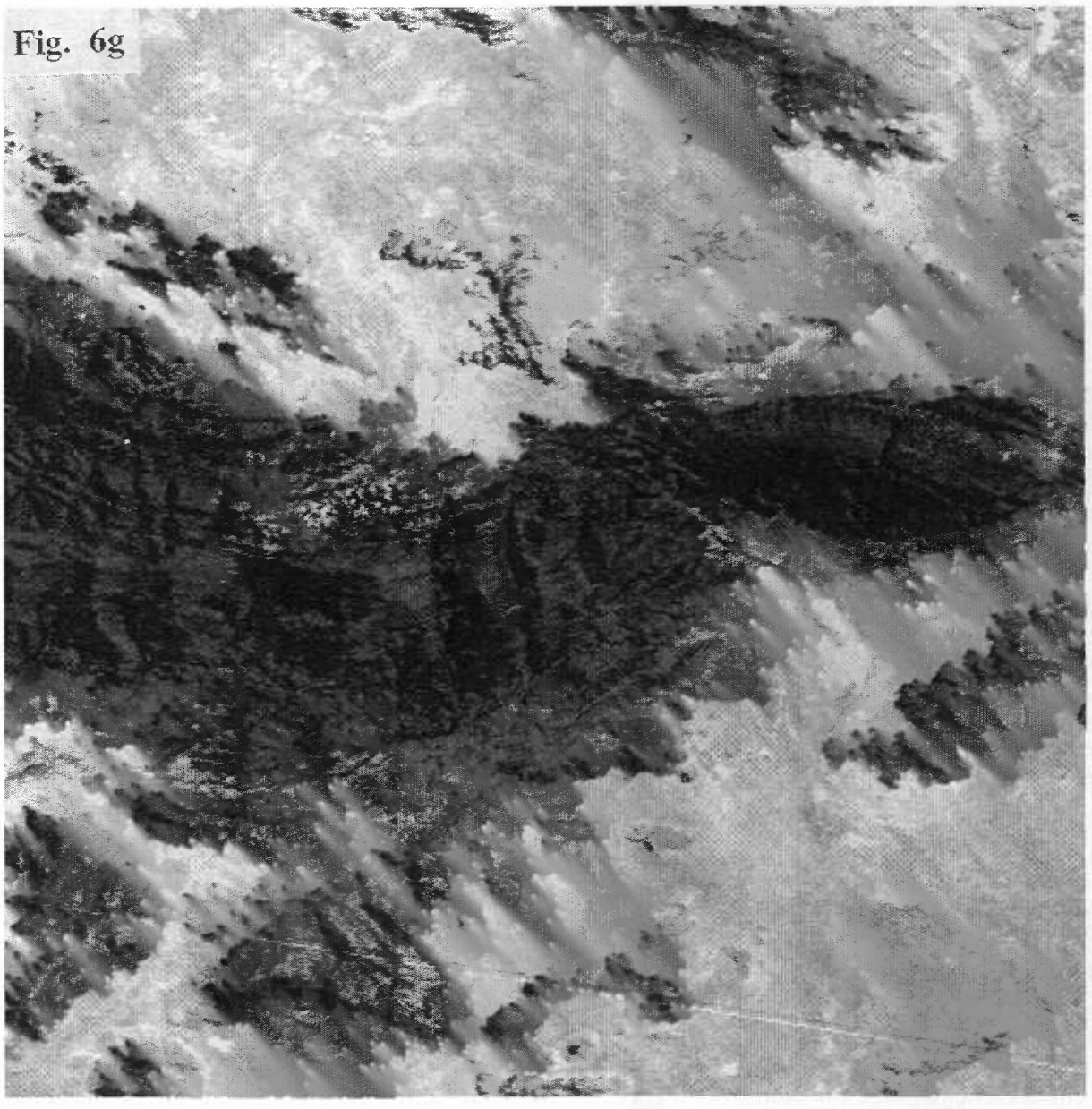

mafic granulites show significantly higher log residual values in LR bands 7 and 5 and lower values in LR bands 4 and 3 when compared to gabbro and from weathered gabbro. This distinction stands out, for example, on RGB log residual 7:4:1 images (mafic granulite - red; gabbro - cyan), allowing the charting of relict little-recrystallized gabbro from mafic granulites in the western Hinckley range. The spectral difference between gabbro and mafic granulite, which have near-identical mineralogy and chemistry, is attributable to the silica-bearing weathering crusts and the finer grained nature of the mafic granulites, a consequence of their penetrative intrusion by granitic veins. This is contrasted with the clay/carbonate rich weathering crusts on the little-recrystallized coarser grained gabbro from which the mafic granulites are derived.

Log residual images allow an effective discrimination between gabbroic rocks and felsic igneous and metamorphic rocks on the basis of differences in LR band 5, which displays higher value in felsic rocks (Fig. 6e). Consequently, images such as RGB log residual 7:5:4 display felsic materials in shades of green (LR band 5), which is combined with red (LR band 7) where the felsic rocks are intruded by swarms of iron oxide-rich mafic dykes and derived mafic debris. Weathered felsic rocks located at topographically high positions below uplifted early erosion surfaces (peneplain) display higher DN values in LR bands 3 and 4 due to clay and associated green vegetation, as represented on RGB log residual 7:4:1 images by green (LR band 4) at Mount Aloysius, Mount West and Ewarara ridge. Felsic and mafic granulites have similar value in LR bands 7 and 5, although the mafic rocks have somewhat lower value in LR bands 3 and 4, and appear therefore in similar colors on RGB log residual 7:5:4 and 7:4:1 images.

The spectral respsonse of laterites is similar to that of ferrogabbro in LR bands 7, 5 and 4 - representing the high abundance of iron oxides in these materials. On RGB log residual 7:5:4 images the high value in LR band 5 results in a distinct deep apple green appearance of laterite - a diagnostic feature for the identification of lateritic deposits. The value of laterite in LR bands 4 and 3 is clearly lower than that of clay-coated weathering surfaces such as occur on felsic granulites and granitoids (Fig. 6c, d). Calcrete deposits along creeks are distinguished by high value in LR bands 3 and 1, by analogy to anorthosite and gabbro where carbonate coatings are important. On RGB log residual 7:4:1 images calcrete shows in blue, but is difficult to discriminate from silcrete, which shows similar spectral profiles. In part this analogy is related to a high evaporative silica content of some calcrete deposits.

Alluvial deposits which fringe, and are mostly derived from, specific bedrock types reflect the source contribution through varying abundance of iron oxide, silica and carbonate. Thus, pediments associated with mafic sources display higher value in LR band 7 (iron oxide-dominated) and LR band 1 (carbonate/clay influence) than those derived from felsic sources (Fig. 5). Alluvial deposits derived from felsic sources have a generally higher value in LR bands 5 and 4, probably due to the effect of free quartz. Alluvial deposits derived from mixed sources display intermediate effects. Dunes show little difference from mixed-source alluvial deposits, reflecting a combined effect of iron oxide coatings and free quartz. Some silt/clay deposits display lower value in LR band 5 and high value in LR bands 3 and 1 - representing lower iron oxide and higher clay components relative to coarser grained alluvial deposits (Fig. 5). Accordingly, alluvium fringing or forming rings around outcrops of felsic granulite, with a higher clay component supporting green vegetation, are displayed on RGB log residual 7:4:1 images in blue (clay) to greenish blue (vegetation on clay-rich soil).

Fireburn effects in alluvial and dune areas are manifest by a higher value in LR bands 4 and 3 relative to old growth-covered dunes (Fig. 5). Thus, on RGB log residual 7:4:1 images old growth areas are displayed in red (LR band 7) and fireburn areas in yellow (red-green mixture of LR bands 7 and 4) and light green (LR band 4 - vegetation). On gabbro bedrock outcrops fireburn areas reflect more strongly in LR bands 4 and 3 and less in LR band 1 as compared to old growth areas. Consequently, on RGB log residual 7:4:1 images fireburn areas show a higher green/blue ratio than old growth areas - as represented by their azur (greenish blue) color. Further, old growth areas reflect slightly more in LR band 7, resulting in a purplish tinge.

Log residual images can be significantly enhanced through LR band inversion of the spectral pattern where the display of a low values of the data is desired. An example is the application to the Geoscan Mark-1 (see section 5) RGB 9:4:1 image of laterite and weathered gabbro north of Wingellina. In this area discrimination between laterite and gabbro is enhanced by inversion of LR band 4, which results in enhancement of the clay component of the weathered gabbro (LR band 4 - green). This, when combined with iron oxide staining (LR band 9 - red), imparts a yellow colour to the gabbro, whereas the laterite is dominated by LR bands 9 and LR band 1.

3.7 BAND RATIO IMAGES

3.7.1 RGB images

The characteristic spectral response of several of the most common surface types - including clay, carbonate, iron oxide, green vegetation and dry vegetation - allow their direct identification by means of band ratios - which render radiance corrections less essential since all bands are affected by similar absorption and interference factors. However, the superposition of spectral sections of several materials complicates interpretations. The relative abundance of these mineral components in the weathering surfaces of specific rock types provides useful fingerprints for primary lithologies. Landsat-5-TM spectra allow identification of iron oxide (hematite - high 3/1, 5/4 and 5/3), clay + vegetation (high 5/7), and green vegetation (high 4/3)(Table E; Fig. 7). Given the limited number and the broad wavelength spectrum covered by Landsat-5-TM bands, the identification of components is complicated by spectral superposition. Since the 3/1 and 5/3 band ratios nearly coincide with the green and dry vegetation spectra, the 5/4 band ratio is better suited for discrimination of iron oxides. Thus, the RGB 5/4:4/3;5/7 image is useful for distinction of iron oxides, green vegetation and clay, respectively. In this image a partial green vegetation cover over clay/carbonate bedrock displays in cyan, whereas fireburn areas show in dark brownish colour. However, the spectral overlap between some materials complicates their distinction, for example: (1) carbonate spectral ratios are similar to clay; (2) the 5/7 ratio of green and dry vegetation is similar to that of clay; (3) goethite ratios are difficult to separate from those of hematite. The effects of histogram stretching, maximizing the range of DN values for each of the ratios on RGB images, changes the relationships between any three displayed ratios, complicating their direct reading from images. However, comparisons are facilitated by single ratio images and ratio tables (Figs 7; Table E). Examination of Landsat-5-TM spectral patterns for training areas in the Tomkinson Ranges indicate systematic differences with regard to some of the principal ratios, summarized below:

Laterite, characterized by high reflectance in band 7 due to iron oxide-rich weathering crusts, displays high 5/4 ratio values (c. 2.7) and high 5/1 ratio values (c. 4.6-5.1), but do

Table E - selected band ratios of dark pixel-corrected mean values of training areas for bedrock and surface type units in the Tomkinson Ranges.

BAND RATIO typical materials	3/1 Fe-oxide + veg	5/4 Fe-oxide	5/1 Fe-oxide + veg	5/7 clay + dry veg	4/3 green veg
1. igneous and metamorphic rocks					
opx-rich rocks-GP	1.2	2.0	3.1	1.05	1.25
cpx-rich rocks-EW	1.3	2.3	3.1	1.12	1.07
gabbro-BR	1.7	1.8	3.5	1.17	1.08
ferrogabbro-BR	1.6	2.0	3.5	1.25	1.11
gabbro-HG	1.4	1.3	2.0	1.12	1.09
weath. gabbro-HG	2.1	1.5	3.3	1.19	1.08
mafic granulite-HG	1.3	2.3	3.3	1.27	1.11
norite-KA	1.8	1.6	2.8	1.12	0.95
leucogabbro-KA	1.6	1.8	3.0	1.26	1.02
anorthosite, TEIZI	1.9	1.6	3.3	1.37	1.04
gabbro-MH, fireburn	1.65	1.6	2.85	1.24	1.09
gabbro-MH, old veg	1.23	1.8	2.43	1.21	1.08
felsic granulites	1.7	2.1	4.2	1.35	1.15
granite gneiss	1.6	2.2	4.0	1.31	1.17
weathered felsic granulites	1.9	1.8	4.1	1.39	1.20
2. duricrust					
laterite-WIN	1.47	2.6	4.59	1.32	1.2
laterite-KA	1.76	2.7	5.17	1.31	1.1
calcrete-PID	1.41	1.8	2.84	1.45	1.1
calcrete-CDM	1.92	2.0	4.30	1.33	1.1
silcrete-WIN	1.27	1.9	2.35	1.48	1.0
silcrete-KA	1.14	2.1	2.52	1.60	1.06
3. alluvial deposits					
alluvium, basic source	1.52	2.0	3.26	1.21	1.05
alluvium, felsic source	2.68	2.1	6.26	1.38	1.10
silt and clay-CDM	2.27	1.8	4.32	1.23	1.04
Ferruginous silt - LW	1.22	2.6	3.16	1.19	1.00
dunes, fireburn	2.14	2.0	4.85	1.31	1.15
dunes, old growth	1.46	2.3	3.79	1.36	1.14
green vegetation Wingellina school	1.69	1.53	3.30	1.43	1.27

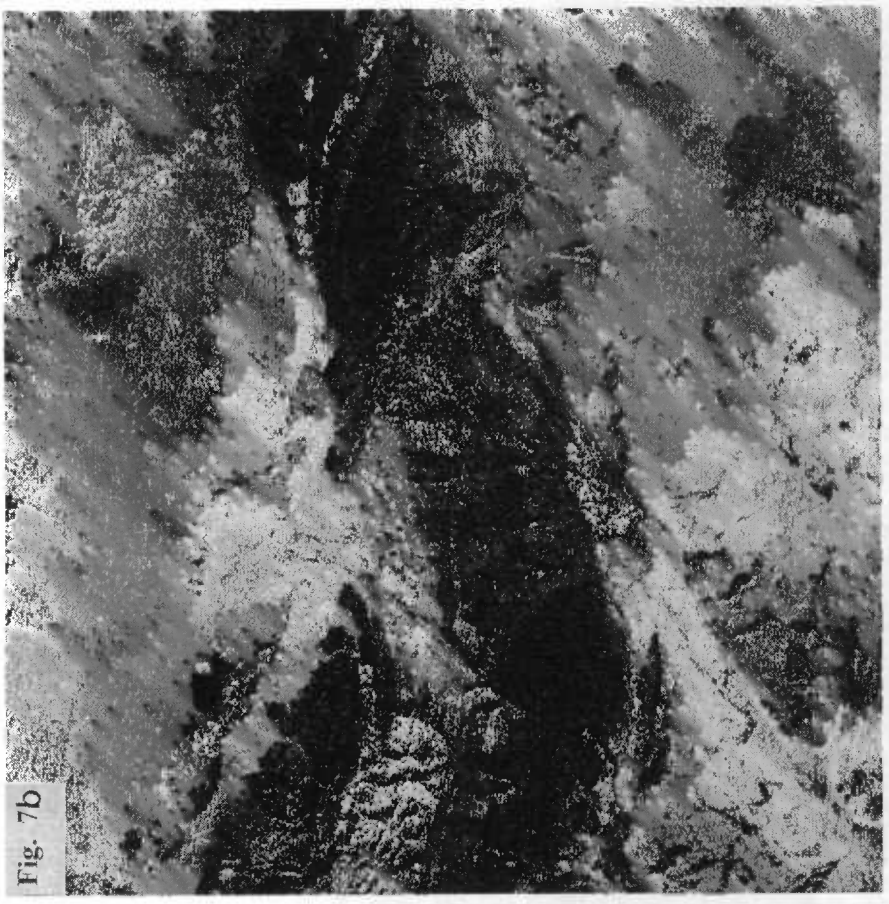

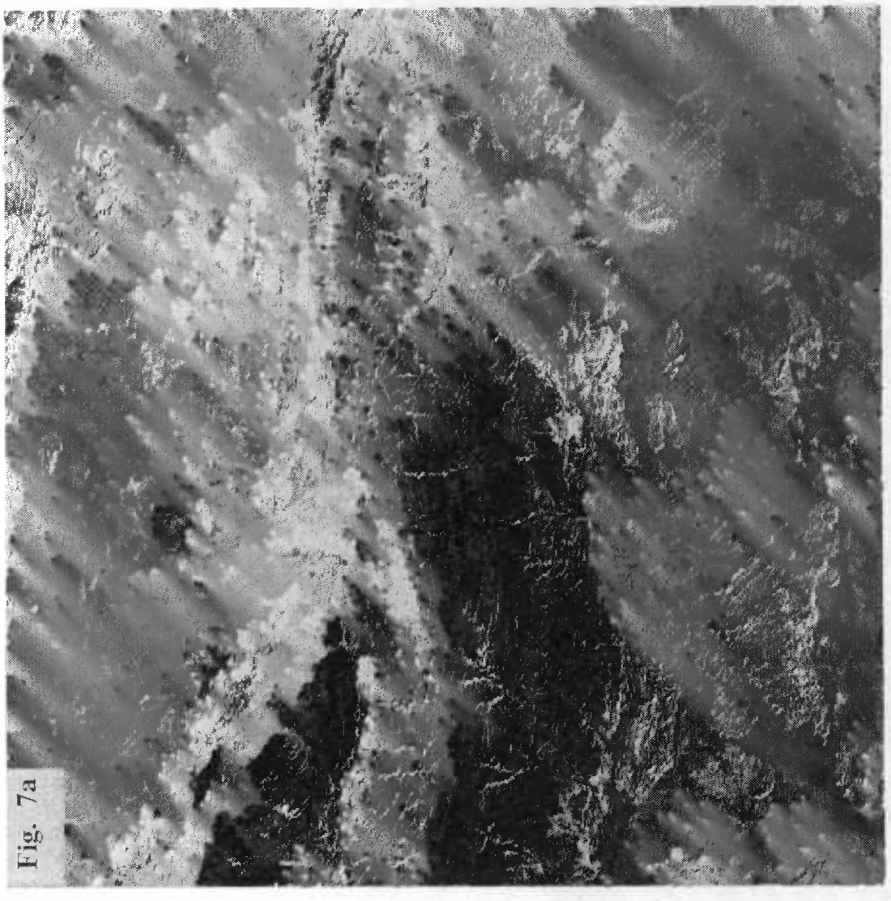

Fig. 7. Band ratio images of the Mount Davies sub-scene. 7a - bands 5/4 ratio, showing high reflectance for iron oxide (pyroxenite, laterite, iron oxide-rich detritus); 7b bands 5/7 ratio, showing high reflectance for clay-bearing alluvium around felsic granulites and calcrete; 7c - bands 4/3 ratio, showing high reflectance for vegetated areas on southern slopes, creeks and strike depressions.

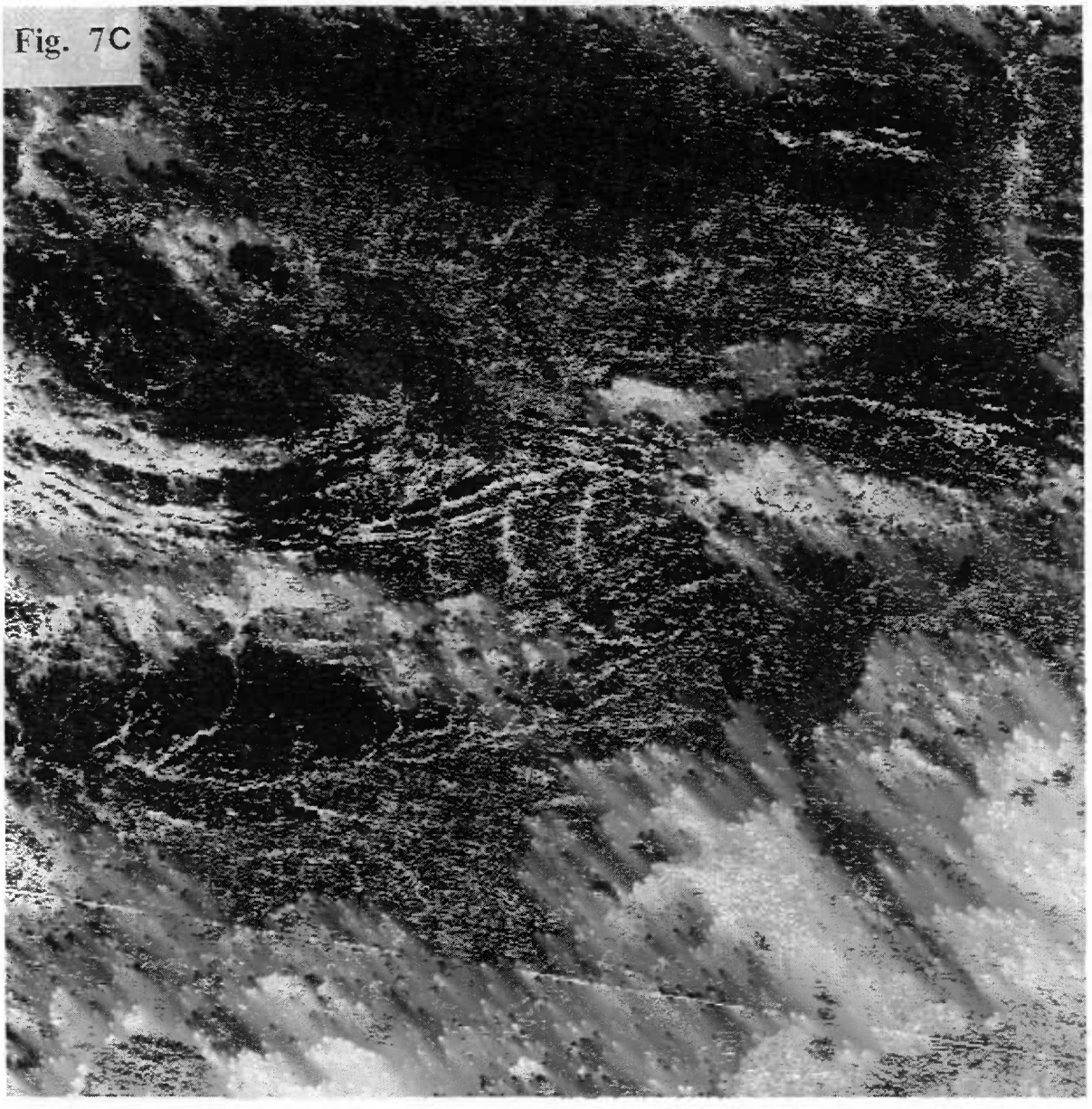

not display high 3/1 ratios relative to other less-ferruginous materials. Clay pans and dry lakes (Champ de Mars, Lake Wilson) do not display the high bands 5/7 ratio values expected for clay, suggesting they may consist principally of silt. The Lake Wilson bed is characterized by high 5/4 band ratio (c. 2.6), signifying iron oxide-rich detritus. Weathered clay-rich felsic granulites and anorthosites have relatively high 5/7 band ratios val;ues (c. 1.4) due to clay/carbonate enrichments, as does calcrete. The high 5/7 ratios of silcrete may betray the carbonate component of silica/carbonate mixtures. The masking effects of dry and green vegetation are partly overcome by calculating the band ratios of devegetated images, using a pixel-unmixing program that subtracts the green vegetation end member from the bands (section 3.9) (Bierwirth, 1990). The results of this analysis indicate consistent lowering of the 5/7 and 5/4 ratios and increases in the 3/1 and 5/1 ratios in green vegetation-removed images as compared to mixed mineral/vegetation images (compare tables E and G).

3.7.2. Single band ratio images

bands 5/4 ratio image: this band ratio has been found useful for the identification of iron oxide-rich materials, including hematite and goethite, since the other common components - clay, carbonate, green vegetation and dry vegetation - have significantly lower ratios (Table E). This ratio is more diagnostic of iron oxides than the 3/1 ratio as the latter is partly masked by the 3/1 ratio of dry vegetation and, to a lesser extent, green vegetation. The Mount Davies sub-scene (Fig. 7) displays very high reflectance for laterite and high reflectance for pyroxenite and oxidized mafic-derived colluvium. Felsic rocks are characterized by higher 5/4 ratios than gabbroic rocks. In mafic terrains fireburn areas show a low reflectance compared to old vegetated areas (Table E).

bands 5/7 ratio images: in this band ratio, traditionally used for the identification of clay and carbonate, the former have similar ratio values to those of green and dry vegetation (Fig. 2). Felsic rocks show higher reflectance than mafic rocks, representing greater abundance of clay in the weathering crusts. Surface types displaying very high DN values in the 5/7 ratio on the Mount Davies sub-scene (Fig. 7) include (1) clay-rich alluvial/arkose girdles around isolated outcrops of felsic granulites; (2) carbonate-rich weathering zones overlying peridotitic rocks at Gosse Pile. Patchy high ratio value zones also occur over gabbro bedrock surfaces, representing vegetation patterns.

bands 4/3 ratio images: The 4/3 ratio values of green vegetation are higher than that of dry vegetation and significantly higher than that of iron oxides, and help to outline vegetated creeks and southern sun-shaded slopes. In the Mount Davies sub-scene (Fig. 7) high reflectance areas outline gullies, creeks, strike depressions over pyroxenite and parts of the southern shaded and thereby better vegetated slopes of Mount Davies and Gosse Pile. Low 4/3 ratio values in parts of Mount Davies correspond in part to recent fireburns with little green vegetation.

3.8 PRINCIPAL COMPONENTS ANALYSIS

3.8.1 Single band principal components

The generally high correlation between bands of the spectral response of common materials in natural terrains requires a method of discriminating spectral patterns which depart from the general norm. Principal components (PC) analysis measures the correlation between band radiance values in each pixel and the mean spectral pattern of the total pixel array. The method quantifies the proximity of each radiance value (DN) to best-fit variance axes

in N-dimensional space - the number of axes equaling the number of spectral channels. The highest PC (PC1) represents best correlated band values whereas lower PCs represent increasingly little correlated spectra of potential interest. Each PC is influenced by all the 6 Landsat-5-TM bands, each band being represented by an Eigen vector which weighs the influence of each band on the relevant principal component. Commonly, particular PCs are influenced by particular surface types, although such correlations may vary within and between images.

Eigen vectors weighing the effect of each of the the 6 spectral bands in each of the 6 PCs (based on bands 1,2,3,4,5,7, excluding the thermal band 6) are tabulated in Table B. The Eigen vectors can be correlated with some of the features on single band principal component grey scale images of the Mount Davies sub-scene (Fig. 8). In general the PC analysis of Landsat-5-TM in the Tomkinson Ranges suggest correlations between low order least-well correlated PCs and superficial vegetation types and fireburn patterns. Thus, whereas RGB images of PCs 1, 2 and 3 outline geological and structural elements, RGB images of PCs 3, 4 and 5 display the distribution of vegetation and fireburn areas. PCs 3 and 4 contain information on the distribution of free quartz in alluvial and dune deposits, as contrasted from weathering-coated quartz in bedrock and from silcrete. Single PC Eigen vectors and images display the following features:

- PC-1 is dominated by bands 2, 3 and 7 (i.e. clay, carbonate, iron oxides). The Mount Davies sub-scene displays both mafic and felsic rock types in high DN values. Gabbro and pyroxenite display high to very high DN values (~200) as do felsic granulites/ granites. However, whereas mafic source-derived alluvium reflects in intermediate DN values [135], felsic source-derived alluvium and dune crests has very low DN values [90]. This difference is interpreted in terms of (1) high bands correlation of the clay-carbonate-iron oxide-dominated weathering crusts in a compositionally wide range of bedrock types, and (2) low bands correlations of free quartz-dominated felsic source-derived alluvium and dunes. The lack of quartz expression in the felsic rocks themselves is attributed to their coating by weathering products such as clay and iron oxides. Calcrete and silcrete show very low band correlations in PC1. Fireburns are displayed by the somewhat higher DN values of old growth. Shade is represented by lower DN values.

- PC-2 shows a strong negative correlation with band 7 (iron oxides), allowing discrimination between iron oxide-rich materials (pyroxenites, ferrogabbro and laterite, intermediate to high DN [~200]) and anorthositic to gabbroic rocks (low DN [160-180], grey to dark grey). Felsic granulite/granite displays intermediate to high DN values [~190]. Fireburn areas on gabbro show lowering of DN values [110] as compared to old growth [130. Calcrete and silcrete show may show low DN values and felsic-derived alluvium and dunes show in black - representing the low bands correlation of free quartz. Green vegetation and thereby creeks show as low-DN dark zones.

- PC-3 is influenced by bands 2 and 5 (clay, iron oxides), and appears to be dominated by free quartz, as suggested by very high DN values of felsic-derived alluvial materials and of dunes. The role of quartz is confirmed by the high negative Eigen vector value (-.723) of the thermal band 6 in the original Landsat-5-TM image (Table A). Interpretations of band 6 are complicated by its sensitivity to atmospheric conditions. The PC3 image is useful for discrimination of fireburns thanks to significantly higher DN values in fireburn areas over bedrock and alluvial deposits. Calcrete and silcrete duricrusts show low DN. PC-3 images display little discrimination between other surface types.

Table F - principal component mean digital number (DN) values for training areas, Tomkinson Ranges.

PRINCIPAL COMPONENT	1	2	3	4	5	6
1. igneous and metamorphic rocks						
opx-rich rocks-GP	193	199	199	201	119	207
cpx-rich rocks-EW	159	204	195	206	110	207
gabbro-BR	150	185	197	203	117	205
ferrogabbro-BR	156	210	192	211	107	208
gabbro-HG	174	163	192	197	123	204
weather. gabbro-HG	165	172	207	190	115	204
mafic granulite-HG	157	197	175	200	119	208
norite-KALKA	150	164	195	206	110	204
leucogabbro-KALKA	146	176	181	200	109	206
anorthosite, TEIZI	120	158	184	191	106	202
gabbro-MH, fireburn	166	174	194	192	115	207
gabbro-MH, old veg	177	183	182	199	118	210
felsic granulites	124	191	181	194	119	203
granite gneiss	147	199	185	196	114	204
weathered felsic granulites	148	185	193	181	114	205
2. duricrust						
laterite-WIN	149	212	181	198	115	208
laterite-KALKA	134	214	182	201	107	207
calcrete-PID	75	154	141	196	130	204
calcrete-CDM	89	184	178	201	117	203
silcrete-WIN	79	138	119	204	124	201
silcrete-Kalka	63	152	94	195	129	198
3. alluvial deposits						
alluvium, basic source	135	189	184	210	114	207
alluvium, felsic source	89	197	197	188	104	209
silt and clay-CDM	112	178	201	203	110	205
silt and clay-LW	115	198	156	232	122	202
dunes, fireburn	109	191	196	194	126	212
dunes, old growth	128	198	173	199	119	211
4. vegetation						
eucalypts, Wingellina	129	166	188	175	142	207

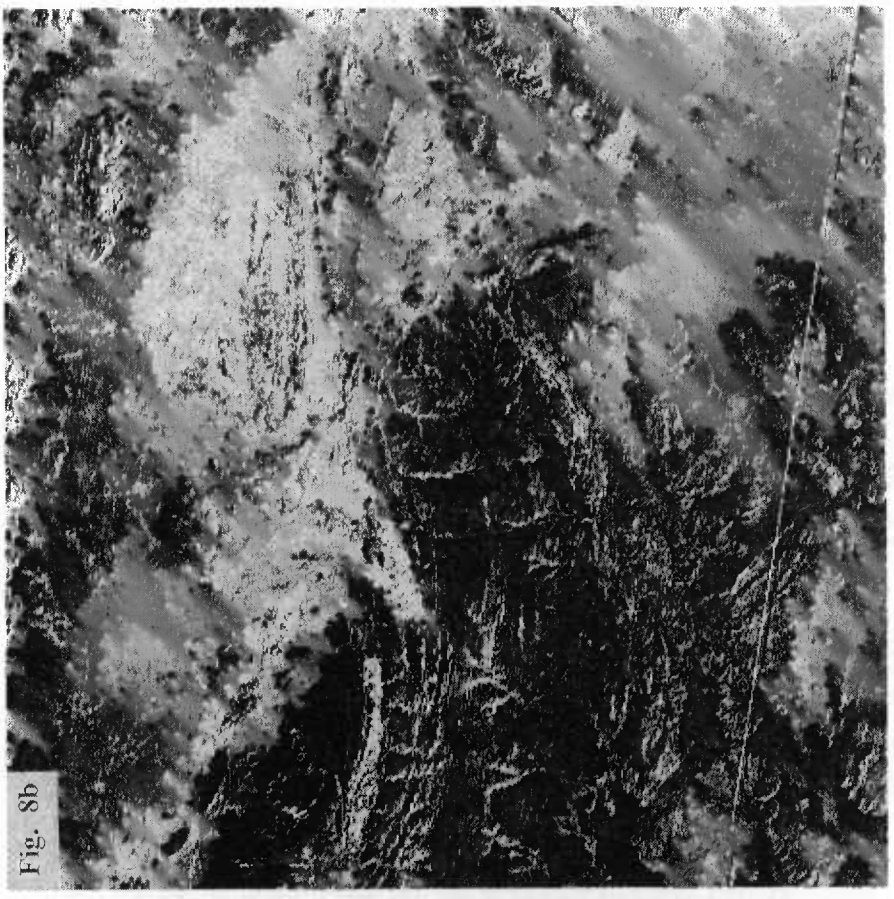

Fig. 8. Principal component images of the Mount Davies sub-scene. 8a - pc1; 8b - pc2; 8c - pc3; 8d - pc4; 8e - pc5; 8f - pc6 (for lithological correlatisons see section 3.8. For geological explanation see Fig. 4.

Fig. 8d

Fig. 8c

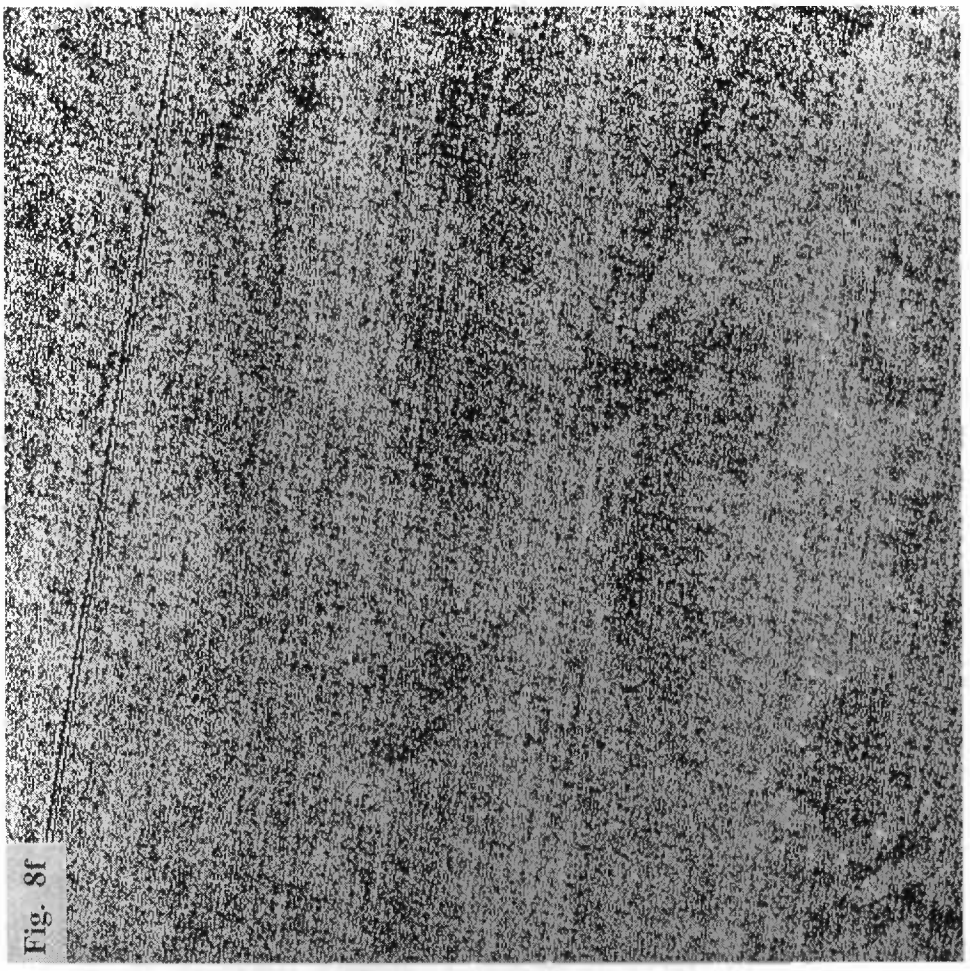

Fig. 8f

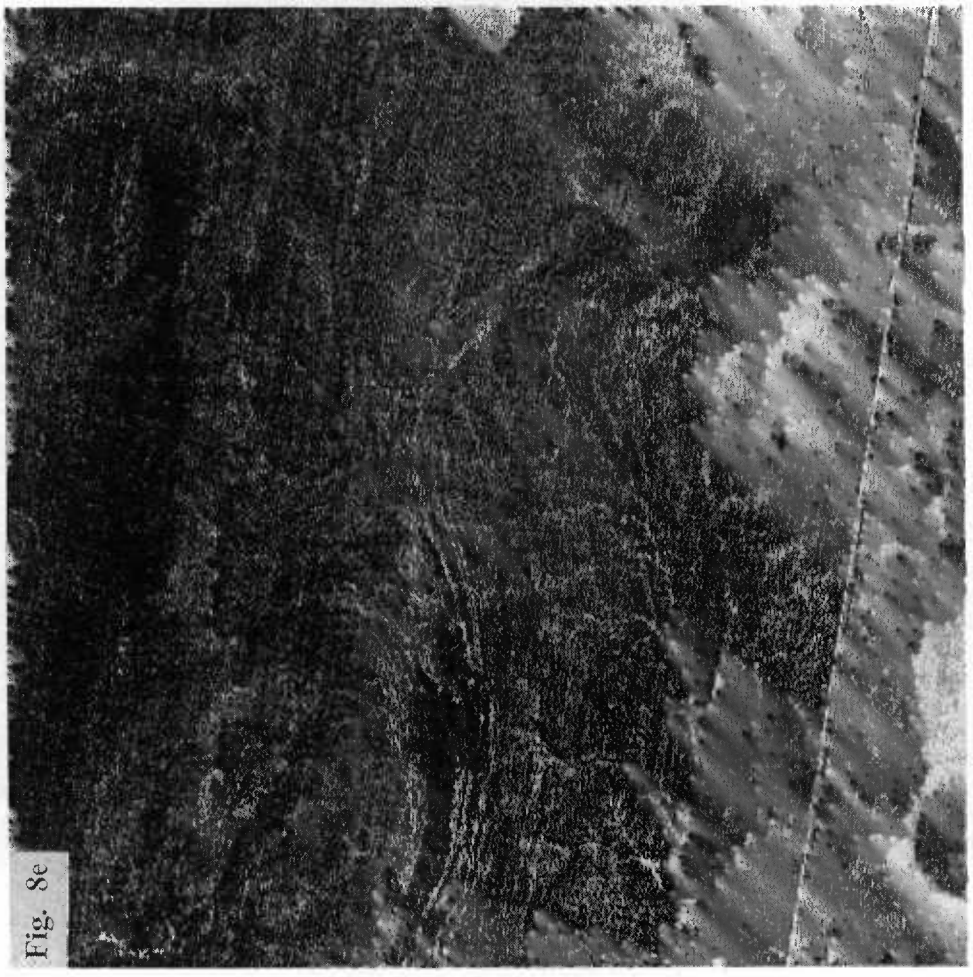

Fig. 8e

- PC-4 shows a strong negative correlation with bands 5 and 3 and displays high DN values for iron oxides and for fireburn areas. The DN values of the latter is in inverse relation to their age, namely young fireburns display higher DN values. PC-4 offers a good discrimination between gabbro and mafic granulites, the latter displaying higher DN values. Felsic materials show lower DN values than mafic materials, and free quartz-bearing felsic alluvium as black areas.

- PC-5 shows a negative correlation with band 1 and a positive correlation with band 4 (green vegetation), which occurs mainly along creeks and depressions, in agreement with the high Eigen vectors in band 4 (.475). Little contrast is shown between mafic and felsic lithologies.

- PC-6 is dominated by negative correlations in bands 4 and 1. The images are very "noisy" and show faint outlines which can hardly be correlated with geological features, possibly reflect old fireburn patterns and dry vegetation patterns.

3.8.2 Principal components of band ratios

Application of principal component analysis to band ratios allow for the discriminating between materials with partly overlapping spectral patterns (Fraser and Green, 1987). Thus, high 4/3 ratio values pertain to both iron oxide and green vegetation and high 5/7 band ratio values pertain to both clay and vegetation. However, iron oxide can be distinguished from vegetation by lower 5/7 ratio values. Likewise, clay can be distinguished from vegetation by lower 4/3 ratios. These discriminations can be made using principal component analysis of pairs of ratios. For vegetation and clay the difference is expressed by principal components analysis of bands 4/3 and 5/7, selecting the green vegetation 4/3 ratio as the highest correlation (PC-1) (showing closest correlation with the overall image pattern) and the clay 5/7 ratio as a second correlation (PC-2) (showing a lesser correlation with the overall image pattern). The discriminative principal component can be combined with ratios in RGB images to display a range of clay/iron oxide variations along with a separate vegetation component. A useful image in this regard is RGB PC-2(clay-dominated) : 5/4 (iron) : 4/3 (vegetation). In this image the visually sensitive red and green colours represent lithological variations and the visually less senstive blue colour represents vegetation. Comparisons between lithological correlations allowed by this image and correlations suggested by log residuals, ratio bands and pixel-unmixed bands suggest superior resolution of surface types, as follows (see frontispiece):

- old growth-covered gabbro - red and purple, representing clay/carbonate weathering crusts and vegetation, the latter being particularly dense in shaded southward slopes that show in deep purple.

- fireburn over gabbro - dark brown to red, representing low DN values clay covered weathering surfaces.

- ferrogabbro - blilliant apple green, representing iron oxide.

- pyroxenite - green-dominated commonly ranging to cyan - representing strong effect of iron oxides (northern Kalka, Ewarara, Latitude Hill, Gosse Pile, merging into cyan where vegetation is important, i.e. southern shaded slopes of Gosse Pile.

- felsic granulite and granitic gneiss - mostly yellow (clay/iron oxide red/green mixtures)

covered in places by blue (vegetation on southern slopes) and red (strong sub-peneplain clay weathering, as on the high levels of Mount Aloysius).

- laterite - marked apple green (iron oxide) to yellow (iron oxide-clay mixture), i.e. east of Kalka and Poonawarra, and cyan where laterite is covered by dense mulga bush (around Wingellina).
- calcrete - orange red, i.e. along creeks and over peridotite (Mount Davies).
- silcrete - show in red.
- mafic source-derived alluvium - show in shades of light green to light orange, represnting the importance of iron oxide and clay.
- felsic source-derived alluvium - show in light red to purple, commonly forming collars around outcrops of felsic granulite, representing the importance of clay and vegetation.
- silt and claypans - showing in light orange to red (Champ de Mars clay pan) and in green (Lake Wilson) - the latter suggesting suspended iron oxide/clay mixture.

3.9 PIXEL UNMIXING ANALYSIS

The pixel unmixing process ivolves the analysis of multispectral data with respect to known reflectance profiles for various mineral and vegetation types. Prior to unmixing, the remotely sensed data must be converted to reflectance. The sensor count value (DN) is related to reflectance by (Bierwirth, 1990):

$$Ci = RiGi + O \quad \ldots (1)$$

$$O = (Lmin + Lp)/K$$

$$G = EgTq/3.14K$$

$$Eg = EoTw \cos(w) + Ed$$

Ci – count value

Ed – diffuse sky irradiance

Eo – solar irradiance at top of atmosphere

Lmin – instrument offset

Lp – path radiance resulting from multiple atmospheric scattering

Ri – reflectance value

Tq – atmospheric transmittance of reflected radiation at angle q to the zenith

Tw – atmospheric transmittance of solar irradiance at an angle W to the zenith

The additive component - O - is generally successfully removed by finding and subtracting the dark pixel (Bi):

$$Bi = RiGi \quad \ldots (2)$$

The AGSO in-house program BERAD on the IIS system was designed to remove the multiplying effects, being the global irradiance - Eg - and the sensor gain factor - K.

In this program, values for average solar irradiance and sensor gains were used to correct the data. These values were obtained from Markham and Barker (1986). The correction for the new value - A - becomes:

$Ai = RiTqi/3.14$ ... (3)

The new spectral curves are still influenced by the atmospheric transmittance Tq curve which causes values of A to be lower in the visible wavelength. A small approximate correction for this effect is implemented in the program BERAD2.

Bierwirth (1990) developed a program based on the simultaneous solution of sets of equations allowing the resolution of specified end members. In this approach, for any particular wavelength interval (band) [i] within any particular pixel, corrected radiance data can be modelled in the following terms:

$R_{[1]} = a_{[1]}A + b_{[1]}B + \ldots x_{[1]}N$

$R_{[2]} = a_{[2]}A + b_{[2]}B + \ldots x_{[2]}N$

etc...

$a_{[n]}$ - reflectance of material a in band n

A - proportion (% area) of material a within the pixel

$b_{[n]}$ - reflectance of material b in band n

B - proportion (% area) of material b within the pixel

R_n - total pixel reflectance in band n

x - number of material types (can not exceed the number of bands)

The method depends critically on the choice of spectrally distinct realistic end-members identified in the field. Similar spectral patterns preclude effective discriminations, for example spectral similarities between clay and carbonate and between hematite and goethite complicates their distinction on Landsat-5-TM images. Model end-members can include dry vegetation and green vegetation (higher 4/3 and 2/3 band ratio than dry vegetation). The number of end members can not exceed the number of bands, namely up to six bands in Landsat-5-TM images (excluding the thermal band 6). Pixel unmixed images representing the proportion of modelled end members in each of the pixels need to be tested against field observations. The program enables subtraction of the model proportions of vegetation end members from the modeled mineral end members and presentation of the latter as devegetated images.

In the present study, field measured end member spectra were selected from a spectral library file (TMSPECLIB, P.N. Bierwirth, pers. comm., 1992). Models tested included the following end members: (1) kaolinite; (2) calcite; (3) haematite; (4) goethite; (5) silica; (6) eucalyptus green vegetation; (7) dry vegetation; (8) spinifex vegetation (similar to green vegetation). Comparisons between pixel-unmixed model images and selected band ratio images confirm the unmixing model with regard to (1) the unmixed clay component, correlates with 5/7 ratio images; (2) the unmixed iron oxide component correlates with 5/4 band images (this ratio is preferred to the 3/1 ratio, where superposition of iron oxide and vegetation occurs), and (3) the unmixed green vegetation component correlates with 4/3 band images (Fig. 7). On the other hand, no discriminations of clay from carbonate, of hematite from goethite and of silica have proven possible:

- kaolinite, representative of clays in general, is suggested in the weathered surfaces of felsic igneous and metamorphic rocks and derived alluvial materials - the latter forming distinct rings and fringes juxtaposed with felsic igneous and metamorphic ourcrops.

- clay/carbonate mixtures are suggested in the weathering surfaces of mafic igneous rocks.
- carbonates and carbonate/silica mixtures are represented by calcrete along creeks and by calcrete rises beneath alluvial surfaces.
- hematite and/or goethite dominate outcrops of orthopyroxenites, ferrogabbro, lateritic deposits and iron oxide-rich alluvial deposits derived from mafic igneous rocks. Attempts to model goethite are unsuccessful, in part due to its spectral overlap with vegetation.
- silica is not discriminated except as a generally high to very high reflectance, i.e. in silcrete open cuts near Wingellina and Pipalyatjarra. Thus, on RGB images containing a silica end member this component is readily confused with other materials, such as clay and/or carbonate.
- green vegetation is well represented along creeks and in fireburn areas covered by young green spinifex regrowth, allowing discrimination of fireburn outlines. These areas offer geological "windows" through which the spectral patterns of mineral components are better manifest than in old growth areas covered by the highly reflective dry vegetation.

In view of the near overlap between the 5/7 band ratio of dry vegetation and clay, removal of the dry vegetation component in the unmixing analysis affects the clay component and needs to be avoided. Comparisons between the original data and devegetated images reveal important differences, particularly where log residual enhancement (band DN/pixel mean DN/image mean DN) of original images and devegetated images are compared. Images from which the dry vegetation component has been removed reveal a major loss of information, particularly with regard to the clay component.

Comparisons between single band pixel-unmixed images and band ratio images indicate the following similarities and differences: The hematite end member band of the pixel-unmixed image (Fig. 9a) shows important features in common with the 5/4 band ratio image (Fig. 7). Both images share very high reflectance for laterite and for oxidized mafic-derived colluvium, intermediate reflectance for felsic granulites and low reflectance for clay/carbonate weathered mafic rocks and for clay and quartz-rich girdles around felsic outcrops. The correlation between the clay end member band of the pixel unmixed image and the 5/7 band ratio image is not as good, although clay/carbonate-rich areas at the centre of Mount Davies and clay/quartz-rich alluvial girdles around felsic granulite outcrops are expressed by high DN values in both types of images. The otherwise poor correlation arises due to superposition of vegetation on the 5/7 ratio, requiring comparisons with devegetated images. A close similarity is shown between the green vegetation end member in the pixel unmixing image (Fig. 9) and the 4/3 band ratio image (Fig. 7). Both images display the greater concentration of green vegetation in creeks, strike-parallel depressions of less resistant lithologies and some southern slopes, i.e. Gosse Pile.

3.10 DEVEGETATED IMAGES

The modelling of end member abundances by pixel unmixing (section 3.9) allows subtraction of the reflectance effect of dry and/or green vegetation end members in each band from the primary (radiance-corrected) Landsat-5-TM band value in order to obtain the devegetated images. However, since field-measured spectra indicate a close coincidence between the 5/7 ratios of dry vegetation and clay, it follows that a significant loss of mineral-related data will occur upon subtraction of the dry vegetation end member. For this

Table G - Radiation-corrected mean band ratios of green vegetation-removed (devegetated) Landsat-TM training areas in the Tomkinson Ranges.

BAND RATIO typical materials	3/1 Fe-oxide	5/3 Fe-oxide	5/1 Fe-oxide	5/4 Fe-oxide	5/7 clay + dry veg	4/3 green vegetation
1. igneous and metamorphic rocks						
opx-rich rocks-GP	2.0	2.0	4.1	1.96	0.59	1.04
cpx-rich rocks-EW	2.9	2.0	6.0	1.90	0.69	0.79
gabbro-BR	3.0	1.6	4.9	1.55	0.69	1.06
ferrogabbro-BR	2.5	2.3	5.6	2.05	0.70	1.11
gabbro-HG	2.4	1.1	2.7	1.10	0.64	1.01
weather. gabbro-HG	3.6	1.3	4.8	1.21	0.69	1.08
mafic granulite-HG	1.9	2.1	4.1	1.86	0.77	1.15
norite-KA	2.8	1.2	3.5	1.56	0.65	1.01
leucogabbro-KA	2.4	1.6	3.7	1.43	0.77	1.09
anorthosite, TEIZI	3.1	1.4	4.3	1.27	0.81	1.11
gabbro-MH, fireburn	2.8	1.4	3.8	1.3	0.73	1.06
gabbro-MH, old veg	1.8	1.6	3.0	1.5	0.71	1.08
felsic granulites	2.8	2.0	5.7	1.68	0.81	1.20
granite gneiss	2.7	2.1	5.6	1.8	0.78	1.16
weathered felsic granulite	3.2	1.8	5.7	1.49	0.81	1.18
2. duricrust						
laterite-WIN	2.2	2.6	5.8	2.11	0.79	1.22
laterite-KA	2.7	2.5	6.7	2.06	0.80	1.21
calcrete-PID	2.3	1.7	3.8	1.42	0.88	1.17
calcrete-CDM	3.2	1.9	6.0	1.63	0.81	1.15
silcrete-WIN	1.9	1.5	2.9	1.34	0.90	1.15
silcrete-KA	1.7	1.9	3.2	1.51	0.99	1.24
3. alluvial deposits						
alluvium, basic source	2.5	1.8	4.6	1.68	0.73	1.07
alluvium, felsic source	4.7	2.0	9.4	1.66	0.84	1.20
silt and clay-CDM	3.8	1.6	6.1	1.47	0.73	1.09
silt and clay-LW	1.8	2.2	4.0	1.98	0.74	1.09
dunes, fireburn	3.8	1.9	7.2	1.63	0.77	1.16
dunes, old growth	2.4	2.2	5.1	1.83	0.81	1.18

reason, only green vegetation subtraction was applied to the Tomkinson Ranges scene. Radiance-corrected reflectance spectra and devegetated estimated spectra are displayed in Fig. 10. The comparison shows (1) a consistent reduction in the 4/5 and 5/7 ratios of the devegetated spectra, consequent on the removal of the positive 5/7 and 5/4 ratios of green vegetation, and (2) a consistent decrease in the 4/3 ratio of the devegetated spectra, due to the removal of the high 4/3 ratio of green vegetation; (3) lowering of the 2/1 and 2/3 band ratios, which are high in green vegetation. Devegetated images of the Tomkinson Ranges show that, whereas sharpening of the images and good definition of some lithological units are obtained, much of the detail shown in the original images and in log residual images and ratio images is lost. This may indicate that green vegetation concentrations help define surface mineral types.

3.11 UNSUPERVISED CLASSIFICATION

Unsupervised image classification involves comparisons between nearest-neighbour pixels, calculation of mid points, and migration of means by an iterative process - grouping analogous spectra into a user-specified number of classes. The method differs from supervised classification where specified spectral types are derived from training areas, a process involving ***a priori*** categorization of the classes, or subjective selection. Unsupervised classification can be performed either on raw spectral data, corrected spectral data or processed images. On classified images each spectral group is given a separate color, allowing its visual distinction. In this study unsupervised classification images produced on the IIS system, using 20 and 30 class selections allow the following correlations:

- A 20-class image differentiates between the following surface types:

1. gabbro.
2. ferrogabbro and pyroxenite.
3. felsic granulites and granites.
4. quartz-rich alluvial deposits.
5. weathered felsic granulites.
6. vegetated dune areas.

- A 30-class images differentiates between the following surface types:

1. mafic and ultramafic rocks.
2. felsic granulites and granites.
3. quartz-rich alluvium.
4. vegetated dunes.

The above suggests that an increase in the number of classes may result in subdivisions whose significance in terms of correlation with surface types is less clear. In view of the limited resolution of classified raw data images, unsupervised classification was performed on geologically particularly useful images, for example RGB pc2(4/3:5/7):5/4:4/3 image (section 3.8). The classification process results in image degradation due to the averaging of pixel arrays, generally diminishing the resolution of individual surface type. Thus, whereas the classified image still allows a discrimination between gabbro, iron oxide-rich ferrogabbro/pyroxenite/laterite, felsic granulite and weathered felsic granulite - its spatial resolution is distinctly inferior as compared to that of the unclassified image.

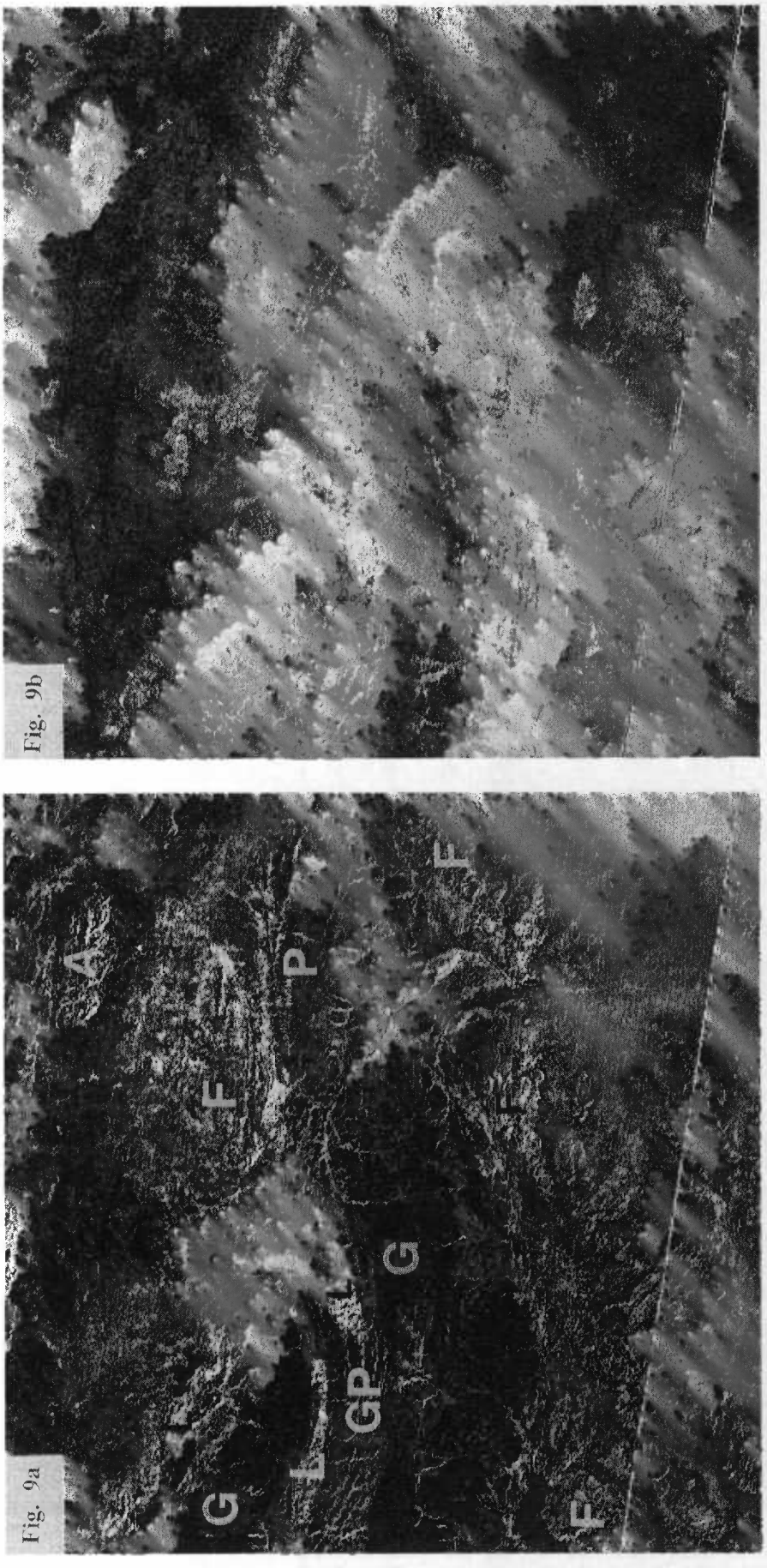

Fig. 9. Pixel unmixing images of the Mount Davies sub-scene. 9a - unmixed hematite end member (for explanation of symbols refer to Fig. 4); 9b - unmixed clay end member; 9c - unmixed green vegetation end member; 9d - unmixed dry vegetation end member (for explanation refer to section 3.9).

Fig. 9d

Fig. 9c

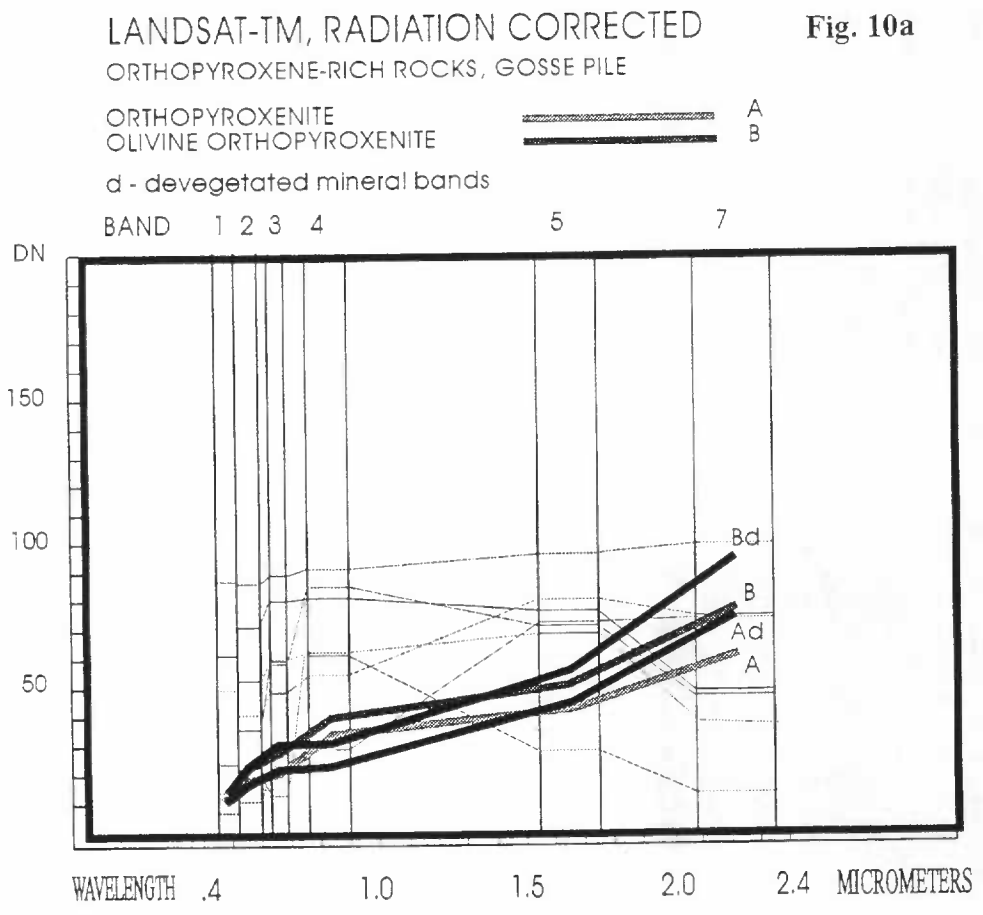

Fig. 10a

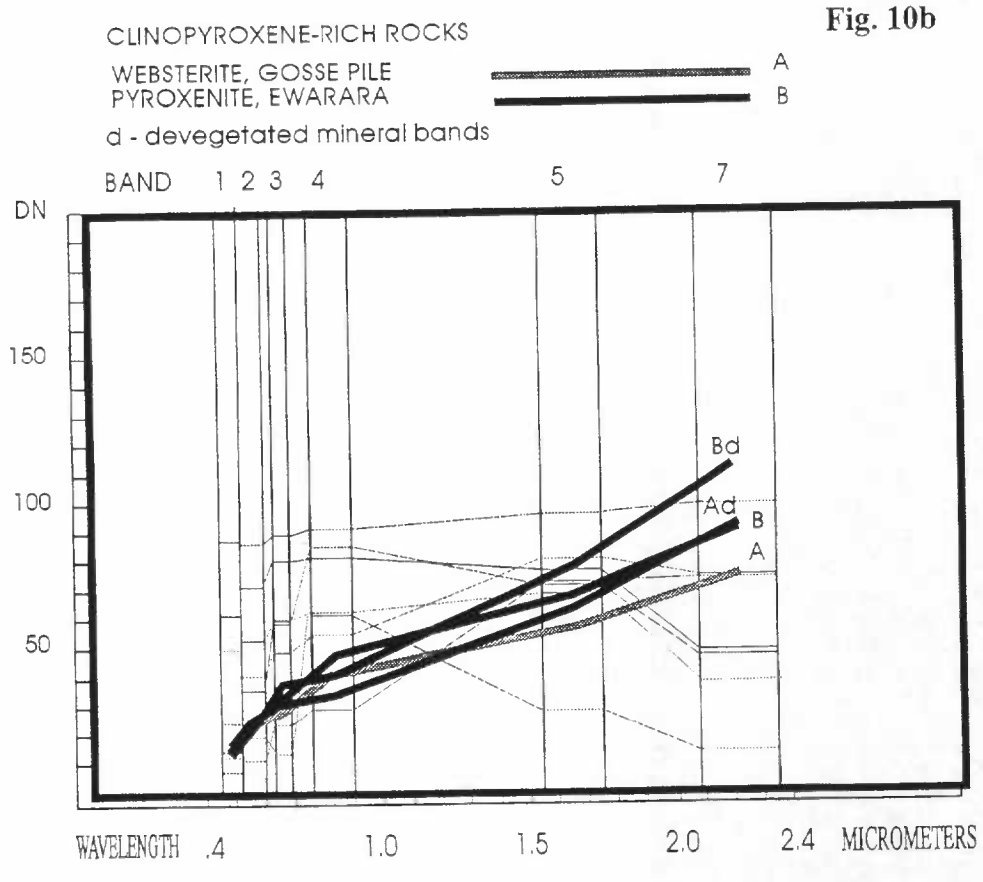

Fig. 10b

Fig. 10. Radiance (atmospheric effects)-corrected and devegetated bands Landsat-5-TM mean data for training areas. Surface types as in Fig. 3. For explanation refer to sections 3.3 and 3.10.

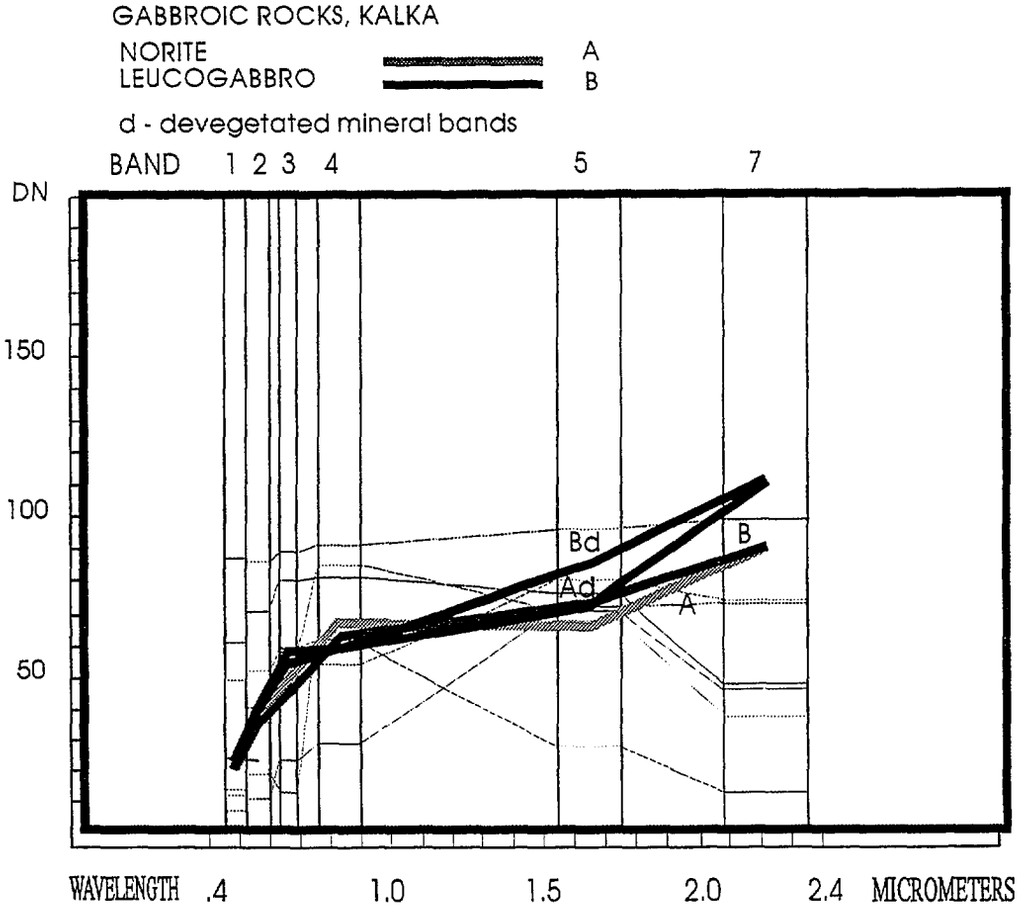

Fig. 10c

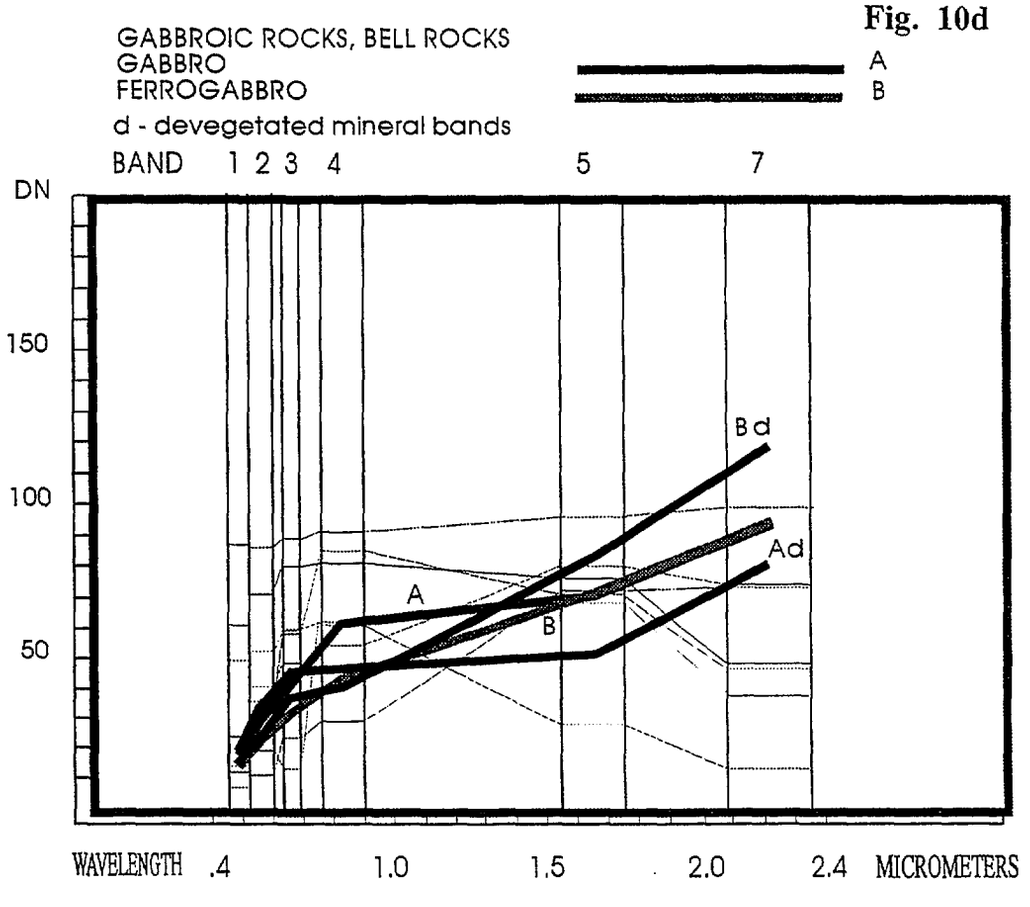

Fig. 10d

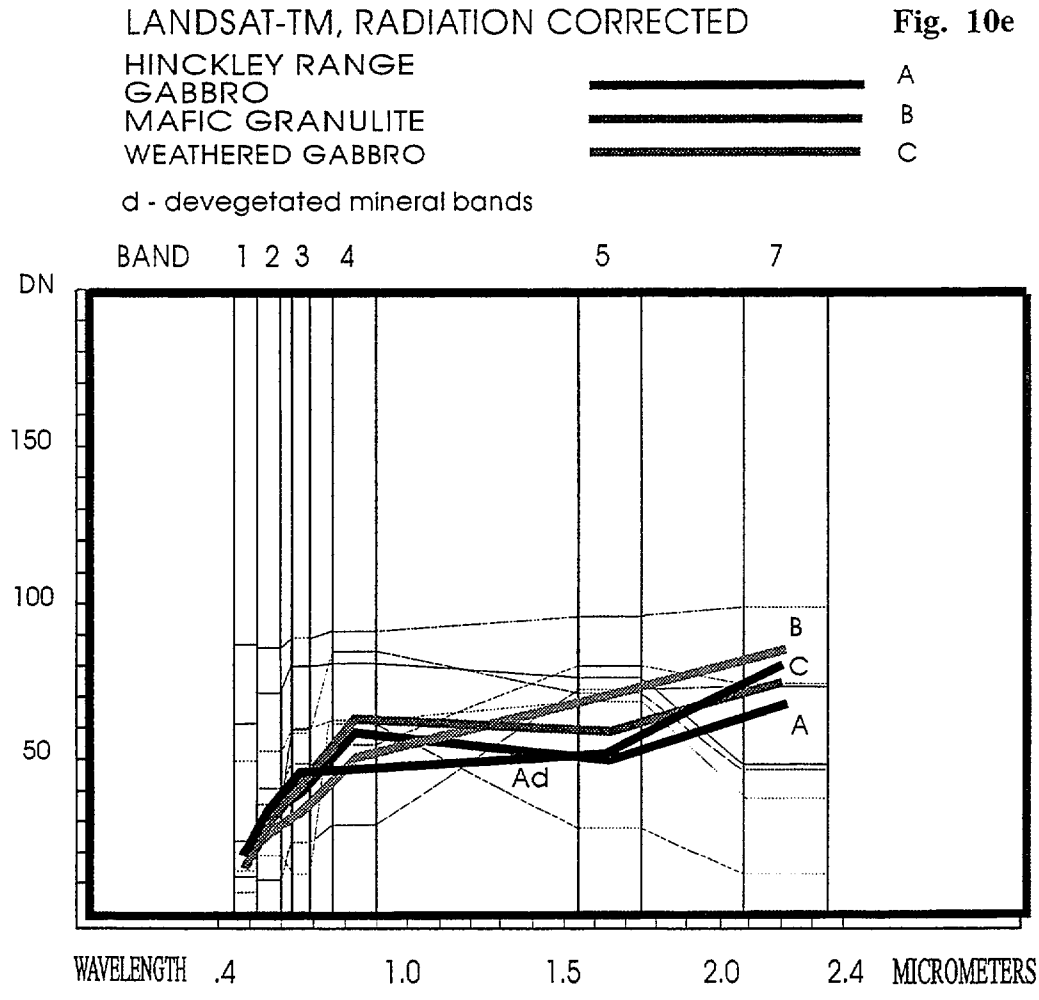

Fig. 10e

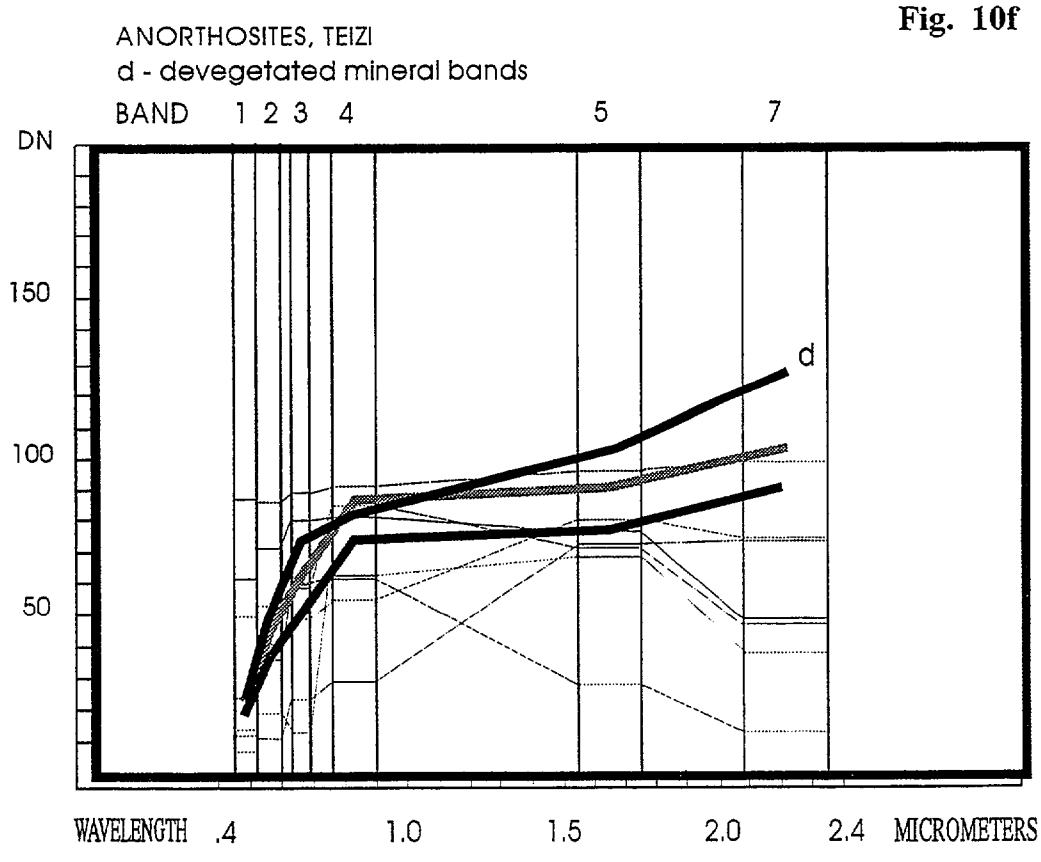

Fig. 10f

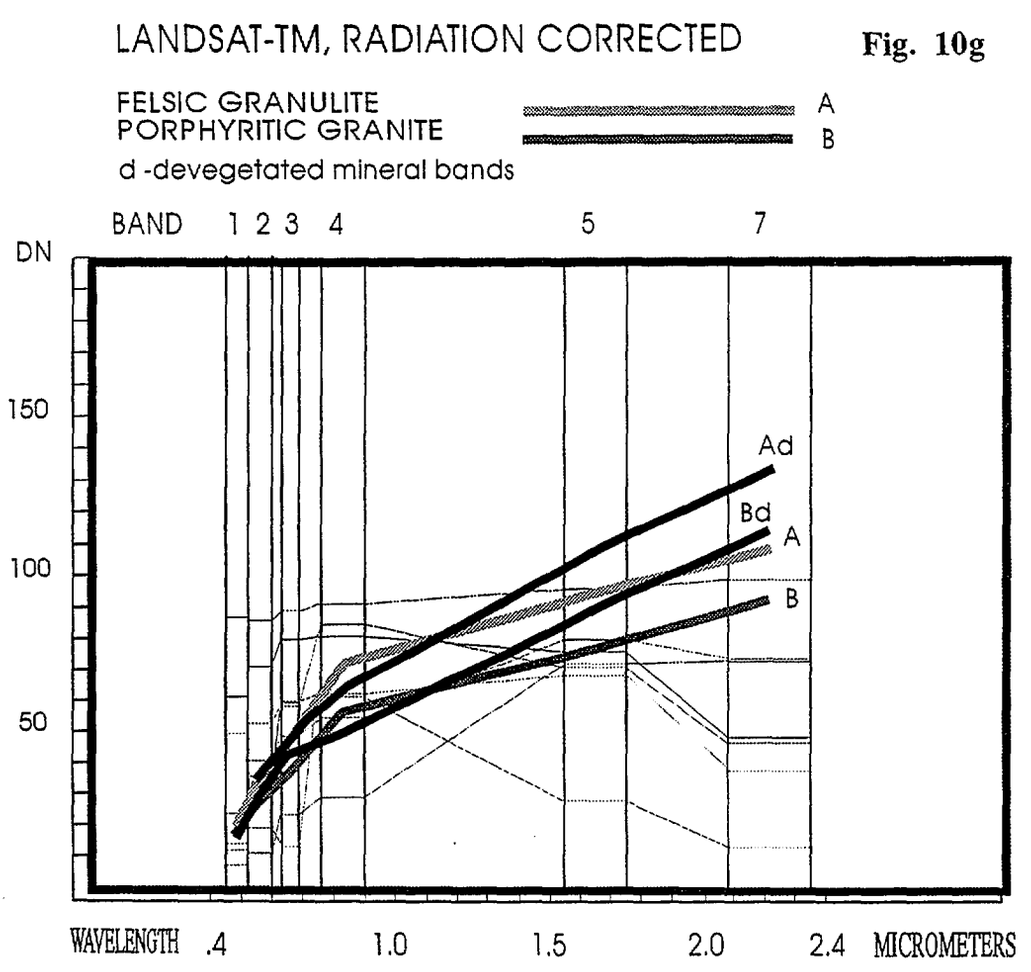

Fig. 10g

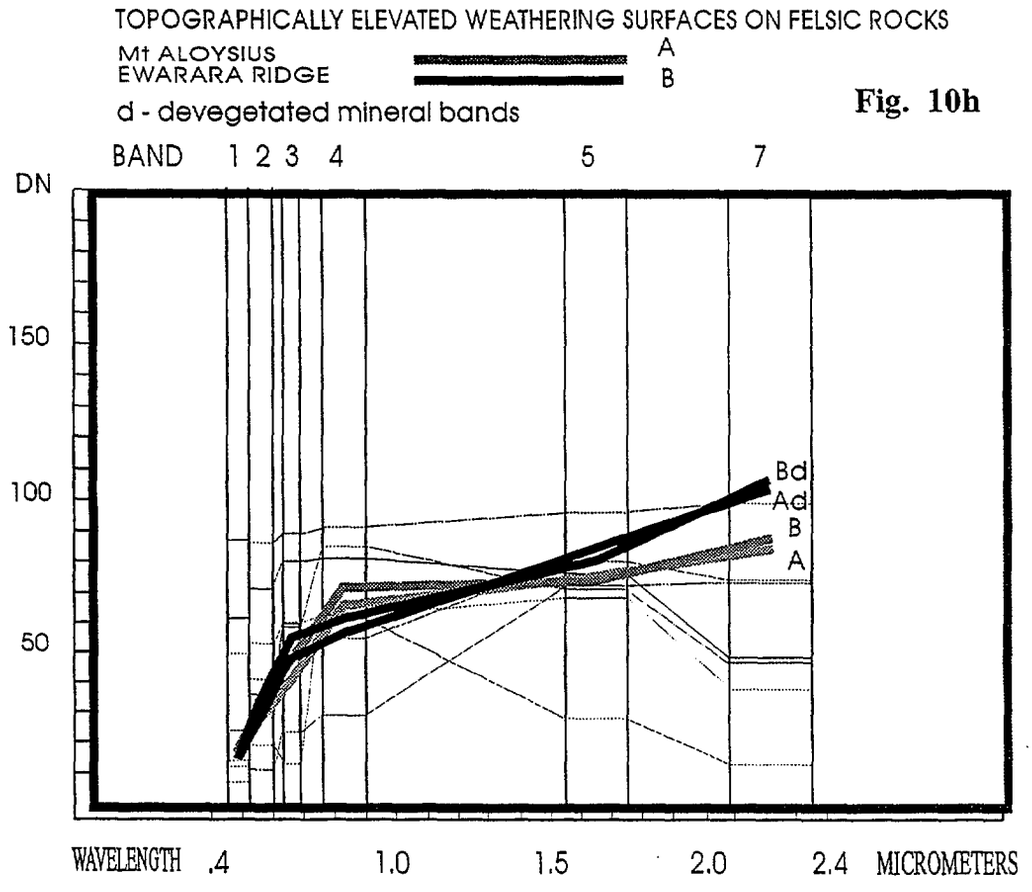

Fig. 10h

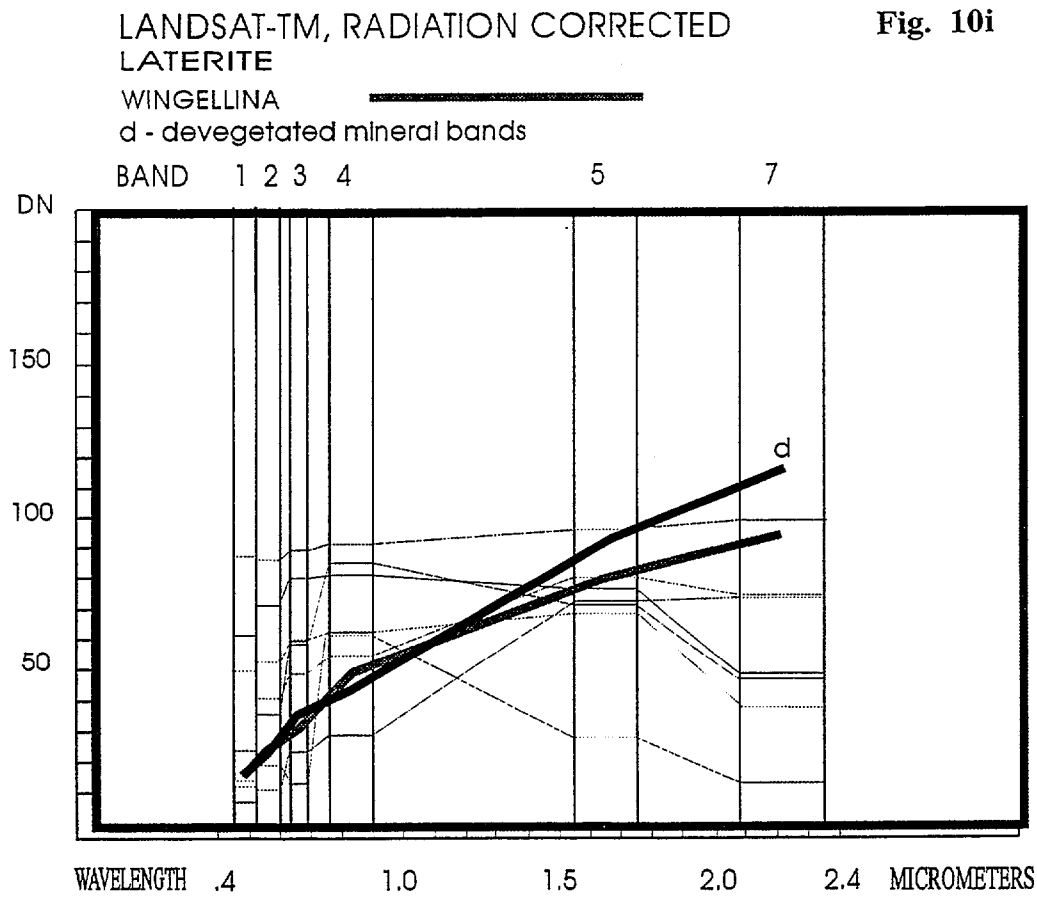

Fig. 10i

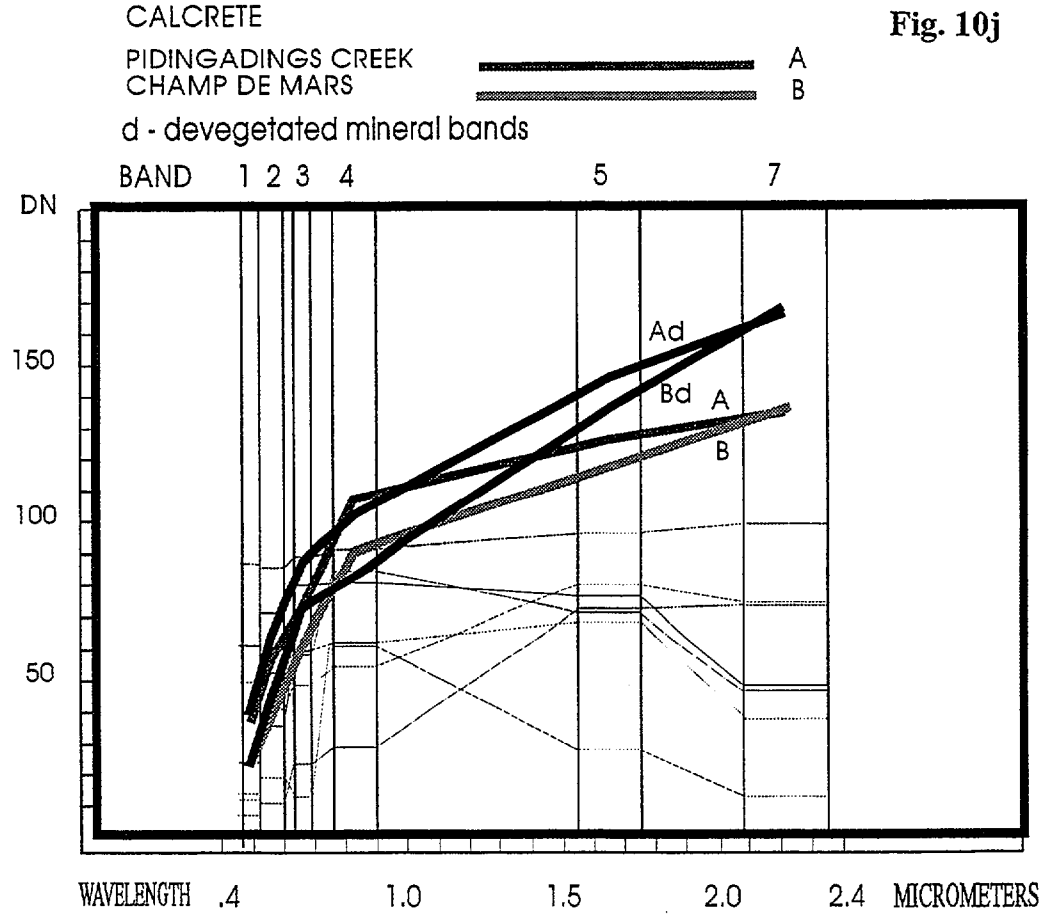

Fig. 10j

Fig. 10k

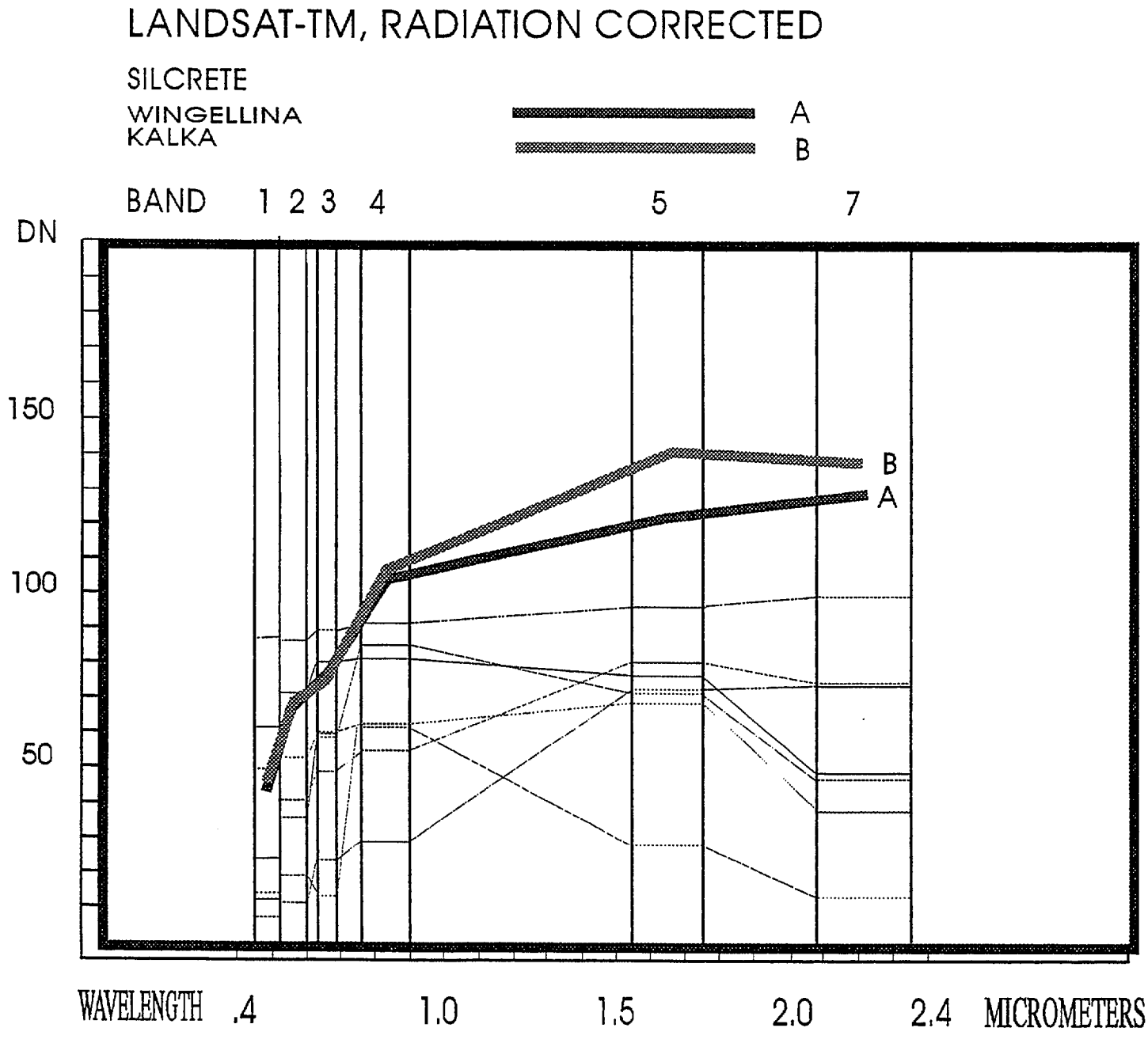

LANDSAT-TM, RADIATION CORRECTED

Fig. 10l

ALLUVIAL PEDIMENT

FELSIC SOURCE — A

MAFIC SOURCE — B

d - devegetated mineral bands

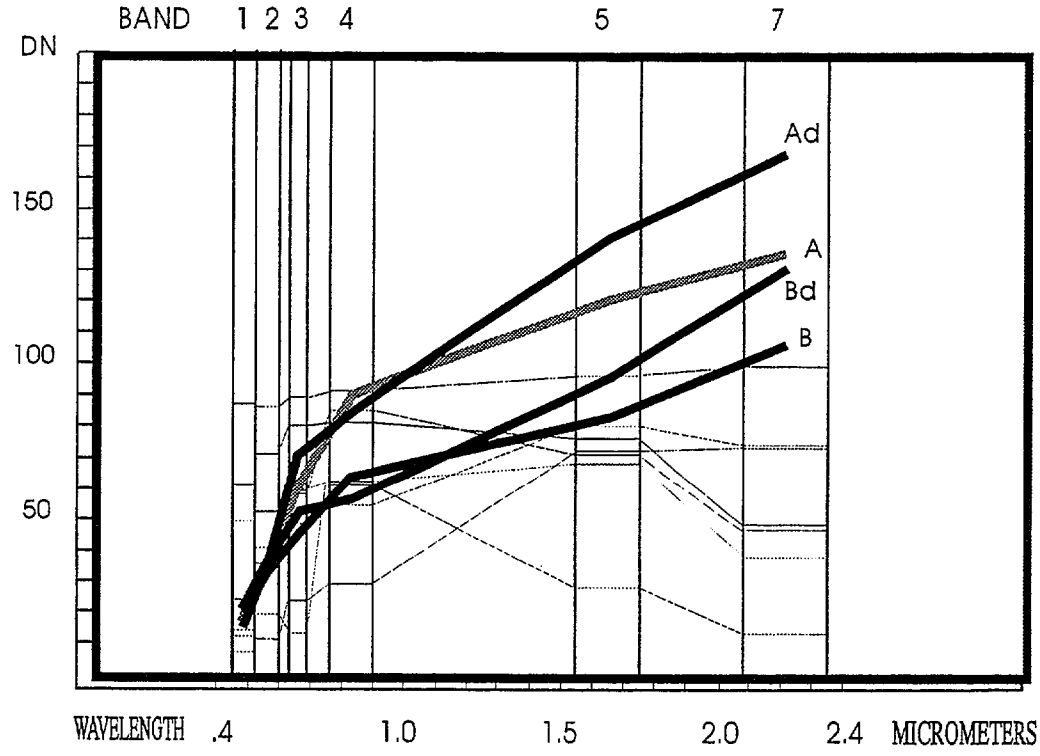

SILT AND CLAY

CHAMP DE MARS VALLEY
LAKE WILSON — A, B

Fig. 10m

d - devegetated mineral bands

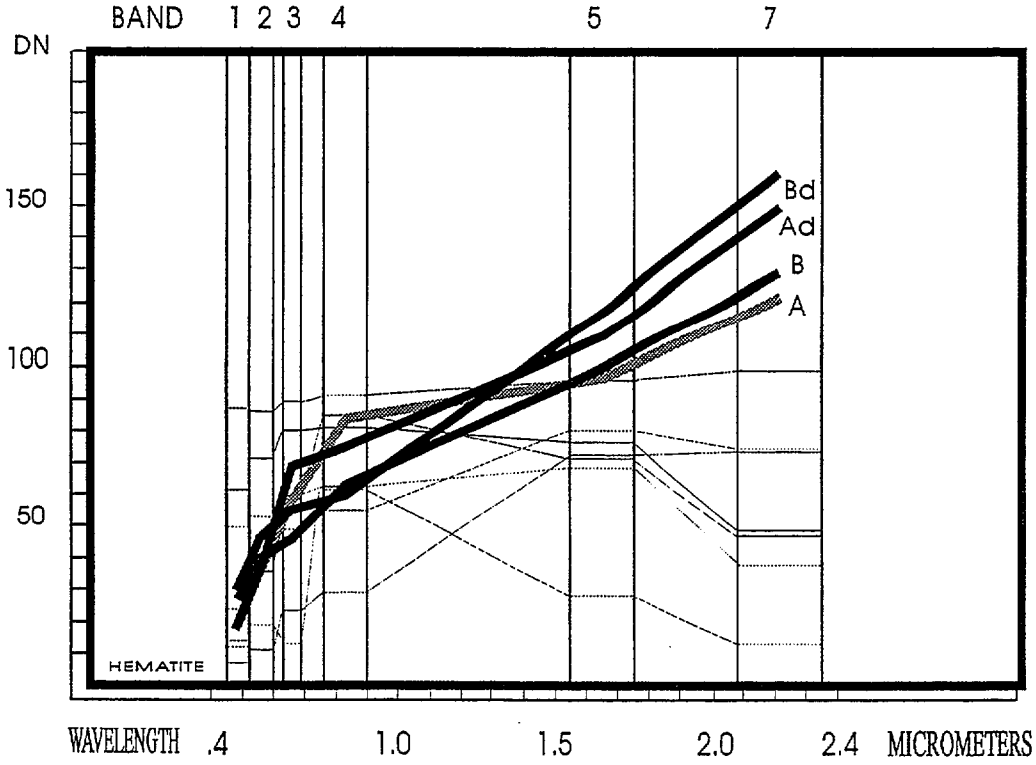

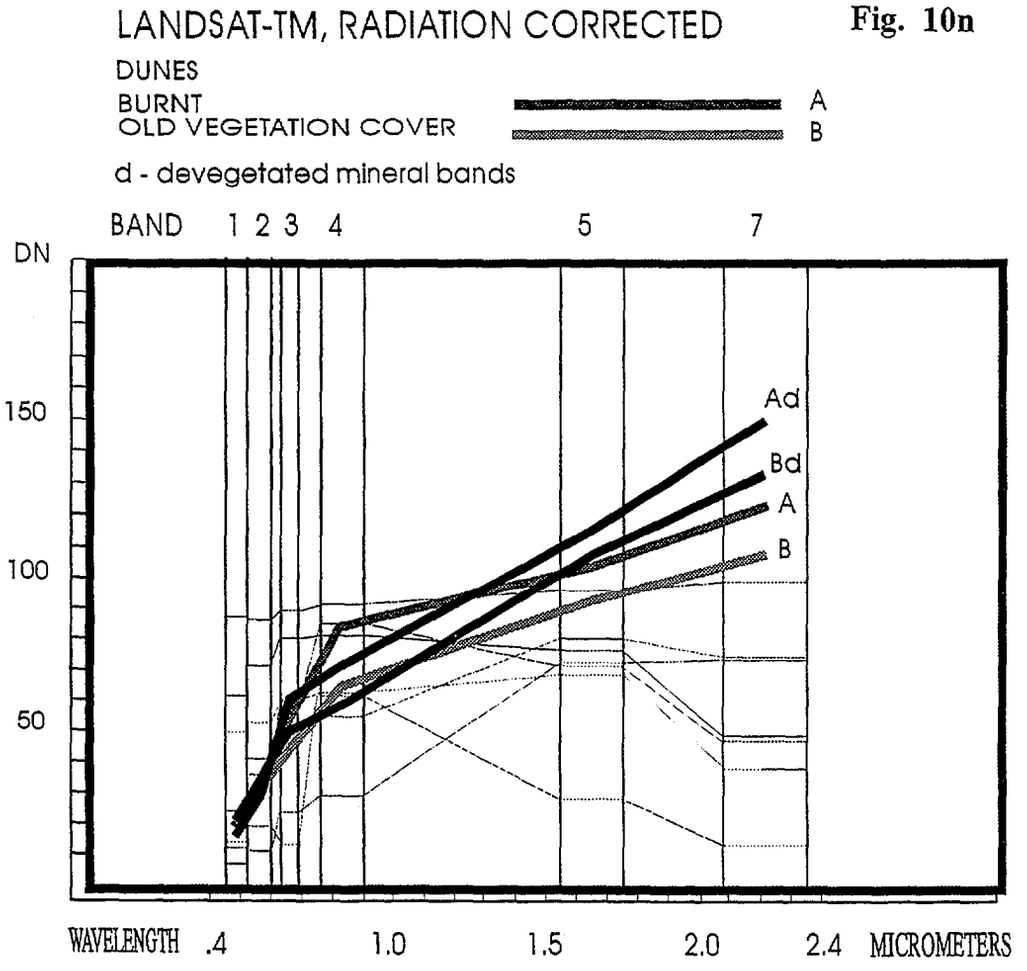

Fig. 10n

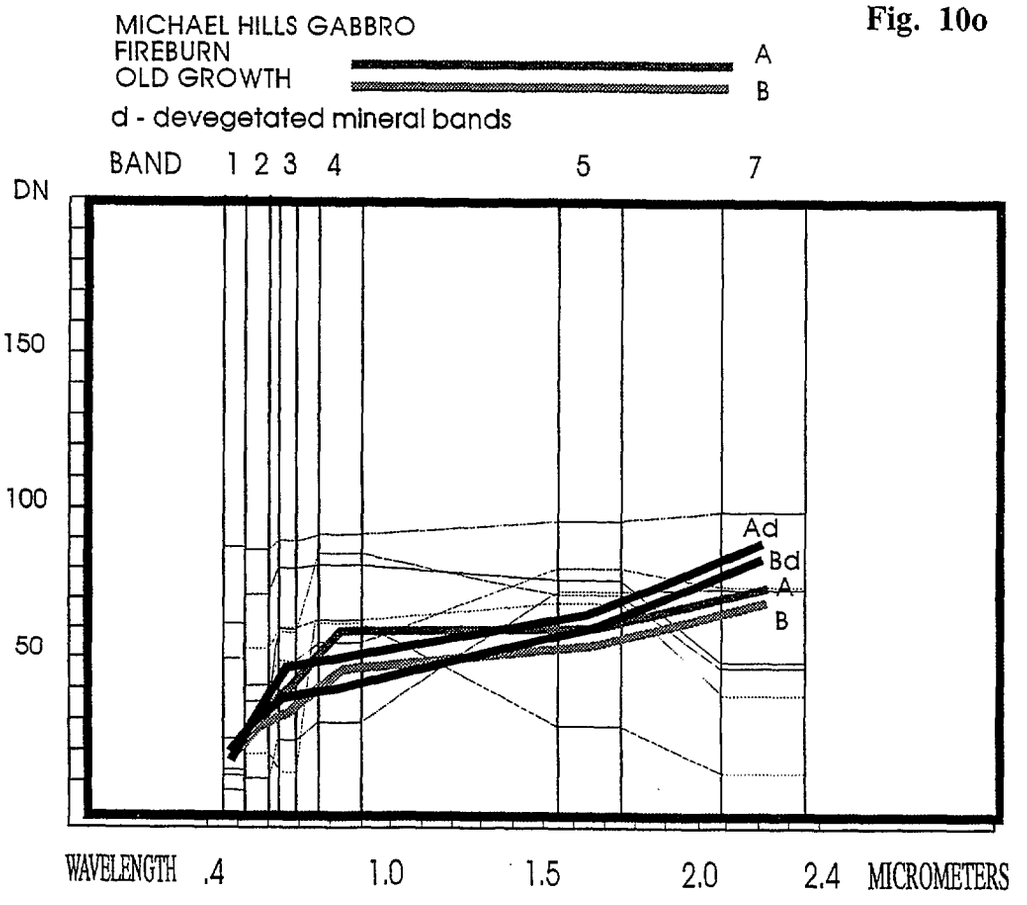

Fig. 10o

4. SUMMARY OF LANDSAT-5-TM LITHOLOGICAL CORRELATIONS

The aim of this chapter is to summarize the observations made in the above sections in terms of a table of individual surface types, enabling their identification from Landsat-5-TM imagery in the western Musgrave Block. Systematic classifications are allowed by comparisons between spectral patterns (Figs. 3, 5, 10). In view of the wide range of image types available and the redundancy of spectral-surface type correlation methods, only the more diagnostic criteria identified in the present study will be listed here It is emphasised that, in themselves the spectral characterisitics are not considered a sufficient basis for independent identification of surface type - except as interpolations and extrapolations of field and structural studies of the terrain and materials in question. Correlations between the spectral features of some of the more diagnsotic images and surface types are summarized in Table H.

Table H - Spectral claissifications of surface types in the western Musgrave Block using Landsat-5-TM images. Note - only the more diagnostic criteria identified in the present study are listed.

image [1] - RGB pc2(4/3;5/7) : 5/4 : 4/3 (clay/carbonate : iron oxide : green vegetation).

image [2] - RGB log residuals 5:4:3 (iron oxide : green vegetation: clay/carbonate).

image [3] - RGB log residuals 7:4:1 (iron oxide : green vegetation: clay/carbonate).

image [4] - RGB 7:4:1

I. Layered mafic-ultramafic intrusions

peridotite, commonly laterite, carbonate and silcrete-coated	image [1] - patchy combination of red, green and white.
orthopyroxenite: iron oxide-rich weathering crusts:	image [1] - green to cyan; image [2] - yellowish red to orange image [3] - purplish red
clinopyroxenite/websterite, iron oxide & clay/carbonate weathering crusts	image [1] - green with red dots. image [3] - purplish red.
gabbro/norite -clay/carbonate/ iron oxide-bearing weathering crusts	image [1] - mainly red; blue where covered by. green vegetation; yellowish to red where covered by dense old dry vegetation (spinifex); brown where fireburnt. image [2] - purple (iron oxide, clay and carbonate). image [3] - cyan (clay/carbonate + vegetation); image [4] - purple.
ferrogabbro iron -oxide-rich weathering crusts:	image [1] - apple green to yellowish green. image [2] - orange to yellowish red. image [3] - brilliant pink
anorthosite - carbonate/clay weathering crusts	image [1] - orange red. image [3] - cyan. image [4] - cyan (higher reflectance than gabbro)

II. Metamorphic rocks	
mafic granulites - clay, iron oxide and quartz-bearing weathering crusts, commonly cut by iron oxide-rich mafic dykes	image [1] - yellow (red/green), cut by green/blue mafic dykes. image [3] - purplish red (iron oxide + clay) with relict cyan patches (gabbro).
felsic granulites - clay, iron oxide, quartz-bearing weathering crusts, cut by iron oxide-rich mafic dykes.	image [1] - felsic granulites - yellow (red/green); mafic dykes - apple green; clay-rich weathering zones - red; shaded/vegetted southern slopes display in cyan. image [2] - felsic granulites: yellowish green, cut by orange red mafic dykes. image [3] - purplish red (iron oxide shed by mafic dykes) and cyan (clay+vegetation) weathering surfaces; image [4] - purple.
III. Felsic igneous rocks	image [1] - yellow (red/green), as for felsic granulites, or in places purple (vegetated clay-rich exfoliated outcrops); image [4] - purple
IV. Volcanic rocks	
mafic/andesitic volcanics	image [1] - yellow (red/green); image [3] - purplish red
felsic volcanics	image [1] - red (clay weathering); image [3] - blue
V. Duricrusts	
laterite	image [1] - apple green, cyan where covered by dense bush; image [2] - apple green to yellow, representing iron oxide and thick vegetation; image 3 - orange red; image [4] - red
calcrete	image [1] - orange zones along creeks; image [2] - blue to purple; image 3 - cyan to blue; image [4] cyan
silcrete	image [4] high labedo (white)
VI. Alluvial deposits	
felsic source-derived pediment	image [1] - pink rings (clay-rich arkose) around felsic granulite outcrops; image [3] - apple green to bluish green; image [4] - cyan (vegetation on clay)
mafic source-derived pediment	image [1] - green to yellow/green colluvium; in places reddish clay-rich alluvial zones; image [4] - red
mixed alluvial deposits	image [1] - yellow/red/blue alluvial plains
dunes	image [1] - dune crests: thickly vegetated - purple; dune valleys: clay/iron oxide-rich - yellow (red/green); heavily vegetated dunes - blue with white lineaments (quartz-rich crests).
silt and clay pans	image [1] - orange/brown areas; green where iron oxide-rich clay occurs
green vegetation	image [1] - cyan; image [4] - green; image [2] - yellowish green; image [3] - apple green.

5. GEOSCAN MARK–I IMAGE INTERPRETATIONS

Two runs of Geoscan 13-band 10 meter-pixel Mark-I imagery flown over the Tomkinson Ranges have been provided by Geoscan, courtesy of Dr J.L. Daniels, for lithological comparisons. The two runs, covering 5 km-wide east-west and north-south strips (Fig. 1), allow further discrimination thanks to the smaller pixel size as well as additional information derived from bands in the thermal range. A comparison between the Geoscan Mark-I band intervals and those of Landsat-5-TM are given in Table I. This section offers only information based on band ratios, whereas further analysis of the Geoscan images will be made elsewhere.

In view of the different band intervals of the Geoscan Mark-I spectra, the data allow correlations with surface type not readily identifed by Landsat-5-TM data, as follows (Honey and Daniels, 1985, 1986):

bands 6/7 ratio - highlights kaolin-rich areas.

bands 6/8 ratio - highlights sericite and smectite-rich areas.

bands 6/9 ratio - highlights carbonate-rich areas

bands 7/8 ratio - positive discrimination of smectites.

bands 8/7 ratio - bright areas for high alunite

bands 11/10 ratio - highlights areas of high free silica.

Comparisons between RGB ratio images of the above bands (6/8:6/9:5/4, 6/8:6/9:11/10, 10:11:12) for the Tomkinson Ranges area allow the following observations and correlations:

1.The 6/8 band ratio is manifest in clay/arkose-rich pediments which fringe felsic granulites and granites, as a patchy pattern over weathered clay-bearing outcrops of felsic granulites and over calcrete.

2.The 6/9 band ratio is manifest over outcrops of gabbro of the Giles Complex.

3.The 5/4 band ratio is manifest over gabbro of the Giles Complex and more strongly on oxidized mafic detritus and alluvium derived from mafic sources - representing iron oxide, although the Geoscan band 5 is different from the Landsat-5-TM band 5 interval.

4.The 11/10 band ratio is manifest over quartz-rich alluvial materials derived from felsic sources and also over silcrete.

Geoscan Mark-I log residual images help to accentuate lithological distinctions. For example, a RGB log residual 9:4:1 image of the Wingellina area clearly expresses the difference between weathered outcrops of gabbro and laterite. Further processing of Geoscan Mark-I images will be reported elsewhere.

6. CONCLUSIONS

To summarize the principal observations made in the present study, the following points are made:

- Landsat-5-TM images furnish an ideal method for fingerprinting and correlating the weathered surfaces of bedrock types, duricrust types and alluvial deposits, provided the composition of the various surface types are first ascertained in the field. Once correlations are established, interpolations and extrapolations of the data can be readily

pursued with a high degree of confidence, provided the morphological and structural patterns of the units in question are taken into account.

- Under the dry climatic conditions which apply in the western Musgrave Block, vegetation and fireburn patterns have only a limited masking effect on the mineral-produced reflectance. In the lack of field calibration with hand-held spectrometer, band ratio images, logarithmic residual images, principal component analysis of vegetation and mineral ratios, and pixel unmixing analysis yield significant correlations with surface types tested in the field.

- The spectral signatures of varying proportions of iron oxide and clay/carbonate are capable of characterizing a wide range of surface types, including individual components of the layered mafic/ultramafic Giles Complex with differing orthopyroxene: clinopyroxen:plagioclase ratios.

- The separation of haematite from goethite and of clay from carbonate on Landsat-5-TM images pose problems. However, in some instances these components can be identified from their mode of occurrence, for example calcrete banks along creeks.

- The identification of quartz on weathered rock surfaces is obscured by thin films of clay and iron oxide. Free abraded quartz in alluvial and dune deposits stands up due to high reflectance and is identified on Geoscan Mark-I images by high bands 11/10 ratios.

- The composition of isolated bedrock outcrops (inselbergs) - which may be too small to identify on Landsat-5-TM images - can be identifed from the associated or encircling wider alluvial haloes. Mafic bedrock sheds iron oxide-rich alluvial haloes and felsic bedrock sheds clay and quartz-rich alluvial haloes.

- The present study points to the importance of studying the composition of weathered surfaces of characteristic lithological types. Thus, the nature of the latter is not necessarily controlled by the major mineral composition of the fresh lithologies, for example, granite vein-intruded mafic granulites display silica and iron oxide-rich weathering surfaces whereas the weathered surfaces of gabbro is dominated by clay/carbonate. Another example is furnished by distinctions between anorthosite bands and plagioclase-rich felsic granulite bands due to the higher clay/carbonate reflectance signature of the former in the visible bands.

- Landsat-5-TM and Geoscan Mark I images are ideal for discrimination of palaeo-weathering surfaces located at high topographic levels and representing relicts of an eroded peneplain. The identification of these surfaces is enabled by the deeper weathering on these rocks, represented by clay and richer vegetation.

- Landsat-5-TM and Geoscan Mark I images can be used to readily identify calcrete duricrust along creeks and elsewhere in connection with searches for suitable target areas for hydrological purposes.

- Although the present study did not focus on the identification and correlation of vegetation types, it is clear from comparisons between the environmental map of the Tomkinson Range (Feeken, 1992) and the imagery that classification of areas dominated by grasses, bush, mulga and Eucalypt habitats can be achieved once the specific spectral differences between these vegetation types are calibrated.

- The lithological surface type variations displayed on the Landsat-5-TM images and on Geoscan images provide information which can not be identified in any other way - including field work - in view of the ability of the reflectance in the infrared range to distinguish surface patterns and variations dependant on mineralogical and geochemical patterns undetected by the human eye in the field and ascertainable only through laboratory testing. In this regard, the routine application of remotely sensed techniques, including image processing using advanced statistical methods, is regarded as essential for the pursuit of modern new generation mapping such as pursued by the National Geoscience Mapping Accord.

ACKNOWLEDGEMENTS

The image processing work on which this report is based would not have been possible had it not been for the generous and patient guidance by J.W. Creasey, in charge of the AGSO remote sensing laboratory. P.N. Bierwirth wrote a part of the section on pixel unmixing. I am indebted to P.N. Bierwirth, P. N. Chopra, L.F. Macias, M. Peljo, A.J. Whitaker and J.R. Wilford for their time and advice. The supervision of the Sun computer system by P. Miller and the provision of Geoscan imagery by J.L. Daniels are gratefully acknowledged. The comments on this manuscript by P.N. Bierwirth, P.N. Chopra, J.W. Creasey, L.F. Macias and C.J. Simpson are gratefully acknowledged.

REFERENCES

ADAMS, J.B., SMITH, M.O., and JOHNSON, P.E., 1986 - Spectral mixture modeling: A new analysis of rock and soil types at the Viking Lander 1 Site. J. Geophys. Res. 91:8098-8112.

ADAMS, J.B., SMITH, M.O. and GILLESPIE, A.R., 1989 - Simple models for complex natural surfaces: A strategy for the hyperspectral era of remote sensing. Proc. 12th Canadian Symp. Remote Sensing, vol. I:16-21

BALLHAUS, C.G., 1993 - Petrology of the Giles Complex, Musgrave Block, central Australia: the Jameson, Blackstone, Bell Rock, Murray, south Mount West, Latitude Hill and Hinckley intrusions. AGSO Record 92/73.

BALLHAUS, C.G. & GLIKSON, A.Y., 1989 - Magma mixing and intraplutonic quenching in the Giles Complex, central Australia J. Petrol., 30:1443-65.

BALLHAUS, C.G. and BERRY, R.F., 1991 - The crystallization pressure of the Giles layered complex: an example for geobarometry in the spinel stability field. J. Petrology 32: 1-28.

BALLHAUS, C.G., GLIKSON, A.Y. and KEAYS, R.R., 1992 - Magmatic evolution and economic potential of the Giles layered igneous complex, central Australia. BMR Research Newsletter, 16:6-9.

BIERWIRTH, P.N., 1990 - Mineral Mapping and vegetation removal via data-calibrated pixel unmixing, using multispectral images. Int. J. Remote Sensing, 11:1999-2017.

CLARKE, G.L., BUICK, I.S. and GLIKSON, A.Y., 1992 - contact relationships and structure of the Hinckley Gabbro and host rocks, Giles Complex, western Musgrave Block, W.A.. BMR Research Newsletter, 17:6-8.

CLARKE, G.L, STEWART, A.J. and GLIKSON, A.Y., 1993 - High pressure eclogite facies metamorphism associated with the Woodroffe thrust. AGSO Res. News, 18:6-7.

DANIELS, J.L. 1974 - The Geology of the Blackstone Region, Western Australia. Geological Survey of Western Australia Bulletin, 123.

FEEKEN, E., 1991 - Environmental mapping in BMR: Cainozoic deposits, landforms and vegetation in the Tomkinson Ranges. BMR Res. Newsletter, 14:7-8.

FEEKEN, E., 1992 - Notes on the 1:100 000 environmental map of the Tomkinson Ranges, Western Musgrave Block, central Australia. AGSO Record 92/34.

FORSTER, B.C., 1984 - Derivation of atmospheric correction procedures for Landsat-5-MSS with particular reference to urban data. Inter. J. Remote Sensing, 5:799-817.

FRASER, S.J. and GREEN, A.A., 1987 - A software defoliant for geological analysis of band ratios. Inter. J. Remote Sensing, 8:525-532.

GLIKSON, A.Y., 1987 - An upthrusted early Proterozoic mafic granulite-anorthosite suite and anatectic gneisses, southwestern Arunta Block, central Australia: Evidence on the nature of the lower crust. Trans. Geol. Soc. S. Africa, 89:263-283.

GLIKSON, A.Y., 1989 - New evidence on the significance of ultramafic components of the layered, Giles Complex, central Australia. BMR Research Newsletter, 10:4-6

GLIKSON, A.Y., 1990 - The Giles Complex, central Australia: new insights into tectonics and metamorphism. BMR Research Newsletter, 12:18-20.

GLIKSON, A.Y., 1992 - NGMA mapping in granulite/gneiss terrains of central Australia. BMR Res. Newsletter, 16:22.

GLIKSON, A.Y. and MERNAGH, T., 1990 - Major pseudotachylite breccia-vein networks, Giles layered mafic-ultramafic complex, western Musgrave Block, central Australia. BMR J. Aust. Geol. Geophys., 11, No. 4, 509-519.

GLIKSON, A.Y., BALLHAUS,, C.G., GOLBY, B.R. and SHAW, R.D., 1990 - Major thrust faults and crustal zonation of the middle to upper Proterozoic crust in central Australia. NATO Advanced Study Institute on Exposed Cross Sections Through the Continental Crust, Kluwer Academic Publishers, Netherlands, 285-304.

GLIKSON, A.Y., STEWART, AJ. and BALLHAUS, C.G., 1991 - Layered mafic/ultramafic intrusions and the deep-seated Proterozoic crust of central Australia (abstract). Geol. Soc. Am. Ann. Conv. Abstracts and Programs, 1991, p.A60.

GLIKSON, A.Y., STEWART, AJ. BALLHAUS, C.G., CLARKE, G.L., SHERATON, J.W. and SUN, S.S., 1994 - Geology of the Tomkinson Ranges 1: 100 000 sheet area AGSO Record, in prep.

GOODE, A.D.T. 1978. High Temperature, High Strain Rate Deformation in the Lower Crustal Kalka Intrusion, Central Australia. Contrib. Mineral. Petrol., 66, 137-148.

GOODE, A.D.T. and KRIEG, G.W., 1967. The geology of the Ewarara intrusion, Giles Complex, central Australia. J. geol. Soc. Aust., 14, 185-194.

GOODE, A.D.T. and MOORE, A.C. 1975. High pressure crystallization of the Ewarara, Kalka and Gosse Pile Intrusions, Giles Complex, central Australia. Contrib. Mineral. Petrol., 51, 77-97.

GOODE, A.D.T. 1978 - High Temperature, High Strain Rate Deformation in the Lower Crustal Kalka Intrusion, Central Australia. Contrib. Mineral. Petrol., 66, 137-148.

GREEN, A.A. and Craig, M.D., 1985 - Analysis of aircraft spectrometer data with logarithmic residuals. Jet Propulsion Laboratory Publ. 85-41, pp. 111-119.

HONEY, F.R. and DANIELS, J.L., 1986 - Rock discrimination and alteration mapping for mineral exploration using the Carr Boyd/Geoscan airborne multispectral scanner. In: 5th Thematic Conference on Remote Sensing for Exploration Geology, Reno, Nevada.

HONEY, F.R. and DANIELS, J.L., 1987 - Application of Carr Boyd Minerals Limited airborne multispectral scanner to spectral discrimination of hydrothermally altered areas. In: 4th Thematic Conference on Remote Sensing for Exploration Geology, San Francisco, California.

MOORE, A.C. and GOODE, A.D.T. 1978 - Petrography and origin of granulite-facies rocks in the western Musgrave Block, central Australia. J. Geol. Soc. Aust., 25, 341-358.

NESBITT, R.W., GOODE, A.D.T., MOORE, A.C. and HOPWOOD, T.P. 1970. The Giles Complex, Central Australia: a stratified sequence of mafic and ultramafic intrusions. Spec. Pub. geol. Soc. S. Afr., 1, 547-564.

NESBITT, R.W. and KLEEMAN, A.W. 1964. Layered intrusions of the Giles Complex, Central Australia. Nature, 203, 391-393.

NESBITT, R.W and TALBOT, J.L. 1966. The Layered Mafic and Ultramafic Intrusives of the Giles Complex, Central Australia. Contr. Mineral. and Petrol., 13, 1-11.

PHARAOH, T.C., 1990 - Aspects of structural geology of the Giles layered mafic/ultrmafic complex, Tomkinson Range, Musgrave Block, central Australia. Bur. Miner. Resour. Record 1990/6.

RICHARDS, J.A., 1986 - Remote Sensing Digital Image Analysis. Springer Verlag, Berlin, 281 pp.

SHAW, R.D., STEWART, A.J. and BLACK, L.P., 1984 - The Arunta inlier: a complex ensialic mobile belt in central Australia. Part 2: Tectonic history. Aust. J. Earth Sci., 31:457-484.

SIMPSON, C.J., 1978 - LANDSAT-5: developing techniques and applications in mineral and petroleum exploration. Bur. Miner. Resour. Aust. Geol. Geophys., 3:181-191.

SIMPSON, C.J., MACIAS, L.F. and MOORE, R.F., 1987 - Differentiation of mafic and ultramafic rocktypes using NS001 and TIMS data (unpubl.)

STEWART, A.J., 1993 - Extension of the Woodroffe thrust in Western Australia. AGSO Res. News. 18:5-6.

STEWART, A.J., SHAW, R.D. and BLACK, L.P., 1984 - The Arunta inlier: a complex ensialic mobile belt in central Australia. Part I: Stratigraphy, correlatisons and origin. Aust. J. Earth Sci., 31:445-455.

STEWART, A.J. and GLIKSON, A.Y., 1991 - The felsic metamorphic/igneous core complexes hosting the Giles Complex. BMR Res. Newsletter, 14:6-7.

SUN, S.S. and SHERATON, J.W.,, 1992 - Isotopic geology of the Giles Complex and environs, Tomkinson Ranges, central Australia, BMR Res. Newsletter, 17: 9-10.

THOMSON, B.P., MIRIAMS, R.C. and JOHNSON, J. 1962. Mann, S.A. 1:250,000 Geological Sheet, Explan. Notes. geol. Surv. South. Aust.

WARREN, R.G., 1983 - Metamorphic and tectonic evolution of granulites, Arunta Block, central Australia. Nature, 305:300-303.